HBRC Journal

Contents

Housing & Building National Research Center

HBRC Journal

EFFECT OF AGGREGATE TYPE ON THE BEHAVIOR OF THERMALLY TREATED SELF-COMPACTED CONCRETE

M. A. Helal
Housing & Building National Research Center, Egypt.
E-mail: mahelal54@yahoo.com
KH. M. Heiza
Minoufiya University, Egypt,
E-mail: khheiza@yahoo.com

ABSTRACT

This paper was conducted to determine the physico-mechanical and microstructure characteristics of self-compacted Concrete (SCC) with different types of coarse aggregate (Basalt, Gravel or Dolomite) exposed to high temperatures for different exposure times. The changes in the physico-mechanical properties of SCC due to the exposure to high temperature were examined. The evaluation of fresh SCC properties was based on the results of slump-flow test, J-ring test and V-funnel flow test. The change in mechanical properties, porosity, absorbtivity, bulk, and real density with temperature at different time of exposure were also recorded. The phase composition and microstructure were investigated by differential scanning calorimetry (DSC). The experimental results showed that the aggregate type has a clear effect on the fresh properties of SCC and also the high temperature has a clear effect on both physico-mechanical and mineralogical composition of different SCC mixes.

Keywords: Microstructure; Physical properties; Self compacted; Thermally treated.

INTRODUCTION

When concrete is exposed to high temperatures it undergoes a series of changes in its physico-chemical structure. These changes occur primarily in the hardened cement paste (HCP) starting from the dissociation of calcium hydroxide (CH) at 400oC, and continue until the complete destruction of the calcium-silicate-hydrate (C-S-H) gel at around 900oC. As a result of these changes, concrete gradually and sometimes sharply loses its mechanical strength and durability [1]. An experimental study was carried out to gain insight into some of the parameters that influence the flow mechanisms of self compacting concrete (SCC)[2]. The results show that the flow behavior of SCC concrete is enhanced with sand aggregate ratio . The amount of coarse pores in both the interfacial transition zone (ITZ) and the bulk paste is generally much higher in the normal concrete, while the porosity is relatively higher in the ITZ than in the bulk paste. The porosity consisted of hollow-shell pores as well as pores with irregular form which lacked sharp boundaries. In the SCC, the porosity is significantly lower and consisted mainly of hollow-shell pores less than about 25 µm. The porosity is evenly distributed between ITZ and bulk paste and distinct preferential formation of hollow-shell pores in the ITZ are not observed, although a weak preference formation is observed, especially at the interface of large aggregates. This may indicate an effect of micro bleeding, which may produce a local increase in the W/C ratio at the interfacial zone, which is much less in the SCC [3-5]. The effect of post fire curing on the strength and durability recovery of fire-damaged concrete were investigated [6]. The test results indicated that the post-fire-curing in substantial strength and durability recovery and its extent depend upon the type of concrete, exposure temperature, method, and duration of recurring. In one case, the recovered strength was 93% of the original unfired strength. The strength and durability performance of normal and high strength pozzolanic concretes incorporating silica fume, fly ash and blast furnace slag were compared at elevated temperature up to 800oC [7]. It

was found that pozzolanic concretes containing fly ash and blast furnace slag give the best performance particularly at temperature below 600oC as compared to the pure cement concretes. The effect of moisture loss at high temperature on the brittleness of concrete was investigated[8]. The results show that when concrete is exposed to high temperature, the brittleness is reduced. The fire resistance capacity of concrete is very complicated because not only concrete is a composite material with components having different thermal characteristics, but also it has properties that depend on moisture and porosity [9]. Behavior of self compacting concrete exposed to elevated temperature was studied [10]. Different normal and self compacting concrete mixes were subjected to different elevated temperatures. The results show that increasing the cement content from 350 kg/m3 to 400 kg/m3 with reduction in the percentage of pozzolana when dolomite is used in self compacting concrete has a reverse effect on all mechanical properties when elevated temperature exceed 200oC. Physico-mechanical properties of normal and self compacting concrete loaded columns subjected to fire were studied [11-12]. The results indicated that columns treated by water after exposed to fire showed severe cracks and decreases in strength in comparison with the columns treated with powder. Also, both the porosity and absorption values increased when cooled by water than those cooled by powder. The effect of high temperature on the physico-mechanical characteristics of SCC treated at temperature rang 200-1000oC for a period of two hours was investigated [13]. The results showed that SCC is considered as a good materials for fire resistance because it has 38% residual strength at 1000oC from its original strength.

EXPERIMENTAL WORK

Materials

The mixtures of SCC were prepared with well-graded quartz sand and different coarse aggregate (Basalt, Gravel and Dolomite) as well as OPC and pozzolana such as fly ash or silica fume. Their physical properties are illustrated in Table(1). Table (2) shows the physico-chemical properties of the viscosity enhancing agent as reported by the manufacturer . Table (3) illustrates the chemical composition of the used OPC, fly ash and silica fume. The absolute volume design method recommended by the ACI code [14] was used to determine the constitutes of self-compacting concrete mixes. The materials required to produce one cubic meter from each mix are given in table (4).

Table 1: Physical Properties of Fine and Coarse Aggregate

Type of Aggregate	Gravel	Dolomite	Basalt	Sand
Loose Density,g/cm^3	1.65	1.44	1.45	1.64
Compacted Density, g/cm^3	1.67	1.63	1.58	1.73
Specific Gravity	2.66	2.73	2.85	2.43

Table 2 : Physico -Chemical Properties of Viscosity Enhancing Agent Viscocrete 5-600 ASTM-C-494 Types G And F.

Viscocrete 5-600	Property
Basis	Aqueous solution of modified polycarboxylate
Appearance	Turbid liquid
Density	1.11 g/cm^3
Ph-value	8 $\pm$ 0.5
Dosage	0.3-2% of cement weight

Table 3 : Chemical Composition of OPC, Fly Ash and Silica fume

ELEMENT	OPC (%)	F.A. (%)	S.F. (%)
Silicon (SiO_2)	20.22	54.66	95.0
Aluminum (AL_2O_3)	5.34	32.07	0.20
Iron (Fe_2O_3)	3.20	2.46	0.50
Iron (FeO)	---	1.23	-
Phosphorus (P_2O_5)	3.20	0.27	-
Calcium (CaO)	62.78	4.11	0.20
Potassium (K_2O)	0.25	0.46	-
Sodium (Na_2O)	0.27	1.61	-
Sulphrus (SO_3)	2.38	1.37	-
Loss on Ignition (LOI)	1.03	1.30	0.50

Table 4: The Mix Constituents of the Self-Compacted Concrete Mixes for 1 m^3.

Mix Code	Cement (Kg)	Coarse aggregate (Kg)	Sand (Kg)	W/C	S.F %*	F.A %**	VEA %***
SCC-D	400	1100	900	0.4	12.5	12.5	2.5
SCC-G	400	1100	900	0.4	12.5	12.5	2.5
SCC-B	400	1100	900	0.4	12.5	12.5	2.5

*   Silica Fume replacement from cement by weight   D Dolomite

**   Fly ash replacement from cement by weight   G Gravel

*** Viscosity enhancing agent addition to cement by weight   B Basalt

Mixing

The used coarse aggregates was washed by water to remove any impurities or clay and kept at room temperature one day before mixing. To prepare the SCC mixes, the dry constituents of cement, both coarse and fine aggregates were mixed for 60 seconds. Water containing VEA, S.F. and F.A. were continuously mixed together for a further four minutes then added to the dry mix.

Casting, Curing and Preparing of Concrete Specimens

The fresh SCC, was molded into steel moulds without any internal or external compaction, i.e. under its own weight. Cubes with dimensions 10*10*10 cm were cast for every type of aggregate to be tested after and before subjecting to an electrical furnace for different periods of

times. Cylinders with 7.5*15 cm and with15*30 cm height were cast and tested to get the splitting tensile strength. After molding, the specimens were cured in the laboratory conditions (70% R.H. and 23 ± 2 ^{o}C) for about one day and cured under tap water up to 28 days then dried at a temperature of 105 ± 5 ^{o} C for 48 hours in the dryer furnace. The other specimens were tested to get the mechanical properties of SCC after 28 days.

Fresh Properties
The slump flow test

This test was used to assess the horizontal free flow of SCC mixes in the absence of abstractions as shown in fig. (1). The test used to determine the mean diameter (D) of the concrete sample spread on base plate after performing a slump test without any compaction. The test Judges the capability of concrete to deform under its own weight against the friction on the surface of the base plate without any external restraint present.
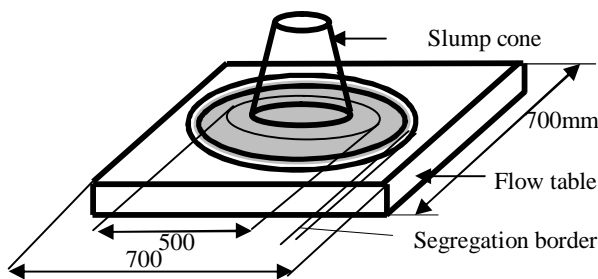
Fig. 1: Slump flow test.

The J-Ring test
This test is used to determine the passing ability and the flow ability of SCC mixes. The test shown in fig. (2), consists of an open steel ring drilled vertically with holes accept threaded sections reinforcement bar. The diameter of the ring of vertical bars is 300 mm and height 100 mm. The ring is generally used in conjunction with the slump flow test or V-funnel test. In the J-ring in conjunction with the slump flow test, the J-ring is centrally placed on the base plate and the slump cone centrally inside it and holds down firmly. The slump cone is filled with concrete as in the slump flow test. The concrete flows through the vertical bars as the cone is lifted. The difference in the height (H1-H2) between the concrete just inside the bars H1 and just outside the bars H2 was measured. Calculate the average of the difference in the height at four locations in mm. Also T50 cm and final spread diameter in two orthogonal directions are measured.
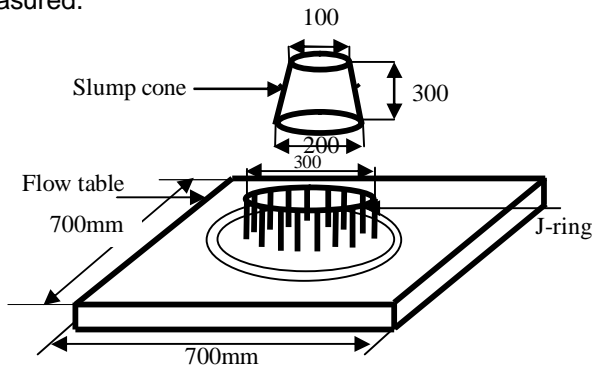
Fig. 2: J-ring Test.

The V-Funnel flow test

This test was used to determine the filling ability (flow ability) of SCC mixes as shown in figure (3). The funnel is completely filled with concrete (about 12 liter) without compaction. After filling the trap door is opened within 10 sec and allow the concrete to flow out under gravity. The trap door is opened and record the time for discharge (the flow time). After the flow time is placed a bucket under its own weight, the apparatus was completely filled with concrete without compacting, open the trap door, after 5 min the second fill of the funnel and allow the concrete to flow out under gravity simultaneously when the trap door is opened and record the time for the discharge (the flow time at T 5 min).
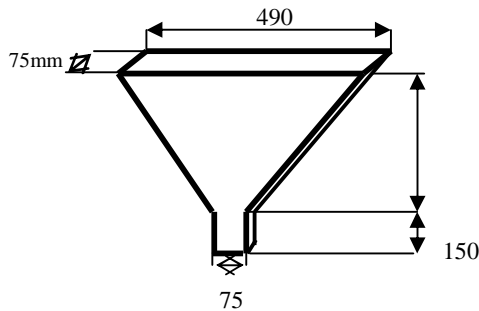
Fig. 3 :V-funnel Test.

Hardened Concrete Properties
Thermo physical tests
Thermo physical properties play a significant rule in the heat and mass transfer in the building materials especially concrete. Density was the most important function governing the transition of heat and mass during the fire period. Also, the porosity and absorption varied with fire growth through the concrete.

Porosity (P) $= ((W_w-W_d) / (W_w-W_s)) \times 100$ (%)   (1)
Absorption (Abs) $= ((W_w-W_d) / (W_d)) \times 100$ (%)   (2)
Density (Row) $= ((W_d) / (W_w-W_s))$ (kg/m^3)   (3)

Where:
   W_d : The dry samples mass,
   W_w : The wet samples mass,
   W_s : The suspended samples mass

Static tests

The compression test was carried out on cubes of (10 x10 x10cm) using hydraulic testing machine of 2000 KN capacity. Indirect tension test was carried out on standard cylinders of dimension 15 cm in diameter and 30 cm in height using also hydraulic testing machine of 2000 KN capacity . Flexure test was carried out on standard beam specimens of dimensions (10 x 10 x 50 cm) using hydraulic testing machine of 100 KN capacity**.**

Exposing the Specimens to High Temperatures

The dried specimens were thermally treated in an electrical furnace at temperature 600°C for one, two and three hours. All heated specimens were left in the furnace to cool down gradually to   room temperature. The influence of high temperature and exposure time on the mineralogical composition and physico-mechanical properties of SCC with different types of coarse aggregate were studied. The specimens after cooling down were tested by a universal

compression testing machine to get the compressive strength after weighing and measuring its dimensions. Then the changes in the mechanical and physical properties of the specimens due to high temperature were examined. The phase composition was investigated by DSC.

RESULTS AND DISCUSSIONS

Properties of Fresh Concrete

Figure (4) shows a comparison between the slump flow time in second for SCC with different types of coarse aggregate. It is clear that SCC-D mix has the lowest value of the flow time which equal to 2 seconds, while the flow time for the SSC-G mix and SCC-B mix were 2.2 and 2.5 seconds respectively. It is clear that the SCC-G mix and SCC-B mix showed an increase in their slump flow time by about 10% and 25% compared to SCC-D mix successively. So, it can be concluded that, SCC containing dolomite as coarse aggregate was the most workable mix for the slump flow time test. This mainly due to that the dolomite absorbs some of mixing water of the concrete therefore the fluability of the SCC-D decreases. The gravel aggregate reduces the mixing water of SCC-G by lower value than dolomite. On the other side, the basalt aggregate contains some alkalis that increases the solubility of some cement constituents therefore, the slump flow time increases.
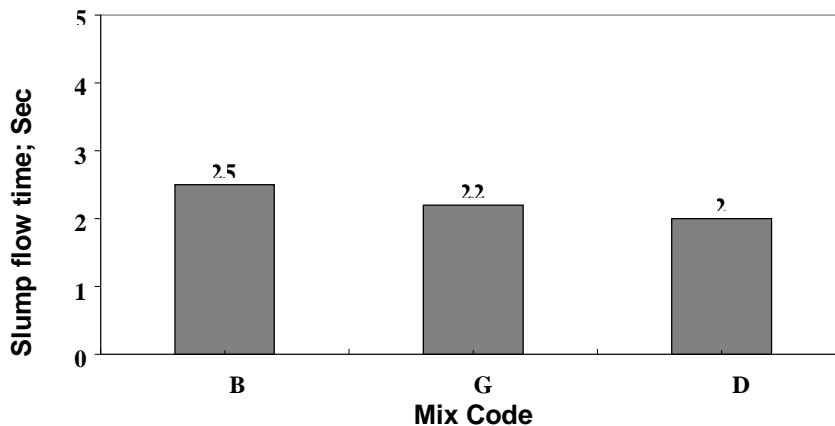
Fig. 4: Slump Flow Time for Concrete with Different Types of Coarse Aggregate

Figure (5) illustrates a relationship between the slump flow diameter in mm and SCC with different types of coarse aggregate. It is clear that the slump flow diameter reached to about 575, 590 and 695 mm for the SCC-B mix, SCC-G mix and SCC-D mix, respectively. So, the SCC-G mix and SCC-D mix increase their slump flow diameter by about 2.60% and 20.86% compared to SCC-B mix. Referring to the slump flow tests, it can be concluded that SCC-D is the most workable one due to the absorption of some of mixing water.
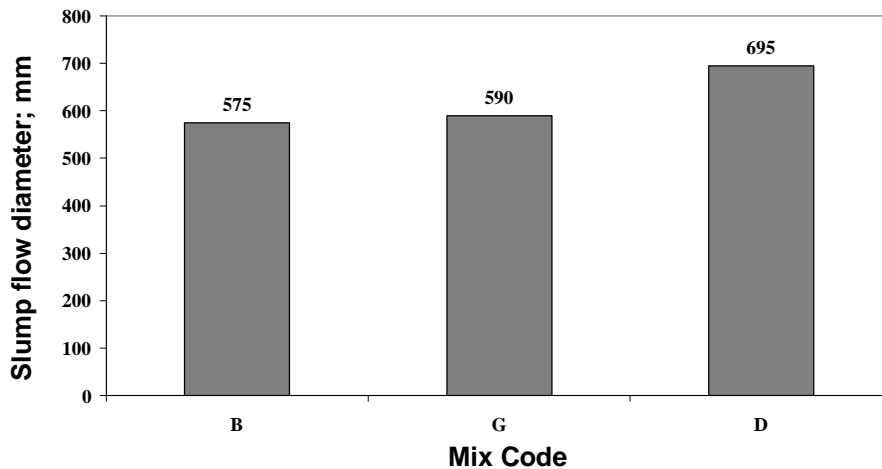
Fig. 5: Slump Flow Diameter for Concrete with Different Types of Coarse Aggregate

Figure (6) shows the relationship between the height difference (H1-H2) in mm of SCC with different types of coarse aggregate. The height difference (H1-H2) reached to about 5, 3 and 2mm for the SCC-B mix, SCC-G mix and SCC-D mix respectively which means that, the SCC-D have the lowest value of (H1-H2) as previously discussed.
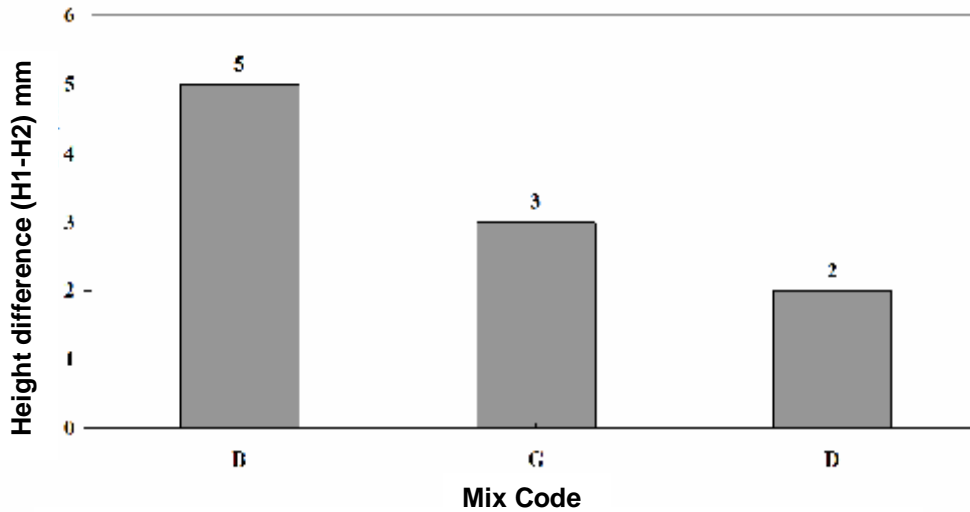
Fig. 6: Height Difference (H1-H2) for Concrete with Different Types of Coarse Aggregate

Figures (7 and 8) show the V-funnel flow time in second and V-funnel flow time T5 in second for SCC with different types of coarse aggregate. It is clear that, the general trend was a decrease in the V-funnel flow time from the SCC-B mix through the SCC-G mix up to the SCC-D mix. These results are in a good agreement with those of slump flow

Finally from the fresh properties of different types of SCC, it can be concluded that, the SCC mixes containing basalt, gravel and dolomite as coarse aggregate have the same trend with difference in magnitude only for the   different fresh properties tests. Also, the SCC-D mix achieves the most workable for the fresh properties of SCC.
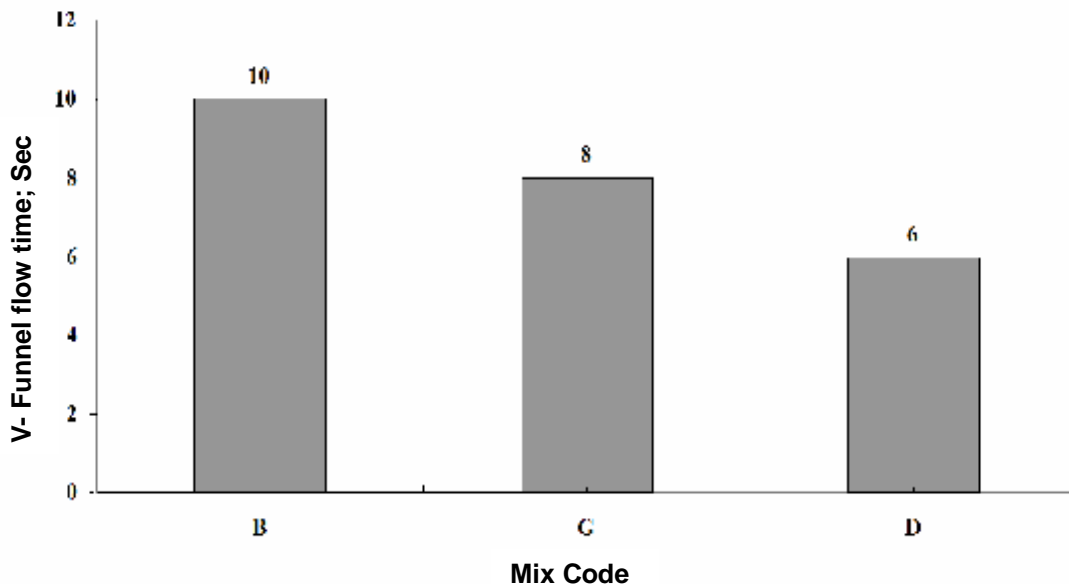
Fig. 7: V- Funnel Flow Time for Concrete with Different Types of Coarse Aggregate
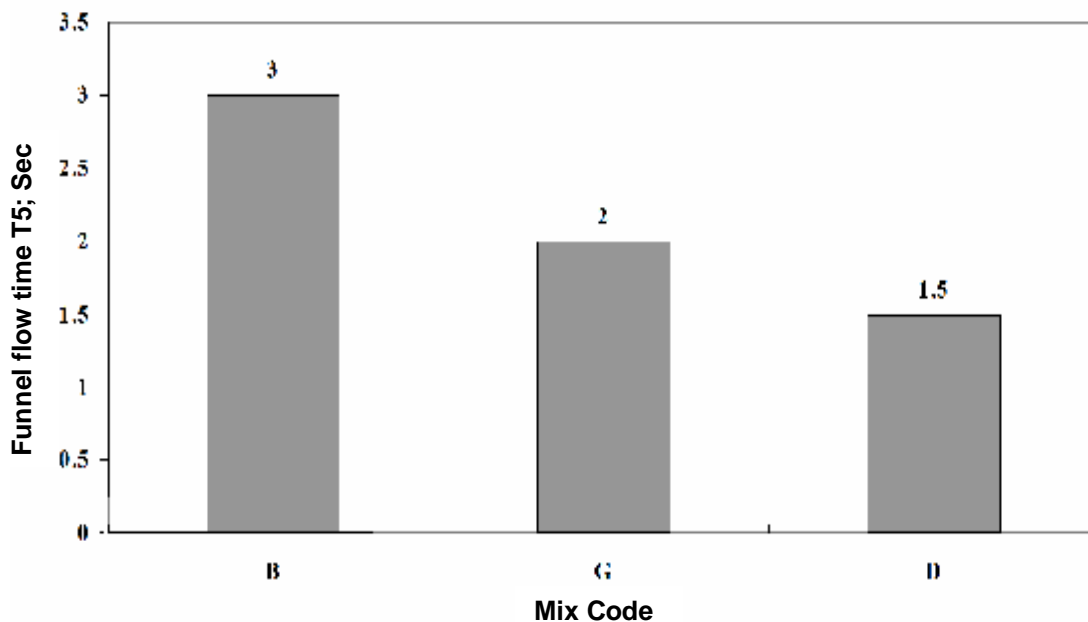
Fig. 8: V- Funnel Flow Time (T5) for Concrete with Different Types of Coarse Aggregate

PROPERTIES OF HARDENED SCC
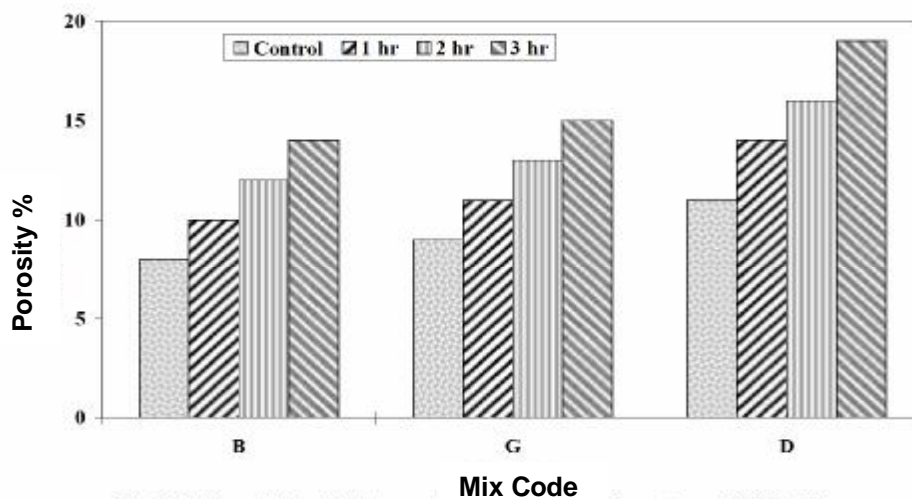
Compressive Strength in High Temperatures

Figure (9) illustrates the relationship between the compressive strength and SCC mixes with different types of coarse aggregate exposed to 600° C for one, two and three hours. It is clear from the figure that, the compressive strength reached 420, 400 and 350 Kg/cm^2 for SCC-D, SCC-B and SCC-G samples at room temperature after 28 days. The SSC-D gives the higher values of compressive strength than those of SCC-B and SCC-G. This is also due to the decrease of the actual mixing water from the absorption of some amount of water therefore the W/C decreases. As the W/C decreases the total porosity decreases and then the mechanical properties increase or the compressive strength increases. SCC-B shows also higher values than the SCC-G due to that the basalt has some pozzolanic reactivity that increases the hydration products. Therefore, the total porosity decreases and then the compressive strength increases. So, the compressive strength of sample SCC-D and SCC-B increased by 20 and 14.28% than sample SCC-G at room temperature. The compressive strength decreased by 25%, 40% and 52.5 for sample B after exposed to 600°C for one, two and three hours, respectively. Also, the compressive strength decreased by 50%, 64.28% and 71.42% for sample SCC-G while by 34.52%, 40.47% and 52.38% for sample SCC-D after exposure to 600°C for one, two and three hours, respectively. This means that, sample SC-G lost 50% of its original compressive strength value after one hour of exposure at 600°C while sample SCC-D and B lost 35% and 25% of their compressive strength values, respectively. This means that the SCC-B is the most suitable concrete exposed to higher temperature. This is due to the pozzolanic reaction of basalt with Ca(OH)$_2$ librated in the hydration of Portland cement. The Ca(OH)$_2$ dissociates at lower temperature than 500oC to CaO which has no binding properties. Therefore, it can be concluded the pozzolanic cement is the most suitable type for SCC subjected to higher temperature.
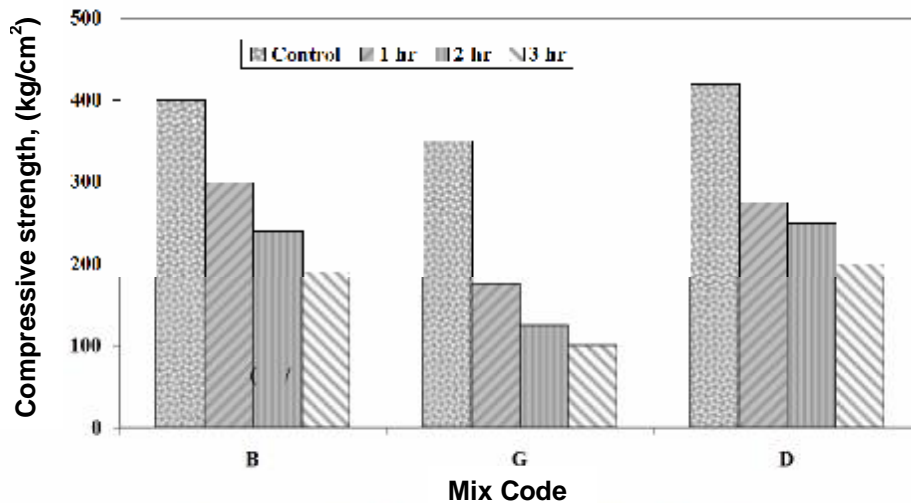
Fig. 9: The Relationship between the Compressive Strength and different Types of SCC with Different Coarse Aggregate and Exposure Time

PHYSICAL PROPERTIES

Figure (10) shows the relationship between the porosity and SCC mixes with different types of coarse aggregate exposed to 600°C for one, two and three hours. The total porosity increases with the time of exposure due to the increase of the dissociated material. The porosity of SCC-B sample increased by 25%, 50% and 75% than its control sample at 600°C for one, two and three hours, respectively. The porosity of SCC-G mix increased by 22.22%, 44.44% and 66.66% than its control sample while SCC-D mix increased by 27.27%, 45.45% and 72.72% at 600°C for one, two and three hours, respectively. It is clear that, the porosity of SCC-G and SCC-D mixes increased by 7.14% and 35.71% than SCC-B mix after exposure time three hours at 600°C, respectively. The SCC-B shows the lowest values of total porosity and the SCC-D shows the higher value. The basalt has also some pozzolanic properties which increase the hydration products and decreas the porosity. On the other side, dolomite-concrete gives the higher values due to the decomposstion of the dolomite aggregate to CaO and MgO. Therefore the porosity increases than the other two types. The SCC-G shows the medium behaviour due to the inrt properties of the gravel.

Fig. 10: The Relationship between the Porosity and different Types of SCC with Different Coarse Aggregate and Time Exposure

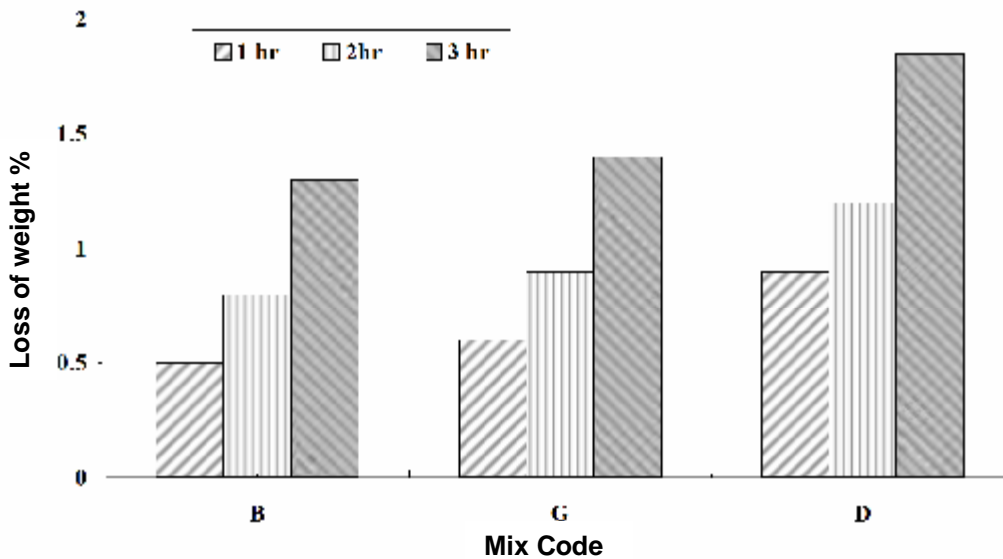Figure (11) illustrates the relationship between the loss of weight for the SCC mixes with different types of coarse aggregate exposed to 600°C for one, two and three hours. The loss of weight increases with   time of exposure for different SCC mixes. The loss of weight reached 0.5, 0.8 and 1.3 % after exposure to 600°C for one, two and three hours, respectively for SCC-B mix. The loss of weight reached 0.6, 0.9 and 1.4% for SCC-G mix while reached 0.9, 1.2 and 1.85% for SCC-D mix after exposure to 600°C for one, two and three hours, respectively. Also, it is noticed that, the loss of weight equal to 1.5 and 2.0 time after 2 and 3 hours compared to one hour of exposure, successively. The weight loss of SCC-B is lower than SCC-G and than SCC-D. This is also due to the dissociation of some of dolomite aggregate which increase the loss on weight. The gravel aggregate is an inert material therefore it shows low loss than dolomite. But, basalt has also a pozzolanic reaction which increases the hydration products and decreases the Ca(OH)$_2$ therefore, the loss on weigh decreases and shows the lowest values.

Fig. 11: The Relationship between the Loss of Weight and SCC with Different Type of Coarse Aggregate and Exposure Time

Phase Composition

Figure (12) shows the DSC thermograms of SCC mixes with different types of coarse aggregate exposed to 600° C for one, two and three hours. The thermograms of SCC mixes at room temperature (SCC-B0, SCC-D0 and SCC-G0) and SCC exposed to 600° C for one, two and three hours (SCC-G1, SCC-G2 and SCC-G3)   illustrate three main endothermic peaks around 100-200, 400-500 and 600°C respectively. The first two peaks in the range 100-200°C are due to the decomposition of the hydration products such as CSH and calcium sulphoaluminate or calcium aluminates hydrates. It is clear that the SCC-B shows higher hydration products due to the pozzolanic reaction of basalt with Ca(OH)$_2$ giving CSH or CAH. The peak area at 450°C is the lowest in the case of SCC-B and decreases in SCC-D and then SCC-G. Also, the decrease of the peak area in SCC-B is also due to the pozzolanic reaction. Dolomite has the intermediate behavior, whereas the gravel has the higher values due to its inert character. The peak located around 450°C represents to the decomposition of calcium hydroxide (CH). The peak located around 580°C is due to the conversion of quartz in SCC-B and SCC-G. But on the other side, this peak is mainly due to the dissociation of dolomite aggregate and not due to quartz convesion. The figure demonstrated that the enthalpy of

Ca(OH)$_2$ phase reached to 2.72, 4.26 and 8.51J/g for the first peak in the mixes SCC-B0, SCC-D0 and SCC-G0 respectively. While reached to 0.556, 0.781 and 1.91 for the second peak. Also, the figure demonstrated that the enthalpy of Ca(OH)$_2$ phase reached to 0.458, 4.09 and 4.16J/g for the first peak in the mixes SCC-G1, SCC-G2 and SCC-G3 respectively. While reached to 1.63, 1.27 and 0.948 for the second peak. So, it is clear that the different type of coarse aggregate and also, high temperature have great effect on the performance of SSC mixes exposed to 600° C for one, two and three hours.
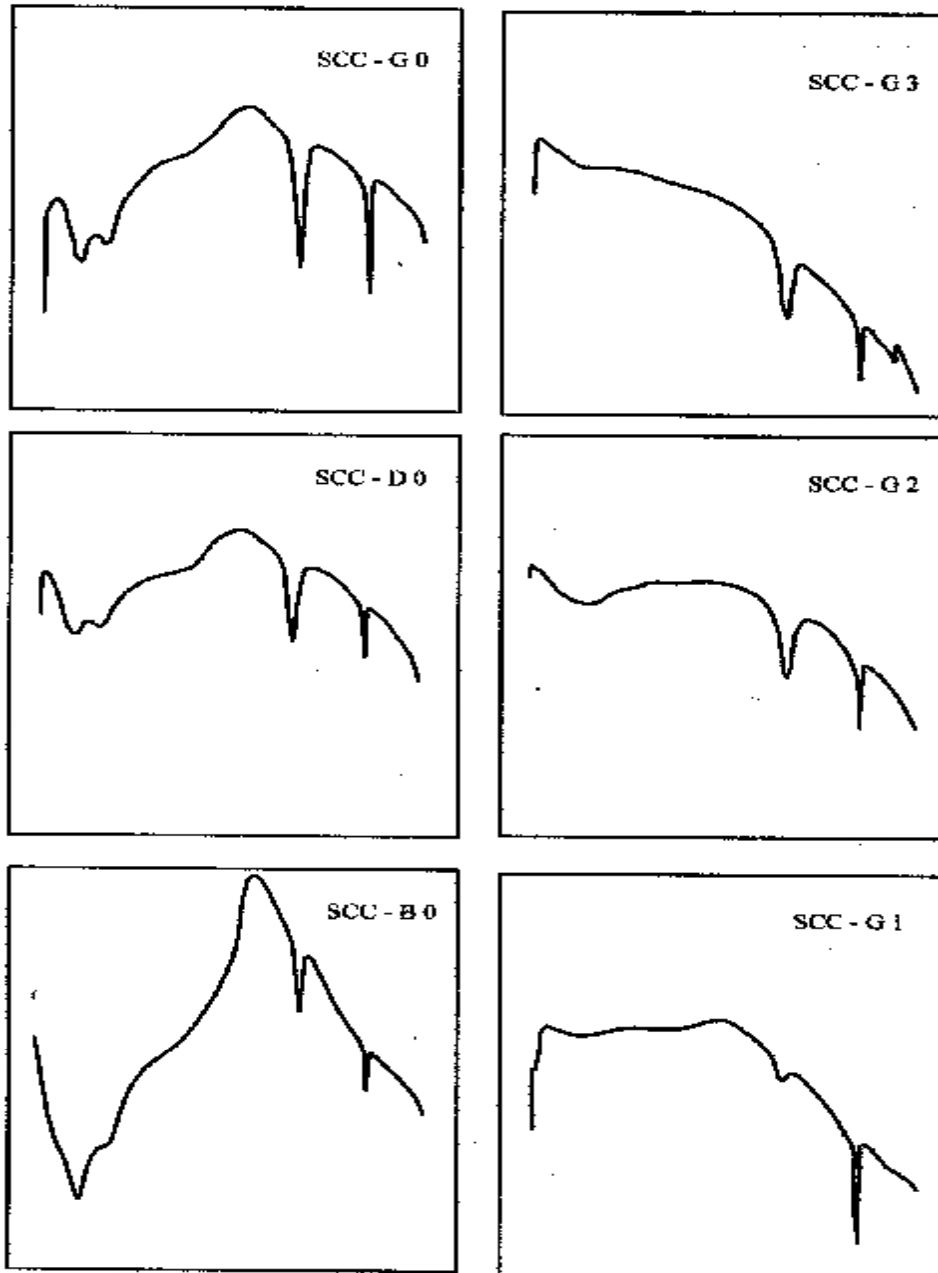

Fig. 12: The DSC Thermo grams of SCC Mixes with Different Types of Coarse Aggregate Exposed to 600° C for One, Two and Three Hours

CONCLUSIONS

The main conclusions derived from this study can be summarized as follows:
1. Self compacted concrete containing dolomite aggregate showed the highest workability comparing to the other mixes.
2. The highest compressive strength was recorded for the SCC-D mix followed by SCC-B and SCC-G respectively.
3. For the different mixes subjected to 600^oC for one, two and three hours SCC-B has the low reduction value followed by SCC-D and SCC-G, successively.
4. The porosity of the different SCC mixes changed according to the aggregate type as it was recorded for the porosity of SCC-D mix which had the maximum value followed by SCC-G mix and SCC-B mix mutually.
5. The porosity increased with the exposure time at 600^oC from one to three hours and the SCC-D had the maximum values compared to the other mixes.
6. The loss of weight of all SCC mixes increased by time of exposure where the SCC-D mix had the maximum value.

The microstructure of the SCC mixes was related as much as possible to the   physico-mechanical characteristics of SCC mixes containing   different types of coarse aggregate and exposed to 600^oC for one, two and three hours.

REFERENCES

1. Z.P. Bazant, M.F. Kaplan, "Concrete at high temperatures", Longman Group, UK, pp.1-20, 1996.
2. M. H. Seleem, A.A. M. Badawy and H.A.Shehab Eldin," Effect of Sand Aggregate Ratio and Type of Coarse Aggregate on The Properties of Self Compacted Concrete", ERJ, Vol.29, No.1, January2006, pp 105-112, 2006.
3. Jolicoeur, C. and Simard, M.A., "Chemical Admixture-Cement Interactions: Phenomenology and Physico-Chemical Concepts", Cement and Concrete Composites 20 , PP. 87-101, 1998.
4. Okamura, H., Ozawa, K., Matsuo, S. and Shimokawd, K.," Evaluation of Superplasticizer for Self-Compacting Concrete Using Mortar Tests", JCA Proceedings of Cement and Concrete, 48, PP 374-379, 1994.
5. Jan Tragardh, " Micro structural Features and Related Properties of Self-Compacting Concrete", Proceedings of the 1st international RILEM Symposium on Self-Compacting Concrete, Ed. Skarendahl and Petersson, Stockholm, Sweden, pp. 175, 1999.
6. Chi-Sun Poon, Salman Azhar, Mike Anson and Yuk-Lung Wong," Strength and durability recovery of fire-damaged concrete after post-fire-curing", Cement and concrete research 31, 1307-1318, 2001
7. Chi-Sun Poon, Salman Azhar, Mike Anson and Yuk-Lung Wong ," Comparison of the strength and durability performance of normal-and high- strength pozzolanic concretes at elevated temperatures", Cement and concrete research 31, 1291-1300, 2001.
8. Binsheng Zhang, Nenad Bicanic, Christopher J. Pearce and David V. Phillips," Relationship between brittleness and moisture loss of concrete exposed to high temperatures", Cement and concrete research 32, 363-371, 2002.
9. S.P. Shah, S.H. Ahmad, " High performance concrete: properties and application, McGraw Hill, 1994
10. M. F. Ali," Behavior of self compacting concrete exposed to elevated temperature and chemical attack", MSC thesis, Faculty of engineering, Cairo university, 2006.
11. M. A. Helal," Physico-Mechanical Properties of Normal and Self-Compacting Concrete Loaded Columns Subjected To Fire", Ain Shams University Journal, Vol. 40, No.4, December,2005
12. KH. M. Heiza and M. A. Helal," Fire Performance of Both Normal and Self-Compacted Reinforced Concrete Loaded Columns", 11th International Colloquium on Structural and Geotechnical Engineering, (ICSGE), Ain Shams University 17-19 May 2005
13. M. A. Helal, KH. M. Heiza and H. Allam " New Building Technology: Properties of Self Compacting Concrete (SCC) with High Temperature" World Renewable Energy Congress VIII (WREC2004), Denver, Colorado, USA, August29-Sep.3, 2004
14. ACI Committee 318," Building Code Requirements for Structural Concrete" (ACI 318-02) and Commentary (318R-02). American Concrete Institute, Farmington Hills, Mich., 369, 2002.

BEHAVIOUR OF SANDWICH FRP WRAPPED RC COLUMNS UNDER ECCENTRIC LOADING

Tarek M. Bahaa
Assistant Professor, Housing and Building National Research Center, Cairo, Egypt
Emails: tarekmbaha@yahoo.com
Hossam Z. El-Karmoty
Assistant Professor, Housing and Building National Research Center, Cairo, Egypt
Emails: hoskarmoty@yahoo.com

ABSTRACT

Fiber reinforced polymer (FRP) composite has proven its efficiency for strengthening reinforced concrete (RC) structure. Recently, the introduction of the sandwich FRP wrapping as a promising technique for strengthening RC columns opened a new field for researches.

This paper investigates the behavior of RC square short columns subjected to eccentric compression loading and strengthened using sandwich and regular FRP wraps. The experimental program comprised testing of seven column specimens. Six columns were strengthened with different FRP schemes while one column was kept unstrengthened. Key parameters included the method of wrapping (sandwich & regular), the type of FRP material (carbon & glass) and the percentage of sandwich wrapping (full & partial).

The results demonstrated that the utilization of sandwich FRP wraps results in load and ductility enhancements higher than those of the regular wraps. The carbon FRP wrapped columns performed better than the glass FRP wrapped columns in terms of strength and ductility. Also, it is recommended to use the full sandwich FRP wrapping, if an enhancement in the load carrying capacity is required.

Keywords: FRP, Wrapping, Sandwich, RC columns, Eccentric loading.

INTRODUCTION

Large numbers of columns in existing reinforced concrete (RC) structures have a serious need to be strengthened due to various reasons related to durability and the design criteria of old structures. Such reasons include mistakes in design or construction, exposure to unpredicted loads or changing the usage of the structures. The fiber reinforced polymers (FRP) was proved to be an effective technique for strengthening RC columns. There have been several studies that investigated the strengthening of axially loaded RC columns using FRP wraps. Despite the fact that eccentric loading are common for columns in practice, a limited number of researches were conducted on FRP wrapped columns subjected to eccentric loading.

Hassan, W. H., [1] investigated the behavior of normal and high strength concrete square short columns subjected to eccentric loading and strengthened with externally applied uni-directional and bi-directional CFRP and GFRP materials. The results of this investigation showed the potential influence of FRP wrapping regarding axial load carrying capacity, flexural capacity, and the overall ductility of tested specimens. The results indicated that the most effective wrapping method in small eccentrically loaded columns was full wrapping with double layers of GFRP laminates which improved the axial load carrying capacity by about 27%. However, wrapping the same specimens with one layer of GFRP stripped laminates gave a slightly lower

enhancement of 24%. Thus, from economic point of view, the study recommended using one layer of stripped GFRP or CFRP laminates as a strengthening technique for biaxially loaded HSC and NSC short square columns.

Li and Hadi [2] conducted a research on the behavior of externally confined high strength concrete columns under eccentric loading. They found that the enhancement of the strength of the plain concrete column specimens under eccentric loading is not so pronounced as for the concrete specimens under concentric loading, especially for the high strength concrete specimens. Hadi [3,4, 5] investigated the behavior of FRP wrapped normal and high strength concrete columns under eccentric loading. The results of these investigations confirmed the latter conclusion that the enhancement of the strength of the plain column specimens under eccentric loading is not so pronounced as for the columns under concentric loading. However, considerable gain in strength and ductility was obtained when reinforcing the columns with vertical CFRP straps and horizontally wrapped.

Mahfouz et al. [6] introduced a new technique for improving the wrapping efficiency through using sandwich wrapping that enhances the stiffness of the FRP wraps. Sandwich wrapping consisted of wrapping the column with two layers of FRP, inner and outer, separated by incompressible material as filling material. The results of this research demonstrated that the sandwich wrapping is a promising technique for strengthening RC columns. Mahmoud et al. [7] investigated the behavior of axially loaded square RC columns strengthened with externally applied carbon fiber reinforced polymer (CFRP) and glass fiber reinforced polymer (GFRP) sandwich wraps. The results of this investigation showed that the use of sandwich wrapping enhanced the ultimate load capacity of the tested columns. Sandwich wrapped columns displayed higher ductility than columns wrapped with regular strengthening method.

The main objective of this research is to investigate the effectiveness of using sandwich wrapping, compared to regular wrapping, for strengthening square RC columns subjected to eccentric compression loading. The main parameters of the study were: method of wrapping, type of FRP material and percentage of FRP wrapping.

RESEARCH PROGRAM

Materials Properties

The concrete mix was made from natural siliceous sand, dolomite from Suez area quarry, ordinary Portland cement (OPC), tap drinking water, and chemical admixture. Testing of these materials was carried out according to the Egyptian standard specifications. The Dolomite had a nominal maximum size of 10 mm. The cement used in this investigation was "Egyptian ordinary Portland cement" which is locally manufactured and complies with the Egyptian standard specifications. Super-plasticizer admixture complies with ASTM C494 Type F was used to achieve a slump of 100 mm. The design cubic compressive strength of the concrete was 30 MPa after 28 days. The proportions of the concrete mix was: 1 (Portland cement): 3.46 (coarse aggregate): 1.73 (fine aggregate): 0.55 (water) by weight. The cement content was 375 Kg/m^3.

Deformed high tensile steel bars of 16 and 18 mm diameter, yield strength of 420 MPa and ultimate strength of 630 MPa were used as main reinforcement for all columns. Mild steel smooth rebar of 8-mm diameter, yield strength of 280 MPa and ultimate strength 410 MPa was used for stirrups.

Carbon fiber reinforced polymers (CFRP) and glass fiber reinforced polymers (GFRP) were used in this study. The stress-strain relationships of CFRP and GFRP laminates are linearly elastic up to failure as reported by the manufacturing company. The used CFRP laminates were manufactured by Sika company and known as SIKA WRAP HEX 230 C. The roll package of laminates had 304.8 mm width, 0.13mm thickness and 45700 mm length. The tensile strength and modulus of elasticity of the laminates are 3500 MPa and 230 GPa, respectively as reported by the manufacturing company. The used GFRP laminates were manufactured by Sika Company and namely as SIKA

WRAP HEX 430 G (VP). The roll package of laminates had 304.8 mm width, 0.17 mm thickness and 50000 mm length. The tensile strength and modulus of elasticity of the laminates are 2250 MPa and 70 GPa, respectively as reported by the manufacturing company. The epoxy paste, which was applied on the column surface, was Sikadure-41. The tensile strength of the epoxy paste equals to 15MPa. Epoxy resin namely Sikadure-330 was used to bond the FRP laminates to the concrete. The flexure modulus, tensile strength and adhesive strength on concrete of the epoxy resin are 3800, 30 and 4 MPa, respectively as reported by the manufacturer.

Local fabricated smooth acrylic plates with thickness 10 mm were used in sandwich wrapping between the FRP inner and outer layers as strips and plates. The acrylic plates are characterized by their good mechanical properties, light weight and reasonable price. The tensile strength, compressive strength and modulus of elasticity of the acrylic plates are 70 MPa, 110 MPa and 3050 MPa, respectively as reported by the manufacturer.
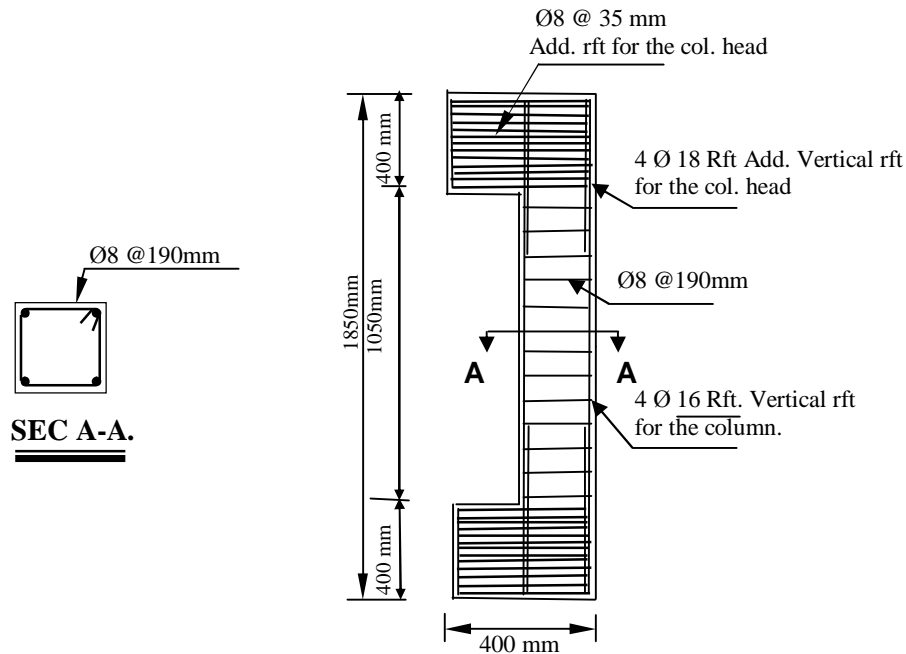
Test Specimens

Seven RC column specimens were tested under the effect of eccentric compression loading. Six columns were strengthened with different FRP schemes while one column was kept unstrengthened as control specimen. All specimens have identical concrete dimensions. The column had a square cross section of 200x200 mm, 1050 mm clear height and 1850 mm overall height including corbel heads. The dimensions of the top and bottom corbels were 200x400x400 mm. Those corbel heads were introduced to prevent premature failure at the end regions of the columns. Figure 1 shows the typical concrete dimensions of the specimens.
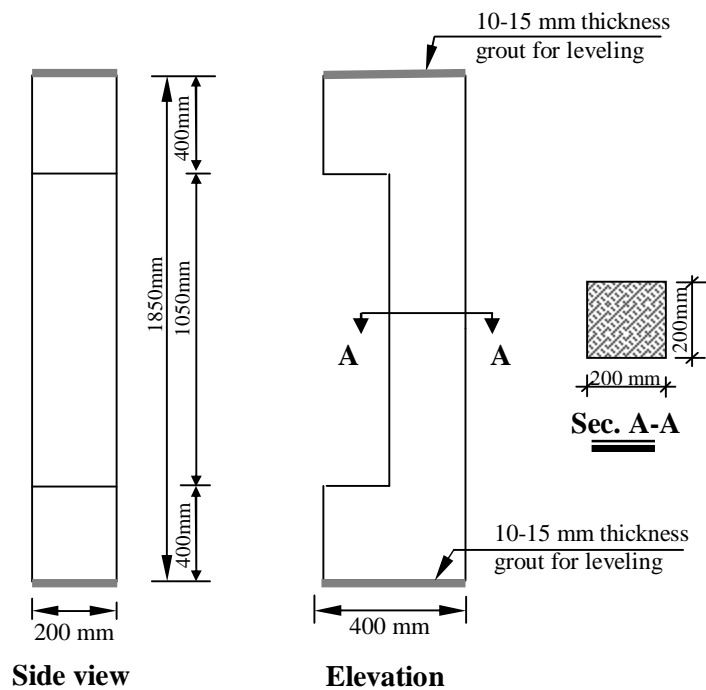
Fig. 1: Concrete Dimensions of the Specimens

The longitudinal steel of the column consisted of four rebars of 16 mm diameter arranged symmetrically in the cross section. Figure 2 shows typical reinforcement details of the test specimens. Steel reinforcement percentage was 2% which is a typical practical value for eccentrically loaded columns. The transverse reinforcement comprised 8 mm diameter peripheral hoops. The hoops were spaced at 190 mm with a volumetric ratio of 0.424%. The hoops had 135-bends extending 60 mm into the concrete core. The core size measured from the center of the peripheral hoop was kept constant at 160x160 mm. To avoid the premature failure at the column ends, the corbels were additionally reinforced with 18 mm diameter deformed rebars. Moreover, transverse ties of 8 mm diameter were concentrated at 35 mm spacing to sustain splitting forces at the loading zones.

Fig. 2: Reinforcement Details of the Test Specimens

The experimental program was designed to investigate the effectiveness of using sandwich wrapping, compared to regular wrapping, for strengthening square RC columns subjected to eccentric compression loading. The investigated variables were the method of wrapping (sandwich or regular), the percentage of sandwich FRP laminates wrapping (full or partial wrapping) and the type of FRP material (carbon or glass). Table 1 presents the FRP strengthening schemes.

Table 1: FRP Strengthening Schemes

Column	FRP sheet type	Wrapping method	Percentage of wrapping
C1	-	-	-
C2	Carbon	Regular	Full length
C3	Carbon	Sandwich	Full length
C4	Glass	Regular	Full length
C5	Glass	Sandwich	Full length
C6	Carbon	Sandwich	Partial wrapping (100 mm Strip@ 100 mm)
C7	Carbon	Combined Regular+Sandwich	Full length* (100mm sandwich Strip@100 mm + 100mm regular Strip@100 mm)

Fabrication of Test Specimens

The specimens were fabricated in the material laboratory of Housing and Building National Research Center in two stages. The first stage was the fabrication of seven reinforced concrete columns and the second stage was the application of FRP strengthening scheme for six of those columns.
Two wood forms were used for casting the specimens. Mixing was performed using a concrete drum mixer. Concrete was cast and compacted using an electrical vibrator for two minutes. The sides of the form were removed after 24 hours. Curing of the specimens lasted for 14 days after casting. The cubic concrete compressive strength of the specimens at the time of testing ranged from 34.4 MPa to 36.9 MPa.

The FRP laminates were applied after the concrete had reached an age of 28 days. Figure 3 shows the steps of application of sandwich FRP strips.   The strengthening procedure was conducted as per the instructions of the manufacturing company of the FRP laminates as follows:

- Preparation of the concrete surface by grinding, and the loose particles were removed using air blower. The sharp edges of the column corners were rounded.
- Application of the epoxy paste (Sikadure-41) on the column surface to fill the irregularities on the concrete surface and rounding the corners of the columns to a radius of 16mm.
- Smoothing the surface of the epoxy past after 24 hour.
- Application of the mixed resin (Sikadur-330) to the prepared substrate using a trowel in a quantity of approximately 0.7 to 1.2 Kg/m^2 depending on roughness of the substrate.
- Attaching the first FRP laminates to the column faces. Rolling the FRP laminate by special laminating-roller to ensure that FRP laminate are saturated in the epoxy, and there is no air voids between the FRP laminate and the concrete surface.
- For regular wrapping, the second layer of the FRP laminate was applied within 30 minutes.
- For the sandwich wrapping, acrylic plates were fix on the first FRP laminates within 30 minutes. Before that the surface of the acrylic plates was roughened on both sides in order to increase the adhesion between the plates and laminates. Also, a special clamp was used to fix the plates in their position till the epoxy hardened.
- Filling and rounding the corners between the plates using the epoxy paste (Sikadure-41) to a radius of 26 mm. Then, Smoothing the surface of the epoxy past after 24 hour.
- Applying the second impregnation resin layer (Sikadur-330) .
- Attaching the second layer of the FRP laminates to the acrylic plates and rolling it.
- The strengthened columns were left in the lab ambient temperature till the time of testing.
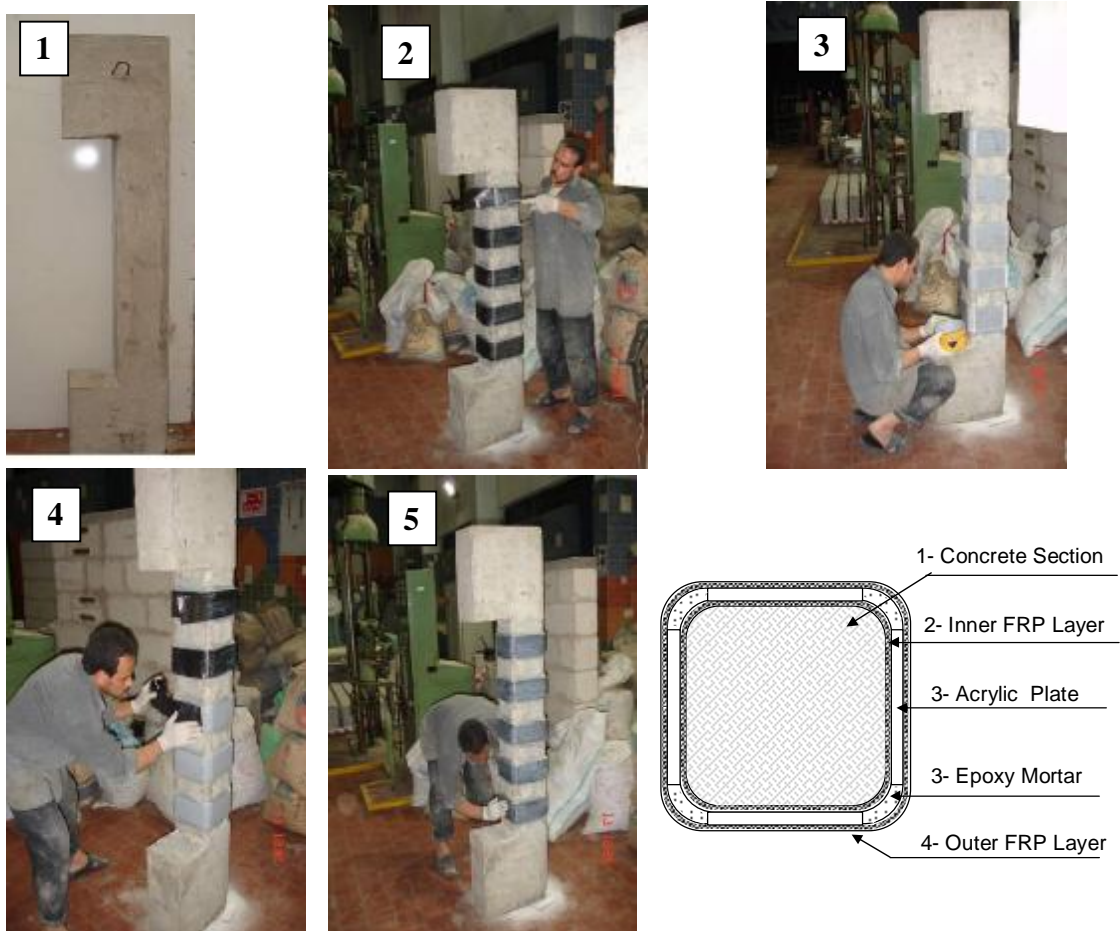

Fig. 3: Application of Sandwich FRP Strips

1- Concrete Section
2- Inner FRP Layer
3- Acrylic Plate
3- Epoxy Mortar
4- Outer FRP Layer

Test Setup and Instrumentation

The specimens were tested up to failure using an AMSLER compression testing machine of 5000 kN capacity. The testing machine consists of lower moving piston which moves on a spherical head covered by a rigid steel plate so that the applied load is always passing through the center of the sphere, and perpendicular to the column's cross section. On the other hand, the upper plate is moving around a fixed sphere. The load eccentricity was achieved using bearing plates of 150 x 150 mm dimensions. The specimen was placed on a lower bearing plate and the load was applied through an upper one. The bearing plates were provided with a spherical part to allow for specimen rotation, i.e. pin-ended specimen. The load eccentricity was maintained at 25 mm throughout the test. This value is considered small eccentricity with respect to the cross sectional dimensions of the tested column. Figure 4 shows test setup and instrumentation of the specimens.
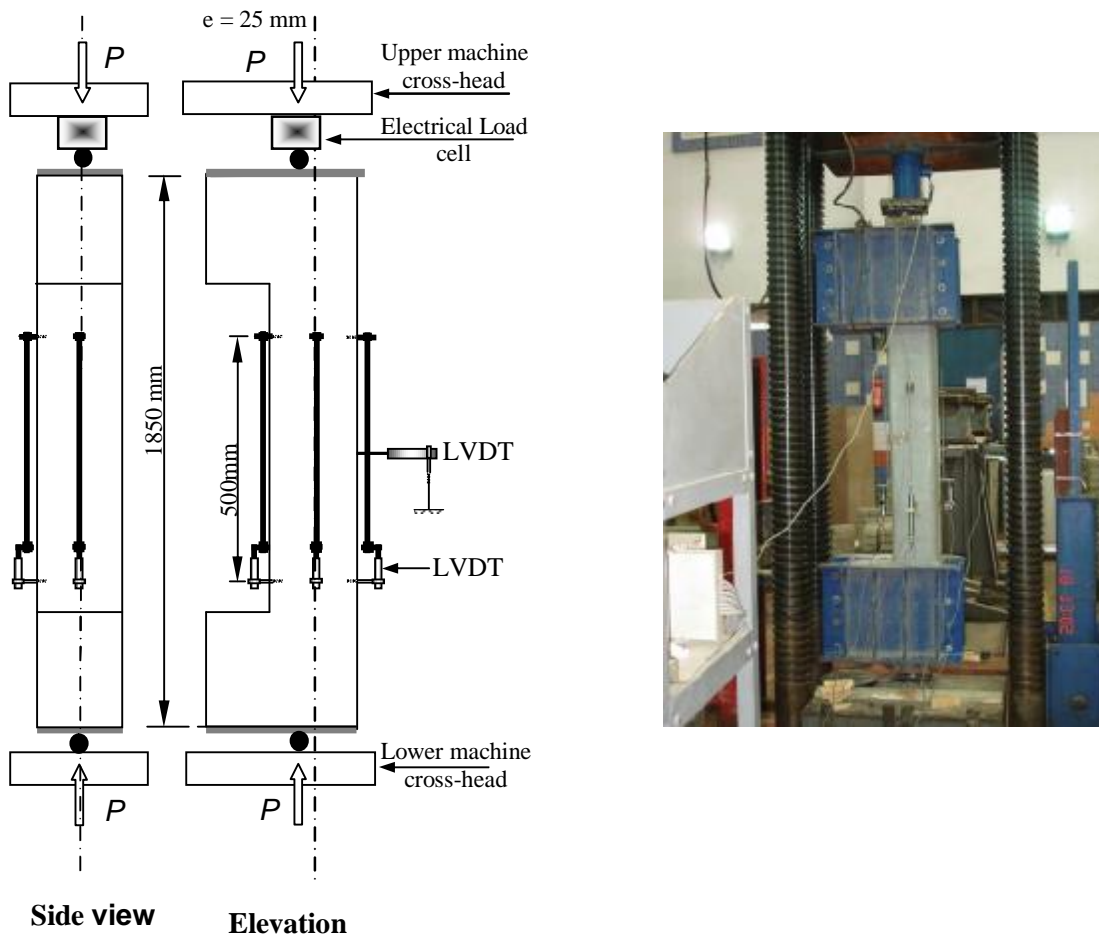
Fig. 4: Test Setup and Instrumentation

A 2000 kN electrical load cell was used to measure the applied load. Axial deformations of the column were measured using linear variable displacement transducers, (LVDTs) over a length of 500 mm. Three LVDT,s were attached to three sides of RC columns as shown in Figure 4. An additional LVDT was positioned to record the lateral horizontal displacement of the column at its mid height. The specimens were instrumented to record strains of steel reinforcement bars as well as strain of FRP laminates. These strains were measured by electrical strain gages. The gages had the following characteristics: gage length 10 mm, gage resistance 119.8 ± 0.2 Ohms, gage factor 2.11 ± 1 %, adaptable thermal expansion 11.7 PPM/Co. and transverse sensitivity

0.2 %. The strain gages were covered by a waterproof coating to protect them from water and damage during casting concrete.

All measurements were read and transformed as micro-strains, forces, and displacements by means of a data acquisition system and stored in a computer. The rate of recording the data was one scan per second.

TEST RESULTS

The cracking behavior and mode of failure of the columns were observed and recorded throughout the test. Major test results are summarized in Table 2. This includes the ultimate load resisted by each column, the associated axial strain at the most compression stressed side, the Mid-height lateral deflection and the toughness. Also, the enhancement in the capacity and ductility of the columns are given.

Table 2: Test Results

| Column	Ultimate load, P_{ci} (KN)	Enhancement in Capacity P_{ci} / P_{c1}	Axial strain at ultimate load	Toughness, T_{ci} (KN.mm/mm)	Enhancement in Ductility $(T_{ci} - T_{c1}) / T_{c1}$ (%)	Mid-height lateral deflection (mm)
C1	883	1	-0.00335	5.3	-	5.087
C2	1007	1.14	-0.00562	17.65	232	7.704
C3	1092	1.24	-0.01199	22.3	320	12.524
C4	958	1.09	-0.00494	16.9	219	6.987
C5	1022	1.16	-0.00728	19.8	274	11.932
C6	901	1.02	-0.00507	13.9	162	8.098
C7	993	1.12	-0.00575	14.7	177	8.205

Modes of Failure

Five mechanisms of failure were observed and recorded during the experimental work. Figure 5 shows the appearance of the column specimens after the conclusion of the test. The unstrengthened column C1 showed the typical cracking behavior of a reinforced concrete column subjected to small eccentric compression. Cracks appeared in the tension face and the concrete cover spalled off in the compression face. At a later stage, the spalling of the cover extended to the side faces. At ultimate load the concrete crushed suddenly causing a significant drop of the load. The longitudinal reinforcing bars experienced inelastic buckling between hoops. The failure of the strengthened columns followed different mechanisms based on the strengthening method.

The failure mode of columns C2 and C4 strengthened using regular full length FRP wrapping started with horizontal cracks of the FRP laminates in the tension side. A fracture sound of the concrete in the compression side was observed. The existence of the FRP wrapping prevented tracking the cracks in concrete cover. Finally, the failure was due to sudden rupture of FRP sheets followed by crushing of concrete. Also, the longitudinal reinforcing bars buckled between hoops in the zone where FRP ruptured. This mode was compression failure; however, it is less brittle than the failure of column C1.

The sandwich FRP wrapped columns C3 and C5 showed horizontal cracks in the FRP laminates. At ultimate load, rupture of FRP wraps took place. The acrylic plates experienced horizontal cracks in the tension side and crushing in the compression side and the FRP laminate rupture. Finally, crushing of concrete in compression and buckling of longitudinal bars occurred.

Column C6 strengthened with sandwich strips experienced cover spalling off in the unconfined areas of the column between the strips. At later stages of loading the unconfined areas at mid height of the column showed crushing of concrete. This was followed by rupture of the sandwich FRP strips at the corner and the acrylic plate was separated from the laminate.

The failure mechanism of column C7 strengthened with combined regular and sandwich wrapping was different from that of column C6. First, the rupture of the regular FRP strip took place. This was followed by the rupture of sandwich FRP strip. The longitudinal reinforcing bars buckled between hoops in the region where the FRP ruptured and the concrete crushed in the compression side.
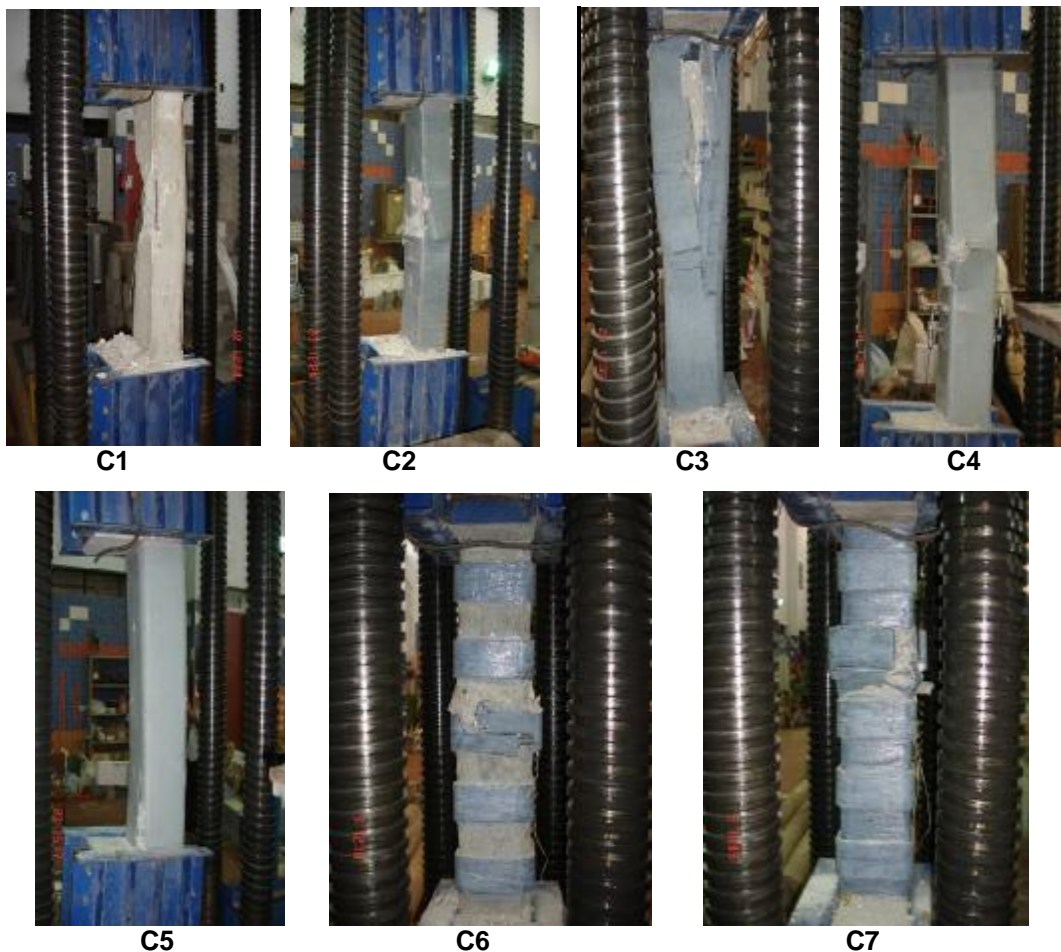
Fig. 5: Appearance of the Columns after the Conclusion of the Test

Mid-Height Lateral Deflection

Table 2 gives the mid-height lateral deflection for all columns at ultimate load level. Generally, the strengthened columns sustained higher deflection than the unstrengthened control column. The latter recorded a deflection of 5.087 mm. Columns C2 and C4 strengthened with full regular FRP wraps displayed higher lateral deflections of 7.704 mm and 6.978 mm, respectively. Columns C3 and C5 with full sandwich FRP wraps displayed deflections of 12.524 and 11.932 which is 146% and 135% higher than that of the unstrengthened column C1, respectively. It is obvious that strengthening with full sandwich FRP wrapping significantly increases the deformation capacity of the columns.

The column strengthened with sandwich FRP strips, C6, and that strengthened with combined regular and sandwich wrapping, C7, experienced close deflection values. These values were 59% and 61% higher than that of the control column, respectively.

Strains in FRP Laminates

Figure 6 shows the load-FRP strain relationships for the strengthened columns C2 through C7. It can be seen that, before ultimate load the developed strains in the FRP laminates were small, less than 0.001. This can be explained that at this loading level, the expansion of the concrete core was small to strain the FRP to noticeable values. Hence, it can be said that at stages of loading preceding the ultimate level, the confinement effect of the FRP wraps is less significant.

At and beyond ultimate load, the FRP wraps acted more effectively and introduced high confinement pressure on the concrete section of the column. For columns C2 through C6, the failure transverse strain of FRP wraps at mid-height zone ranged from 0.0029 to 0.0036. On the other hand, column C7 strengthened with combined regular and sandwich FRP strips recorded a lower strain value in sandwich wrap that equals 0.0021 at failure. This can be attributed to its mechanism of failure that started with the rupture of the regular FRP wraps and consequently causing a load drop and a release of a part of the strain developed in the sandwich FRP wraps.
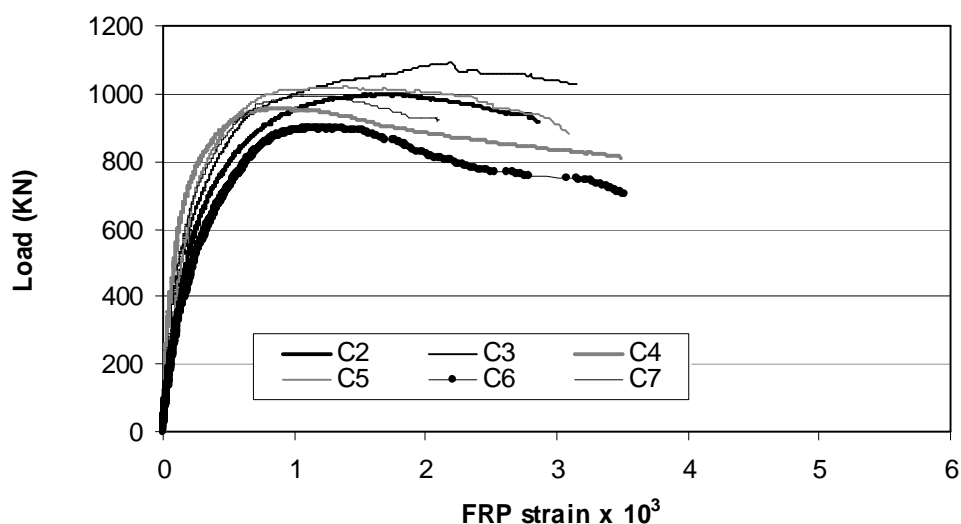

Fig. 6: Load-FRP Strain Relationship for the Tested Columns

Toughness and Ductility Enhancement

Toughness of the columns is defined as the area under the load-axial strain curve till the point on the descending branch where the load drops to 80% of its ultimate value. When needed, this point was determined by means of extrapolation such in case of columns C2 and C3. Toughness values of the tested columns were calculated and given in Table 2. These values represent the energy absorption capacity, i.e. ductility, of the columns. Moreover, the toughness values were used as a measure of the ductility to assess the enhancement in the ductility of the columns due to strengthening with FRP wraps.

As seen in Table 2, column C3, strengthened with full sandwich CFRP, showed a toughness value equals 22.3 kN.mm/mm, which is the highest value among the tested columns. The enhancement in the ductility of the tested columns with respect to the control column is listed in Table 2. The enhancement values ranged from 162%, for column C6 that strengthened with sandwich FRP strips, to 320% for column C3, strengthened with full sandwich CFRP. It can be noted that columns strengthened with full sandwich wrapping showed remarkable enhancement in the ductility.

EFFECT OF MAJOR TEST VARIABLES

The main objective of this research is to investigate the effectiveness of sandwich wrapping using acrylic plates as sandwich material for square concrete columns subjected to eccentric loading. The main parameters of the study were: method of wrapping, type of FRP material and percentage of FRP wrapping.

Effect of Wrapping Method

Two method of FRP wrapping were studied, regular and sandwich systems. Figure 7 shows the load-longitudinal compressive strain relationships for columns C1, C2 and C3. Strengthening with regular and sandwich CFRP systems increased the ultimate load capacity by 14 and 24 percent compared to the control column, respectively.

Figure 8 shows the load-longitudinal compressive strain relationships for columns C1, C4 and C5. Strengthening with regular and sandwich GFRP systems increased the ultimate load capacity by 9 and 16 percent compared to the control column, respectively. It can be noted that strengthening the columns using FRP sandwich wrapping system enhances the ultimate load carrying capacity of the column to a level higher than the level achieved by regular FRP wrapping system.

The enhancement in the load carrying capacity of FRP sandwich wrapped columns can be referred to the presence of the acrylic plates that increased the stiffness of the wraps. Hence, this increased the passive pressure on the concrete core, i.e. more confinement. In addition, the higher stiffness of sandwich wraps compared to the regular wraps enables it to deform in a uniform manner and thus reducing the variation in confinement pressure distribution around the concrete section, i.e. a higher effective confining pressure.

On the other hand, the enhancement in the ductility was more pronounced. The ductility enhancement of columns C2 and C4 with regular FRP wraps were 232% and 219%, respectively, while those of columns C3 and C5 with sandwich FRP wraps were 320% and 274%, respectively. It is clear that the FRP wraps, whether regular or sandwich, result in distinctive gain in the ductility of the column. The confinement effect of the wraps enables the concrete core to withstand higher strains without significant reduction in the load, i.e. axial strain ductility. Also, this allows for higher rotational capacity of the column section. Accordingly, the two main sources of ductility for eccentric columns, axial strain and curvature ductility were improved.

The ductility enhancements due to the use of sandwich FRP wraps were 37% and 25% higher than those of the regular FRP wraps. This indicates that the sandwich FRP wraps outperform the regular FRP wraps in enhancing the ductility of the columns.

It can be concluded that the utilization of sandwich FRP wraps results in load and ductility enhancement higher than those of the regular wraps. It is worth mentioning that the load enhancement ratios of the eccentric columns tested in the current research are significantly lower than those reported by Mahmoud et al. [7] for sandwich FRP wrapped columns tested under concentric loading. This observation is in line with the results reported by Hadi [4]. He found that when load eccentricity is introduced on RC columns, the effectiveness of the regular FRP wrapping significantly decreases.
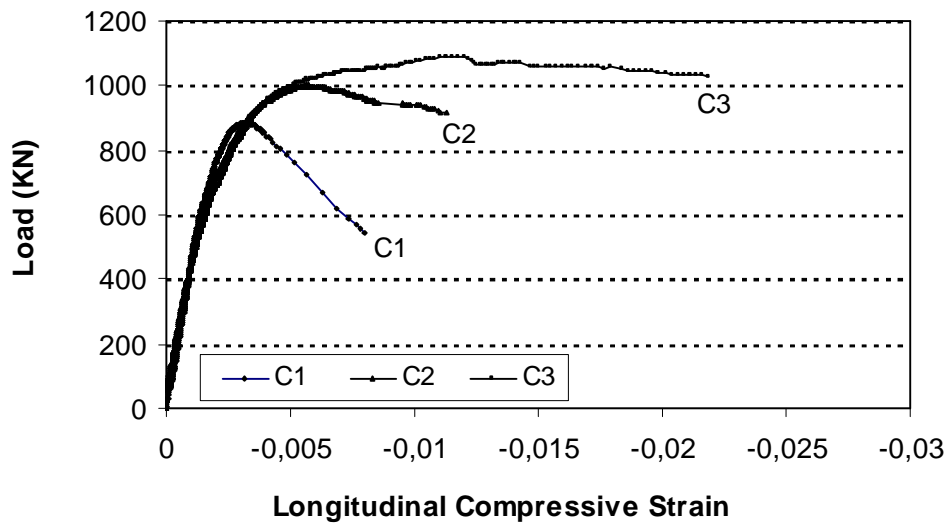
Fig. 7: Effect of Wrapping Method-CFRP Wraps
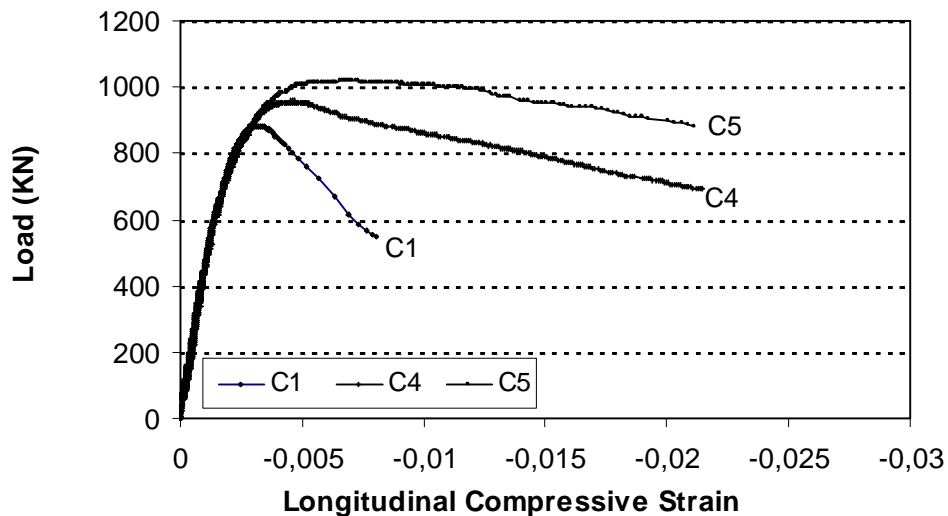
Fig. 8: Effect of Wrapping Method-GFRP wraps

Effect of Wrapping Material

Two types of FRP material, carbon & glass, were investigated. Figure 9 shows the load-longitudinal compressive strain relationships for columns C1, C2 and C4. Strengthening with regular CFRP and GFRP wraps increased the ultimate load capacity by 14 and 9 percent compared with the control column, respectively. The ductility of columns C2 and C4 increased by 232% and 219% compared with the control column, respectively.

Figure 10 shows the load-longitudinal compressive strain relationships for columns C1, C3 and C5. Strengthening with sandwich CFRP and GFRP wraps increased the ultimate load capacity by 24 and 16 percent compared with the control column, respectively. The ductility enhancement of the CFRP strengthened column C3 was 320% which is higher than that of the GFRP strengthened column C5 that recorded a value of 274%. So, the carbon FRP wrapped columns performed better than the glass FRP wrapped columns in terms of strength and ductility.

It can be concluded that for both regular and sandwich wrapping methods, the CFRP wrapped column displayed higher enhancement in load carrying capacity and ductility than the GFRP wrapped column. This can be interpreted as the CFRP composites have higher tensile strength and elastic modulus compared to the GFRP composites. This results in higher strength and stiffness of the CFRP wraps.
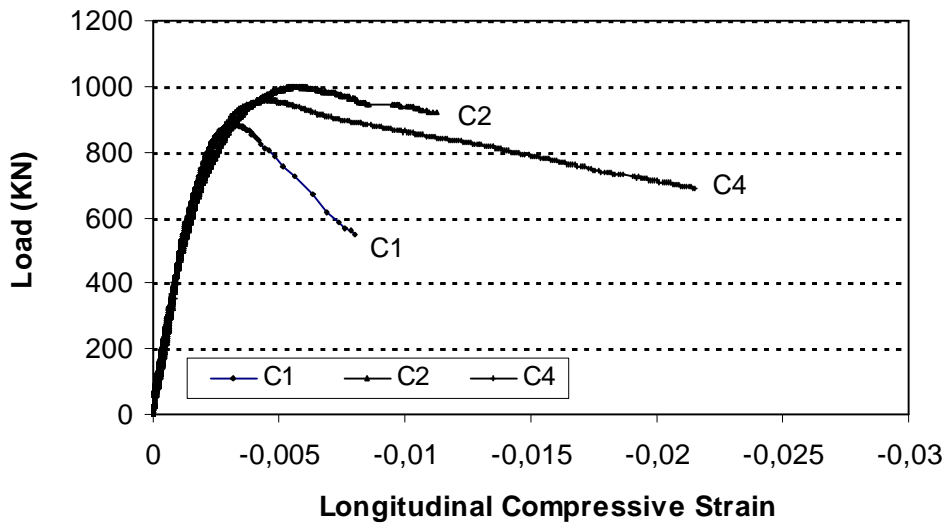
Fig. 9: Effect of FRP Material in Case of Regular Wrapping
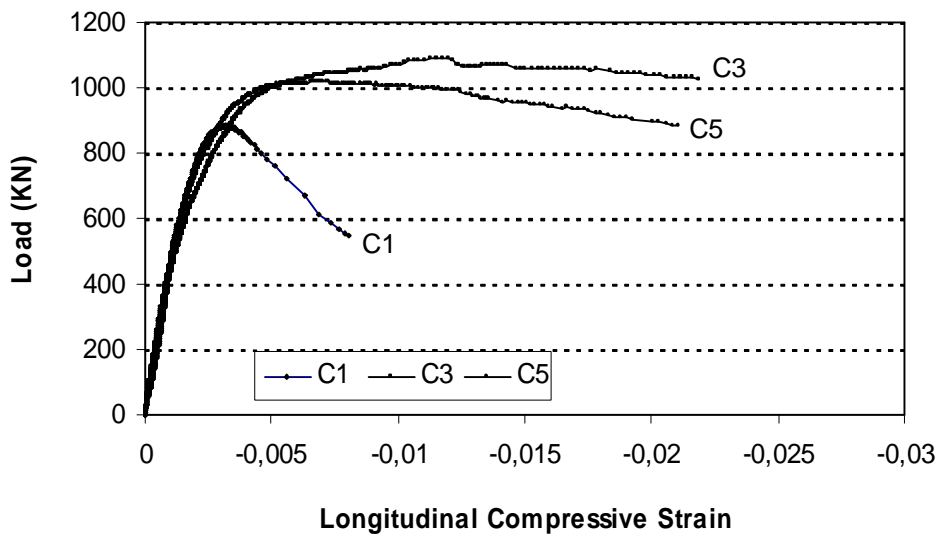
Fig. 10: Effect of FRP Material in Case of Sandwich Wrapping

Effect of Percentage of Sandwich Wrapping

The effect of percentage of sandwich wrapping was studied for full and partial wrapping. The load-longitudinal compressive strain relationships for columns C1, C3 and C6 are presented in Figure 11. Strengthening the column with full sandwich CFRP wrapping increased the ultimate load capacity by 24 percent compared with the control column. On the other hand, partial sandwich CFRP wrapping did not enhance the ultimate load carrying capacity of the column. This can be explained through the failure mechanism of the column provided with partial sandwich wrapping. It started with the compression failure in the unconfined zone and so made

the column performance dominated by its weakest zone, i.e. the unwrapped zone. Till further research is done in this area, it is recommended to use full sandwich FRP wrapping, if an enhancement in the load capacity is required.

The ductility of columns C3 and C6 increased by 320 and 162 percent compared with the control column, respectively. In other words, the enhancement in ductility for the partial wrapping was about half the value of the full wrapping. This can be attributed to the failure mechanism of the column provided with partial sandwich wrapping as explained above.
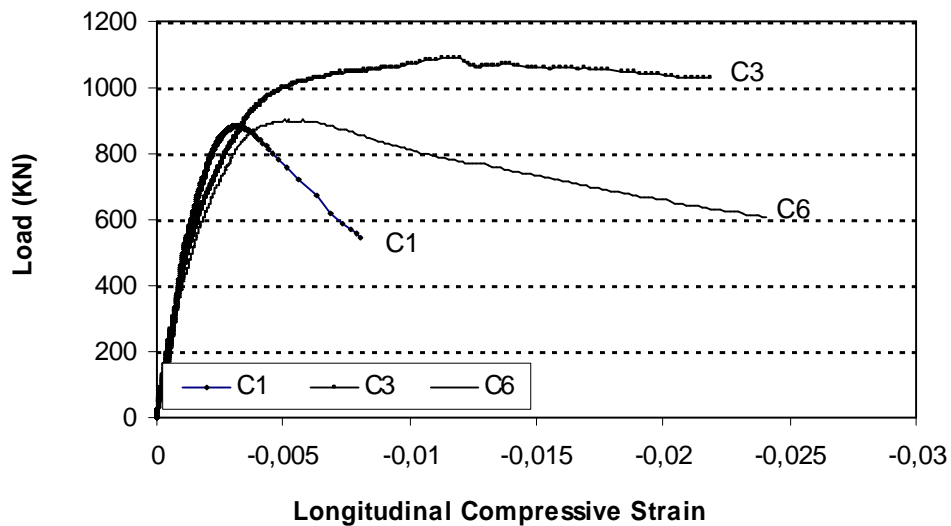
Fig. 11: Effect of Percentage of Sandwich Wrapping

Effect of using Combined Regular and Sandwich Wrapping

The effect of using combined regular and sandwich wrapping strips was investigated. Figure 12 shows the load-longitudinal compressive strain relationships for columns C1, C3, C6 and C7. Column C7 which was provided with combined regular and sandwich wrapping showed enhancement in the ultimate load capacity by 12% compared to the control column C1. This enhancement value is 12% less than that of column C3, provided with full sandwich wrapping, while it is 10% higher than that of the partially sandwich wrapped column.
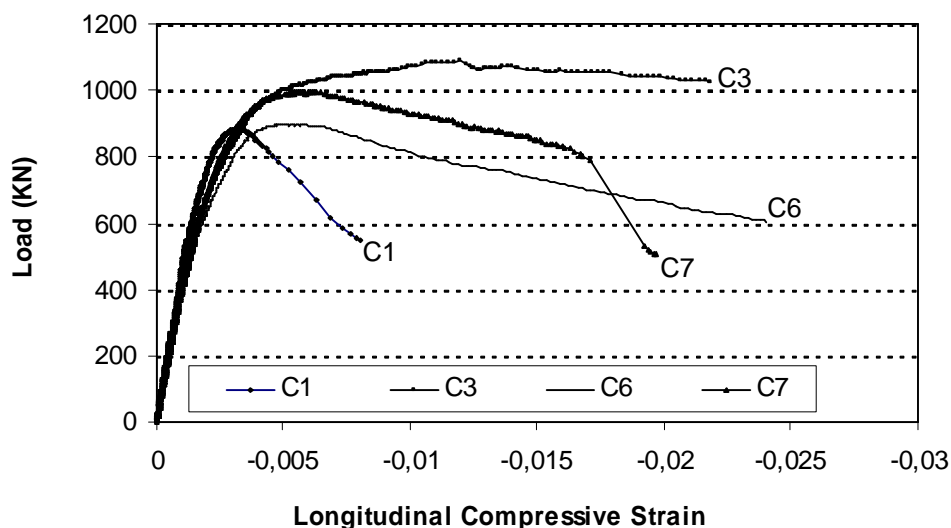
Fig. 12: Effect of Combined Regular and Sandwich Wrapping

On the other hand, the enhancement in the ductility was more significant. The ductility of column C7 increased by 177% compared to the control column C1. So, It can be concluded that the combined wrapping scheme outperforms the partial sandwich wrapping. However, it is still not as effective as the full sandwich wrapping.

CONCLUSIONS

The research presented in this paper included testing of seven eccentrically loaded square RC columns to evaluate the effectiveness of using sandwich FRP wrapping compared to the regular FRP wrapping. Based on the obtained test results and analysis and within the scope of the investigated parameters, the following conclusions were drawn:

1- External FRP wrapping of RC columns subjected to eccentric compression loading improves their structural performance in terms of load carrying capacity and ductility. However, the enhancement in the ductility was more pronounced, up to 320%.
2- The failure of sandwich FRP full wrapped columns was due to crushing of the sandwich plate in compression followed by rupture of the FRP wraps. Finally, crushing of concrete in compression and buckling of longitudinal bars occurred.
3- The wrapped columns sustained higher lateral deflection than the unstrengthened one.
4- Before ultimate load level, the developed strains in the FRP wraps were less than 0.001. At and beyond ultimate load, the FRP wraps acted more effectively and introduced high confinement pressure on the concrete section of the column.
5- The FRP sandwich wrapping system is more effective strengthening technique than the regular FRP wrapping system. This can be attributed to the presence of the sandwich plates that increased the stiffness of the wraps.
6- Strengthening the columns using full FRP sandwich wrapping system led to enhancements in the ultimate load and ductility up to 24% and 320%, respectively.
7- For both regular and sandwich wrapping methods, the CFRP wrapped column displayed higher load carrying capacity and ductility than the GFRP wrapped column.
8- Strengthening the column with partial FRP sandwich wrapping resulted in ductility enhancement of 162%, however, no effect on the load carrying capacity was observed.
9- The combined wrapping scheme, (regular strips +sandwich strips) outperforms the partial sandwich wrapping. However, it is still not as effective as the full sandwich wrapping.

REFERENCES

1. Hassan, W. H. (2004), "Behavior of Biaxially and Uniaxially Loaded Short High Strength Concrete Columns Strengthened Using Fiber Reinforced Polymer Laminates", M.Sc thesis, Cairo University.
2. Li, J., Hadi, M. N. S. (2003), "Behavior of Externally Confined High-Strength Concrete Columns Under Eccentric Loading", Composites Structures, Vol. 62, pp.145-153.
3. Hadi, M. N. S. (2007), "Behavior of FRP Strengthened Concrete Columns under Eccentric Compression Loading", Composites Structures, Vol. 77, pp. 92-96.
4. Hadi, M. N. S. (2007), "The Behavior of FRP Wrapped High-Strength Concrete Columns under Different Eccentric Loads", Composites Structures, Vol.78, pp.560-566.
5. Hadi, M. N. S., "Behavior of FRP Wrapped Normal-Strength Concrete Columns under Eccentric Loading", Composites Structures, Article in Press.
6. Mahfouz, I., Shahraman, S. and Rizk, T. (2001), "Wrapping System For Strengthening Structural Columns or Walls" United States Patent, No. 6,219,988, April 24.
7. Mahmoud, KH., Fouad, E., Ramadan, M.O., and Abd-Elalim, A. (2004), "Behavior of Axially Loaded Square RC Columns Confined with Sandwich FRP Wraps", International Conference: Future Vision And Challenges For Urban Development, Cairo, December.

BRIDGE REHABILITATION UNDER ADVANCED MANAGEMENT AND NON-TRADITIONAL STRUCTURAL APPROACHES

Hesham A. Mahdi

Assis. Professor Sixth of October University, Consultant Engineer of Bridges, Cairo, Egypt
Email: heshamnecb@menanet.net

ABSTRACT

The high capital investment in bridge construction, the use of high-technology construction methods, combined with the increasing need for expanding the service life of bridges and a better considerate of the deterioration/corrosion mechanisms in concrete, has led to efforts to develop rational tactics for bridge maintenance against severe environmental and loading conditions.

In this paper, the subject of rehabilitation of concrete bridges has been treated at the aim to attain some consistent interpretations that may be constructive in our appraisal of reliability and to endeavor an assessment of the level of reliability of bridges in Egypt as well. A simple formulation of a tolerable risk level will be attempted, approximate frequency and potential reasons for bridge collapse shall be provided. The purpose is rather to give an understanding of how the concept of safety is phrased and to discuss the level of reliability required for our bridges.

The research introduces sophisticated structural analysis implementing finite element method and an advanced constitutive model of concrete as combination of smeared cracking model and biaxial fit modifying uni-axial Drucker-Prager plastic model. The paper illustrates the testing program of a deteriorated concrete bridge that suffered serious deterioration due to bad concrete material, lack of appropriate maintenance and service loads that exceeded the designed values. It involves the application of the suggested numerical analysis to assess the structural behavior of the bridge under both the designed loading and the current service loading as well. Moreover, the paper underlines the various rehabilitation processes and the large-scale repair as a practical model for applying the recommended study under the umbrella of reliability requirements.

Keywords: reliability, serviceability, restorability, performance index, finite element

INTRODUCTION

In our coursework with design, check, and approval of bridges design with due regard to reliability issues, we are confronted with the following questions:
   a- Are we conservative? posed by Owners, Consultant Engineers
   b- Is this safe enough? posed by the media and politicians
Those who are responsible for codes for design and those who are approving the design of bridges are expected to make safe and reasonable choices with regard to reliability. Their choices are crucial for people's life and health and for large capital investments as well. By choosing loading level, loading factors, material strength and partial material factors in accordance with "Egyptian Code of Practice" ECOP and enforcement of rules, the safety of our bridge shall be assured.
The question of whether we are too conservative can therefore be answered in the negative. It may seem that the opposite is the case that our reliability is not at the international level when all types of collapse are included. This is hardly due to regulations, design rules or standards; the main reasons are:

> §   Lack of requirements to check the height of vehicles and their loads
> §   Lack of maintenance and rehabilitation

There is a room for improvement in those two points as all transport vehicles exceeding the height or loads must be banned or subject to individual dispensation from the rules.

Accordingly, it is vital to discuss whether we have a safety perspective for our bridges in Egypt and to attempt to arrive at some elucidations that might be productive in our assessment of reliability. The paper shall be limited to the following main themes:

1. What level of reliability do we have in Egypt?
2. How often do our bridges collapse?
3. What is the status today in relation to reasonable requirements? Are our bridges safe enough or are we too conservative in our designs?

This shall be discussed in a general way, without resorting to difficult and mathematical models. The material presented in the forms of statistics is not precise to satisfy scientific requirements. However, our target is to reach a perceptive of how safety rules are formulated and at what level they should aim.

There is presently a vast body of literature on damage detection and structural condition monitoring with the aim of eventually developing a non-destructive evaluation methodology. Large collection of papers on many issues and difficulties involved in implementing damage detection strategies in structural systems are found in Natke (1988)[1] and Natke (1993) [2]. More specialized works, together with experiment set-ups for validation/comparison were presented by Stubbs [3] and Pandy [4]. Besides, a representative work on field implementation of particular detection strategies on a highway bridge, Biswas [5] and Farrar 6].

Ahmed K. Sanli [7] had presented non-destructive evaluation methods of deteriorated bridges using proof load tests to detect the bridge ability to carry a specified live load.

Safety Requirements

The international standard ISO 2394[21] "General principles on reliability for structures", annex E.4 "Specified reliability levels" says:

"Structural reliability is important first and foremost if people may be killed or injured as a result of collapse. An acceptable maximum value for the failure probability in those cases might be found from a comparison with risks resulting from other activities. Taking the overall individual lethal accident rate of 10^{-4} per year as a reference, a value of 10^{-6} seems reasonable".

The maximum allowable probability of failure of the structure depends on the conditional probability of few or many persons being killed, it also depends on the economic consequences of loosing the structure. Finally, it is up to the politicians and the decision makers to judge whether the proposed annual probability is acceptable or not.

For prestigious bridges as Nile bridges and bridges on highways with heavy traffic as Cairo-Alexandria road and other bridges located in the Delta highway networks, the risk of collapse should be lower than 10^{-5} (an annual probability of 10^{-6}). In the meanwhile, bridges with little traffic, a slightly higher risk can be accepted (an annual probability of 10^{-4}). When single members of a structure approach their defined maximum stresses in the ultimate limit state, there may still remain a reserve of carrying capacity before the whole system collapses. Defined design values of material parameters in the ultimate limit state are often lower than the actual resistance developed in the structure at collapse. When a bridge structural member reaches the yield and a plastic hinge develops, the structural system alters and a redistribution of internal forces will take place in the statical system of the bridge. The extent and importance of the redistribution will vary from bridge to another. Besides, some Codes of bridge design stipulate conservative conditions for moment distribution as BS 5400, part 4, 1990[8] as follows:

1. Checks are to be made to ensure that adequate rotation capacity exists at sections where moments are reduced.

2. Proper account is taken of changes in transverse moments, transverse deflections, and transverse shears as a consequent on redistribution of longitudinal moment by means of a special investigation based on a non-linear analysis.
3. Depth of structural members considered is less than 1200 mm
4. Shears and reactions are taken as those calculated either prior to redistribution or after redistribution whichever is greater.

Consequently, it is arduous to state plainly with any conviction that such redistribution effect will lower annual probability of fail to an average of 10^{-5} as we would have planned.

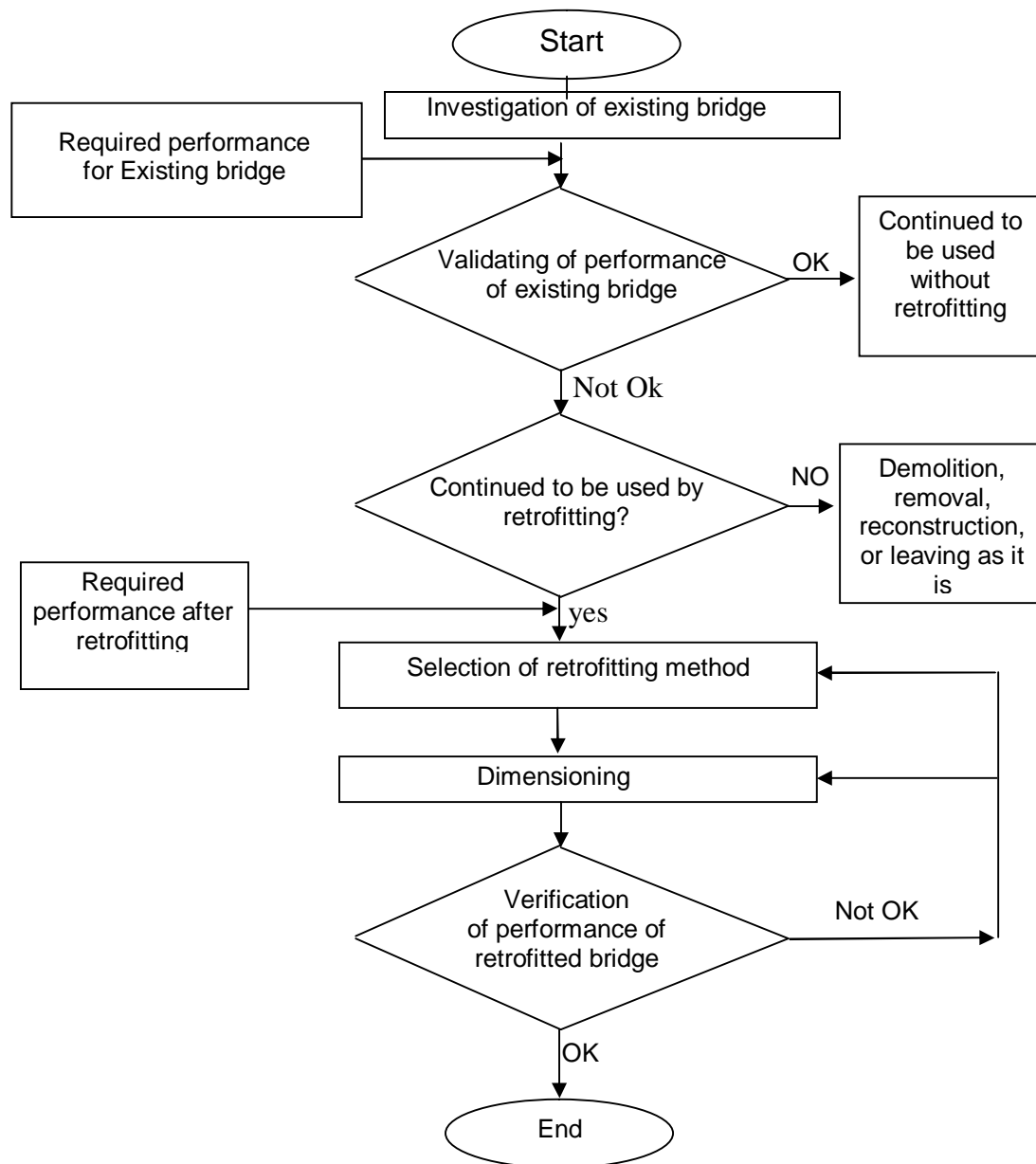## Bridge's Reliability Level and Retrofitting System

Early this year, the author, H. A Mahdi 2006[9] proposed a management system for bridge maintenance based on performance index including (structural integrity, serviceability, and easy maintenance….etc.). It was supported that performance of bridges can be classified into six main categories:

Social and environmental responsiveness ability to minimize unfavorable effects on surrounding environment. Former researches as Ayman H.H. Khalil [10] used controlled truck excitation in performing tests, where the environmental conditions affect the natural frequency of bridge structures. Structural safety: ability to avoid causalities due to structural failure. Serviceability: capability to make users feel contented with the bridges. Constructability: ability to assure safety during construction. Easy Maintenance: ability to make usual inspection/maintenance simple and to restore deficiency and tapering performances economically and technically. Easy demolition and recycling: ability to make demolition and recycling easy.

For Bridge structures, a set of performance items are required quantitatively depending on category, usage, and value of the bridge. In the proposed system, Hosny A [11] evaluated performance of bridges as a function of time, considering time-dependent deterioration due to loading and environmental attack. This is why durability of bridges is not listed in the above categories. Durability can be implicitly considered by evaluating all other performance items along the time.

In order to establish the existing level of reliability it is crucial to record the number of bridge collapses over a number of years, their type, and the reason of collapse. Unfortunately, no official statistics for bridge collapse in Egypt exist. Without authorization (to our best knowledge), we recorded 10 bridge collapses over a period of 25 years at an average rate of 0.40 bridge collapse every year. It is significant to emphasize that collapse does not necessary dictates a complete failure of the bridge but may imply severe problems that may deter the traffic or the safety of crossings underneath. Moreover, it is worth to highlight that there have been no mortal accidents with serious injuries in connection with bridge collapse in Egypt. According to our local survey, reason of collapse for the only 10 available samples (no absolute figures to be widely accepted on other bridges) is summarized as follows:

Collisions of Ships and Vehicles	4.0%
Foundations settlement	0.0%
Lack of Maintenance	39%
Traffic Overloading	30%
Construction faults and lack of Q.C	25.0%
Design faults	2.0%

Fig. 1: Flow Chart of Bridge's Retrofitting Design System after Mahdi, H.A (2006)[9]

The Egyptian Code of Practice ECOP guidelines (2003) provide a level of reliability which is common in most parts of the western world, nevertheless, there are some fields where ECOP - after due consideration- have decided to be more impudent and others have conservative requirements. H. A Mahdi 2006[9] proposed a flow chart of a retrofitting design system for bridges as presented in Fig.1, where a combination of monitoring, testing and structural analysis has to be assembled in order to take the true verdict of demolition/elimination, maintenance/rehabilitation or leaving the bridge as it is. Besides, the system goes beyond the rehabilitation process evaluating the performance of the retrofitted bridge and decides whether the selected retrofitting scheme is convenient for the bridge or a further system has to be conducted.

Proposed Numerical Analysis for Open Deck Reinforced Concrete Bridges

The structural performance of bridges is proposed to be assessed by a detailed FEM analysis using the commercial software DIANA package [12]. The FEM analysis can confirm whether the serviceability conditions of the bridge (as deflection and cracking of the structural elements under the designed and actual acting loads) are compatible with the service tolerable limits.
In this paper, a constitutive model for concrete including smeared crack model is implemented in the finite element analysis using flat shell elements Fig. 2.
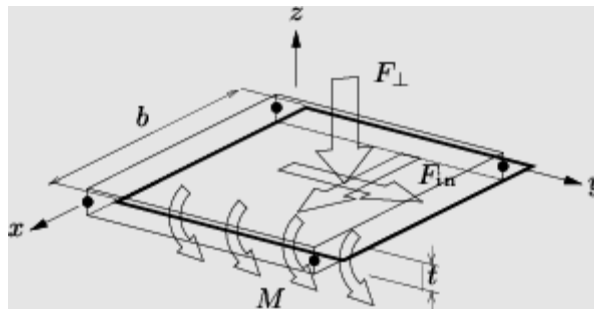
Fig. 2: Flat Shell Element as defined in DIANA[12]

The elements are basically combinations of a plane stress element and a plate-bending element and there is no coupling between membrane and bending behavior. Generally, the membrane behavior matches with plane stress element except the primary stresses, which are defined in terms of moments and forces, rather than Cauchy stresses. The bending behavior is based on the Mindlin-Reissner theory that conforms to Mindlin plate bending element. In the Mindlin-Reissner plate theory the transverse displacements and rotations of the mid surface normals are independent and obtained by employing an isoparametric interpolation respectively from the translations and rotations in the nodes; this technique includes transverse shear deformation. The shape functions used here are taken from Simo and Rifai [13] and from Andelfinger and Ramim [14].
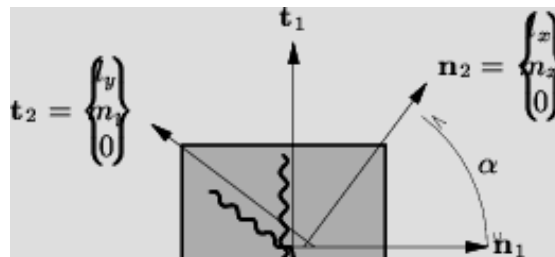
Fig. 3: Multi-directional fixed crack model

As most of the aged bridges under renovation and probing suffer from cracking, it is prudent to allow for cracking of the concrete in the analysis. The elementary feature of the decomposed crack model is the decomposition of total strain into an elastic strain ε^e and a crack strain as ε^{cr}

$$\varepsilon = \varepsilon^e + \varepsilon^{cr}$$

The sub-decomposition of the crack strain ε^{cr} gives the possibility of modeling a number of cracks that simultaneously occur.
The basis feature of this multi-directional fixed crack concept is that a stress σ_i and strain ε_i^{cr} exists in the n-t coordinate system that is aligned with crack I as shown in Fig. 3.

a. Crack Initiation:

A fixed smeared crack model with a constant stress cut-off criterion is implemented in the analysis. The cut-off value equals the tensile strength of concrete corresponding to the concrete class as determined from the concrete cores of the existing concrete member, i.e. a crack arises if the major principal tensile stress exceeds f_t as delineated in Fig.4.

Fig. 4: Crack initiation as function of tensile stress

b. Cracking parameters:

The relation between the traditional cracking parameters --the reduction factor of the Young's modulus "μ" and the reduction factor on the shear modulus ß can be derived as shown in Fig. 5 ignoring the coupling between the normal stresses and the shear stresses, as coupling results in unnecessary level of sophistication. Accordingly, the crack stresses are solely governed by the corresponding crack strains.
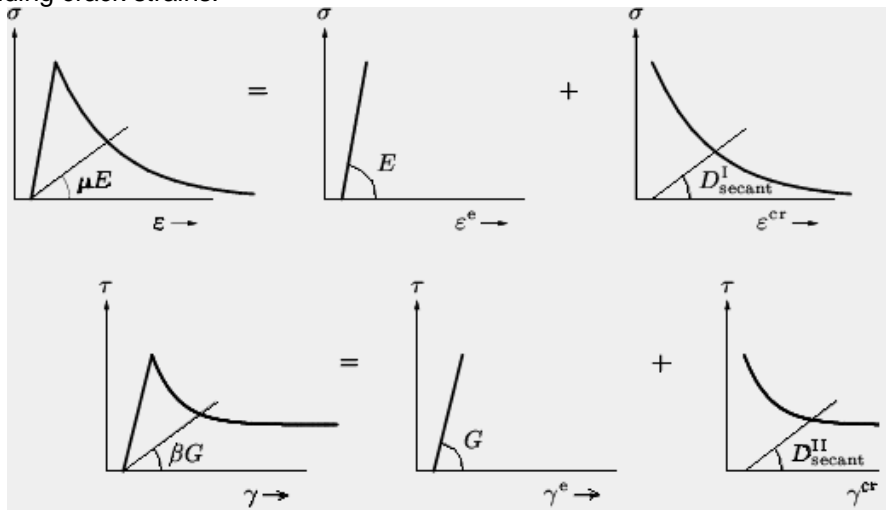
Fig. 5: Relation between Traditional and Secant Crack Parameters

Finally the stress-strain relationship after De Borst and Nauta [15] is:

$$D^{I}{}_{\sec ant} = \frac{m}{1-m}E \quad \textbf{and} \quad D^{II}{}_{\sec ant} = \frac{b}{1-b}G$$

Finally, the stress-strain relationship can be expressed as follows:

$$
\begin{Bmatrix} s_{xx} \\ s_{yy} \\ t_{xy} \end{Bmatrix} = \begin{bmatrix} \dfrac{mE}{1-mu^2} & \dfrac{muE}{1-mu^2} & 0 \\ \dfrac{muE}{1-mu^2} & \dfrac{E}{1-mu^2} & 0 \\ 0 & 0 & \dfrac{bE}{2(1+u)} \end{bmatrix} \begin{Bmatrix} e_{xx} \\ e_{yy} \\ g_{xy} \end{Bmatrix}
$$

c. Concrete physical plasticity model using bi-axial fit

In view of the fact that bridge elements (top slab) is subjected to transversal and longitudinal stresses, the constitutive behavior of concrete under biaxial states of stress has to be taken into account. The biaxial state is in general different from the constitutive behavior under uni-axial loading conditions. The experimental data of concrete subjected to proportional biaxial loading show the influence of the lateral compressive stress on the strength of the material. Experiments by Kupfer and Gerstle [16] produced the data as shown in Fig. 7 with the biaxial fit of the Drucker-Prager failure surface.
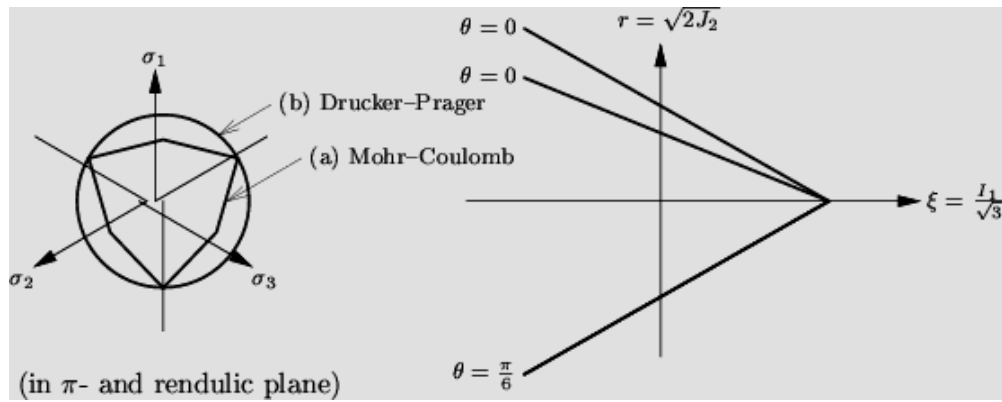
Fig. 6: Drucker-Prager Model

The maximum compressive strength increases approximately 16% under conditions of equal biaxial compression and about 25% increase is achieved at a stress ratio of $s_1/s_2=0.50$. The parameters of the Drucker-Prager failure surface Fig. 6, the friction angle f and the cohesion c, are calibrated with the following procedure.

The relation between the uniaxial stress $s_3=-f_c$ and the equivalent cohesion $\bar{c}$ are given by:

$$
\bar{c} = f_c \frac{1-a_f}{b} = f_c \frac{1-\sin j_o}{2\cos j_o} \quad\text{..(1)}
$$

if the friction angle is constant, the uni-axial fit is given as:

$$
\bar{c} = f_c \frac{1-a_f}{b} \quad\text{..(2)}
$$

The biaxial fit is calculated by substituting the stress vector in case of a plane stress state

$$
\begin{Bmatrix} -af_c \\ -af_c \\ 0 \end{Bmatrix} \quad\text{..(3)}
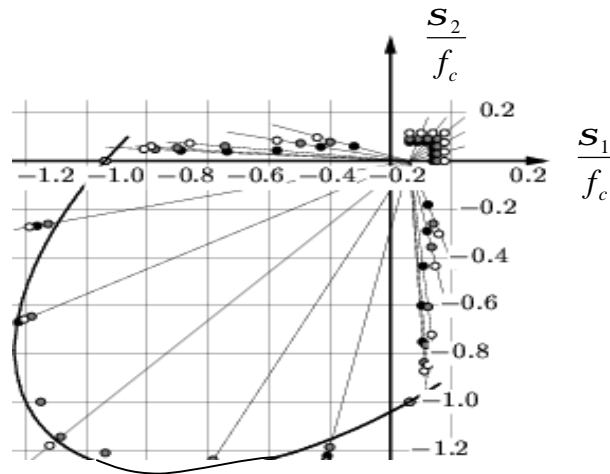$$

Fig. 7: Biaxial fit of Drucker-Prager after Kupfer and Gerstle [16]

With *a* the multiplication factor for the biaxial strength. Substituting the stress vector into the equation of the failure surface of Drucker-Prager yields the following condition

$$af_c - 2a_f af_c - b\bar{c} = 0 \quad \therefore \quad \bar{c} = af_c \frac{1 - 2a_f}{b} \quad\text{...(4)}$$

Solving (1) and (4) for a_f, given the factor *a*, results in

$$a_f = \frac{a - 1}{2a - 1} = \frac{2\sin j_0}{3 - \sin j_0} \quad\text{..(5)}$$

This is solved for $\sin f$

$$\sin j = \frac{3a_f}{2 + a_f} = \frac{3a - 3}{5a - 3} \quad\text{...(6)}$$

Finally, the cohesion is derived from the uniaxial compressive strength and the friction angle f according to

$$\bar{c} = f_c \frac{1 - \sin j_o}{2 \cos j_o} \quad\text{..(7)}$$

For a normal strength quality concrete, the ratio between the uni-axial compressive strength and the biaxial compressive strength is approximately 1.16 which results in a friction angle $f_0 = 10$ degrees and a cohesion $c = 0.42 f_c$

Reliability assessment of Kheneza Bridge over Nubaria water canal

On 1986, the construction of Kheneza Bridge was completed over Nubaria water canal, the bridge is 98 m length and 10.0 m width constructed with the aim of connecting the highway transportation networks of Cairo Alexandria desert road through Sadat City and the highways located at the west of Delta to Behira Governorate. The structural system of the bridge is an open deck three reinforced concrete girders spaced 3.50 m in the transversal direction over which a top slab was cast 20cm thick Fig. 8.

The statical system of the bridge is composed of a simple span 24 m length resting on an overhanging span of 34 m and double cantilever 8.00m each.

After the construction of the bridge, many aggregate quarries were constructed in the vicinity and the bridge was subjected to higher loading level compared to that originally designed on to the extent that reached more than 120% of the designed live load (30 tons).
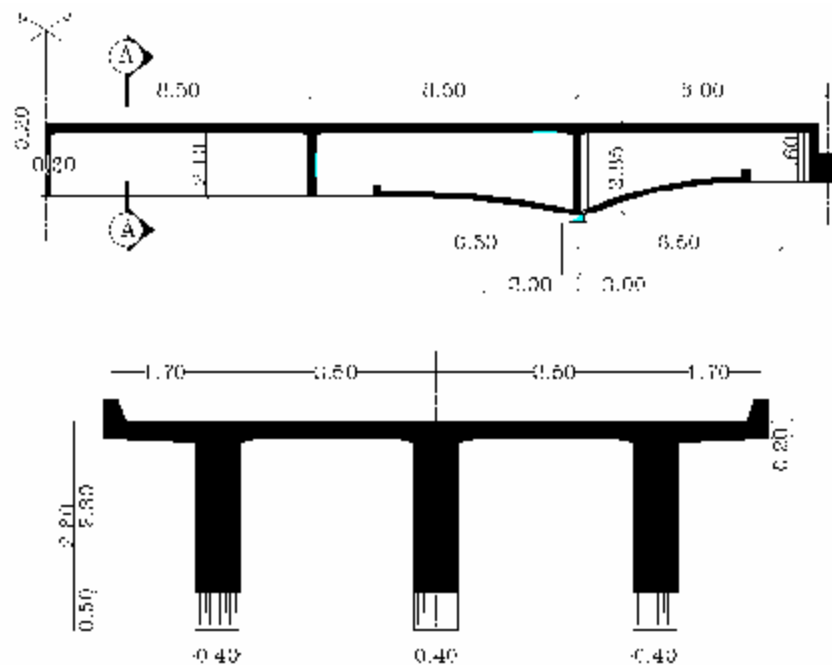
Fig. 8: Longitudinal and Cross sections of Kheneza Bridge over Nubaria Canal

Inspection, Testing, Evaluation of Results and Structural Integrity

In view of AASHTO [17] and Norwegian Bridge management systems (BRUTUS) [20], several types of inspection were conducted to the bridge:

Inventory Inspection

Such inspection is defined as the zero time reference. It was considered as the base line of structural conditions and the identification and listing of any existing defects. Inspection details were recorded in the taking over Certificate and after the expiry of the defects liability period. The inspection recorded honeycombing, bug holes in the piers, evidence of cold joints, irregular surfaces caused by improperly aligned forms that are attributed to poor workmanship.

Routine Inspection:

It is a periodic inspection that took place after a certain time interval measured from the zero time reference. The visual inspection proved a deteriorated state and prevailing of diagonal cracks in the top slab that have been recorded after five years of use due to the construction of quarries and the start of very heavy trucks passing. The inspection was carried every 3 years and ended with an overlay slab 15 cm thick over the existing one.

In-Depth Inspection

After a given age of the bridge (15 years), another profound inspection was carried out to evaluate the old remedy of the top slab. The top had been subjected to severe cracking, spalling (development of fragments in the shape of flakes detached from the main body of concrete) and disintegration (loss of small particles and individual aggregate particles) owing to an extreme excessive truck loading and lack of convenient maintenance (Fig. 9). The inspection proved that the situation was aggravated by the following:
1. High deflection values of the longitudinal members ranging from 4.0 cm to 6.0 cm
2. Collision of heavy trucks attacking bottom level of the main girders at the side spans of the bridge crossing the banks of the river due to lack of adequate clearance(3.75m), resulting in severe cavitations initiated by such repeated impact forces

3. The recurrent collision resulted in crushing of the concrete cover, failure bond between the concrete and the heavy steel bars at the bottom fibers of the girders, in addition to the suspension of the steel bars with the trucks leading to an inevitable pulling out of the steel from the concrete girders as shown in Fig. 9.
4. Severe corrosion of the steel bars and complete separation of the bottom concrete layer (laminated concrete) in addition to the severe honey combing of concrete
5. Assembly of calcareous dust around the cast-steel bearings of the bridge to the degree that hinders the displacement of the bridge as designed.
6. Concrete of Columns and pile caps exhibited brown oxidized spots that were almost interconnected reflecting severe corroded matrix.
7. The recurrence of the heavy truck loading refuted any suspicious as to the obvious lack of control that can prevent 60 tons heavy trucks or even more to cross the bridge.
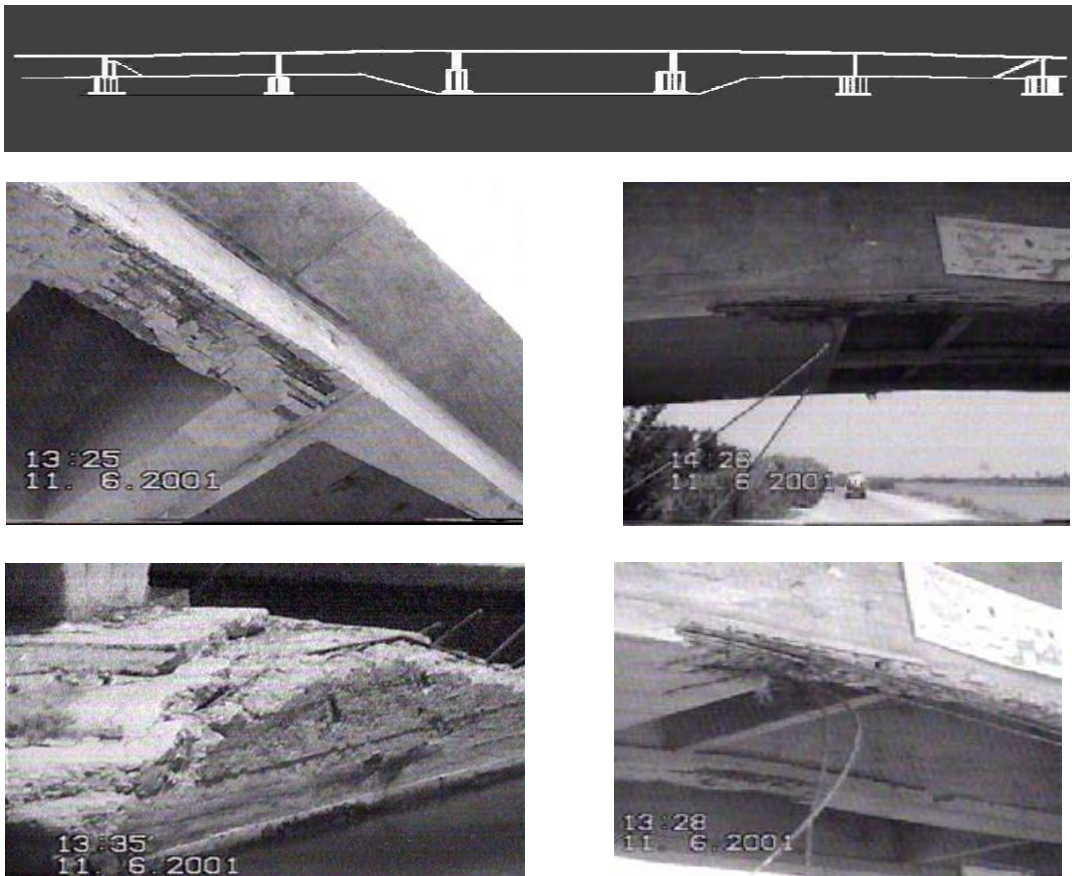
Fig. 9: Deteriorated State of the Bridge Exhibiting Concrete Distress

Accordingly, rebound hammer test (ASTM C 805) was implemented to determine qualitatively the uniformity of the bridge concrete. Ultrasonic tests (ASTM C 597) were procured to determine the depth and extension of cracks as well as the uniformity of concrete. Concrete cores were extracted at the best location at the aim of determining quantitatively the concrete strength values and analyzing the concrete gradients. Concrete cores had been taken from the top slab, girders, columns and pile caps where an obvious spatial variation in the concrete cubic strength was recorded ranging from 120 kg/cm^2 to 180 kg/cm^2 for the slab and girders where the weak records were attributed to the carbonated concrete. Concrete strength of pier shafts and pile caps ranged from 220-250 kg/cm^2. Break-off tests (ASTM C 1150) were conducted for wet chemistry analysis to determine cement content, chloride content and sulfate content. Results of Chemical analysis conveyed direct deterioration of concrete due to sulphate attack in the cement matrix for the super-structural elements. The sulphates - originated from aggregates- caused an expansive reaction that led to cracks in the affected concrete.

Chemical tests also proved indirect deterioration due to reinforcement corrosion, cracks, and spalling originated from the volume increase when iron reacts with oxygen. Moreover, concrete carbonation proved to take place that is the process in which carbon dioxide from the aggressive environment enters the concrete and reacts with the hydroxyl ions, which lead to a drastic reduction of pH-value below 9.0. The carbonation depth over which the pH-value had dropped reached 15 cm in the concrete girders due to the porosity of the concrete cover at most of locations (bad workmanship) .

Results of Numerical Analysis

The most outstanding outcome of the FEM analysis "Fig.10" under both design loads and the designed concrete strength is summarized in Table (1) as follows:
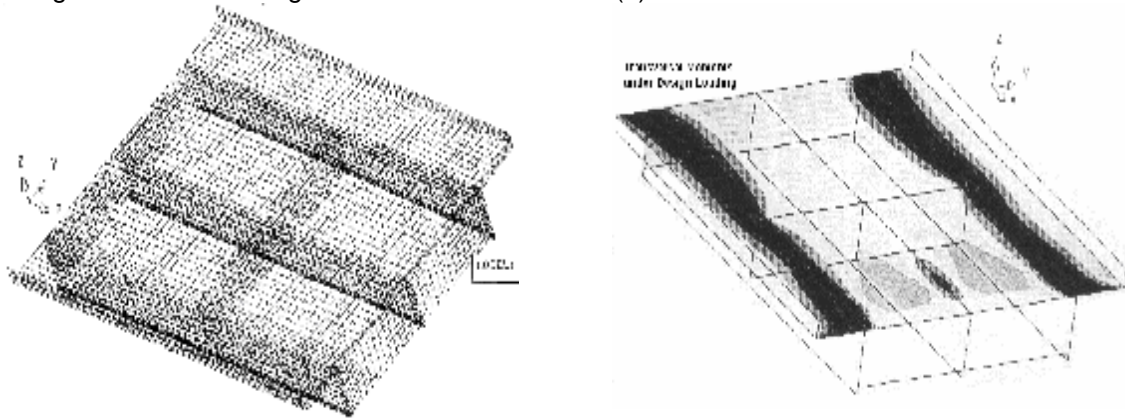
Fig. 10: Finite Element Idealization of the Simple span

Table 1: Structural analysis for the bridge using C300

State	Design loading (30 tons)	Actual Truck Loading
Mid- Span Deflection	23.5 mm	35 mm
Maximum concrete stress in top slab	58 kg/cm^2	75 kg/cm^2
Stresses in steel bars	1450 kg/cm^2	2200 kg/cm^2

Table (2) clearly reflects the perceptible increase in mid-span deflection when the FE was repeated taking into account the deteriorated in-situ concrete properties in view of testing result

Table 2: Structural analysis for the Bridge using current concrete status

State	Design loading (30 tons)	Actual Truck Loading
Deflection	27mm	45 mm
Maximum concrete stress in top slab	57 kg/cm^2	73 kg/cm^2
Stresses in steel bars	1610 kg/cm^2	2396 kg/cm^2

Remedial and Rehabilitation Procedures:

Based on assessing the deterioration level and the drastic changes in the bridge's performance level including the significant threat to the bridge function, remedial actions were conceded through a comprehensive plan. The repair procedure can be summarized as follows:
   a- Strengthening of all the six columns of the bridge using concrete jackets.
   b- Grouting cracks in the pile cap concrete surfaces by injecting with high viscosity epoxy resin which is a combination of epoxide and polyurethane at a pressure 0.010 N/mm^2
   c- Restore and fortify the transversal beam above the columns to accommodate the new bearings to provide for the increase of reactions due to the actual live loading level.

d- For the beams of the overhanging span, a new concrete jacket was cast confining from all sides the old beams and connected using a bottom slab of thickness 15 cm in the 6.00 m from the supports to accommodate the new longitudinal compressive stresses.

e- Demolishing of the superstructure side spans (simple spans) over the canal side banks due to the high corrosion and damage induced by the vehicle collision and recast using high quality concrete of C45.

Fig. 11: Remedy Process of Kheneza Bridge

f- All pile heads were repaired and injected at the connection of the pile with the pile cap to assure full compatibility with the cap surface

g- Top slab thickness was increased to 22 cm as the old design thickness proved to be inadequate to withstand the new traffic loading.

h- Cross girders were increased at maximum spacing 5.0 m instead of the old spacing (8.50m) in order to increase the deck torsional rigidity specifically when the deck was exposed to unsymmetrical truck loading 60 tons.

Besides, the solution of the vehicle collision to the bottom frame of the longitudinal girders was treated by lowering the ground level 1.750 m below the existing level and casting a U-shape culvert to retain the slopes of the canal bank thus providing a clearance of 5.50 m below the bottom level of the new structural member.

Finally, the finite element had been conducted using the repaired dimensions and concrete properties, where the following difference in the mid-span deflection is discernible as a percent of the design state and the final state after repair to the current deteriorated state "Fig. 12".
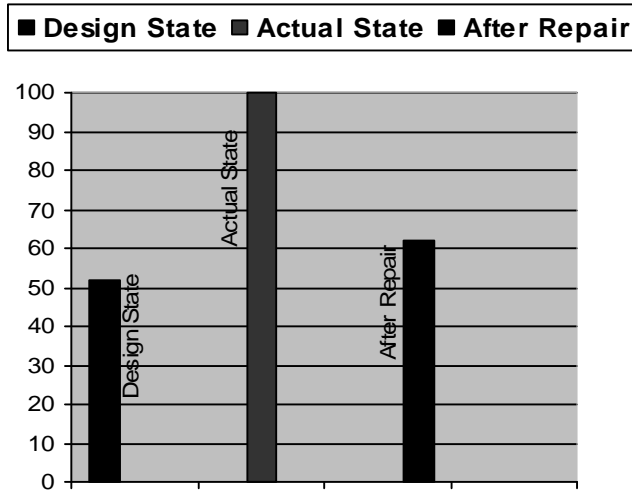
Fig. 12: Service Conditions as a percent of the Actual State before Repair Process

Design state   : is the result of design values using 30-ton truck and concrete C300
Before Repair   : is the state of 60-ton truck loading and deteriorated concrete state
After Repair   : is the state after rehabilitation under 60-ton truck loading.
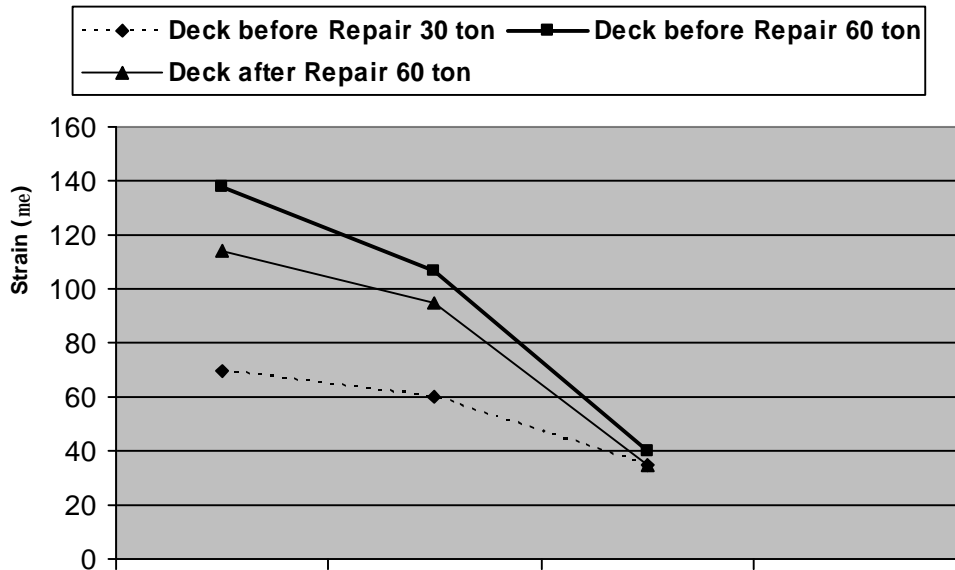
Fig. 13: Strain at Mid span due to truck loading before and after repair

CONCLUSIONS

This paper underscores the importance of defining the reliability of aged bridges especially those constructed during the period of the seventies and the eighties before the first code of reinforced concrete came to the surface that put obvious regulations to quality control issues and design. The bridge taken as case study suffered a plenty of negative parameters due to bad quality control of material and lack of professional workmanship. Moreover, the paper can shed the light on some procedures concerning bridge assessment and future design tasks as follows:

1. Old bridges must be thoroughly revised in respect of present and future traffic needs to avoid the recurrent situation of being subjected to high loading levels exceeding the design limits.
2. Non-destructive testing of concrete (as ultrasonic testing) is fruitful for providing only qualitative data regarding the present concrete and can be perceived as powerful guide for decisive quantitative tests like concrete cores to be conducted at its best locations.
3. Periodic inspection of bridges at a time span not exceeding five years is crucial with an assessment of the quality of material to avoid gratuitous deterioration. The inspection might be reduced to a maximum of two years for bridges located in severe environment.
4. Developments in numerical analysis techniques with accurate problem idealization is a dominant means, when enhanced by consistent constitutive model of the material under study. Precise results can be obtained that can make expensive loading test of old bridges dispensable.
5. Crack model of concrete in the structural analysis provides constructive results in particular the effect of cracking of top slab –due to its transversal behavior- on the concrete Young's and shear modulii and the successive distribution of longitudinal stresses. The crack model highlights the significance of using high quality concrete in the bridge superstructure irrespective of the quantity of the steel bars utilized.
6. Even though analytical models may confirm that a bridge have a reserve load carrying capacity, because of serious defects as concrete distress, fatigue cracks, corrosion and concrete spalling, the reserve may be used and the bridge may be in an unsafe condition. Accordingly, inspection, testing, retrofitting and reliability assessment must be undertaken under the umbrella of performance-based design technique

REFERENCES

1. Natke, H.G. and Yao, J.T.P (1988), "Structural Safety Evaluation Based on System Identification Approaches", Proc. Workshop at Hambrecht/Pfatz, Frieder Vieweg and Sohn, Braunschweig, Germany.
2. Natke, H.G., Tomlinson, G.R. and Yao, J.T.P (1993), "Safety Evaluation Based on Identification Approaches Related to Time Variant and Nonlinear Structures", Proc. Workshop at Hambrecht/Pfatz, Frieder Vieweg and Sohn, Braunschweig, Germany.
3. Stubbs, N. and Osegueda, R. (1990), "Global Damage Detection in Solids-Experimental Verification", International Journal of Analytical and Experimental Modal Analysis, Vol. 5, No. 2, pp.81-97.
4. Pandy, A.K, Biswas, M. and Samman, M.M. (1991), "Damage Detection from Changes in Curvature Mode Shapes", Journal of Sound and Vibration, Vol. 145, pp. 321-332.
5. Biswas, M., Pandey, A.K and Sammnan, M.M (1990) "Diagnostic Experimental Spectral/Modal Analysis of a Highway Bridge", International Journal of Analytical and Experimental Modal Analysis, Vol. 5, pp. 32-42.
6. Farrar, C., Duffey, T.A., Goldman, P.A., Jauregui, D.V. and Vigil, J.S. (1996) "Finite Element Analysis of the 1-40 Bridge over the Rio Grande", Los Alamos National Laboratory Report LA-12979-MS, Los Alamos NM, January.
7. Ahmed, K. Sanli and Mohammed B. Fahmy (2000), "Nondestructive Evaluations of Bridges", Bridge Engineering Conference, 26-30 March, Sharm El-Sheikh, Sinai, Egypt, pp. 225-237.
8. British Standards 5400, Steel, Concrete and Composite Bridges: Part 4: 1990, "Code of Practice of Concrete Bridges".
9. Hesham A. Mahdi and Askar M, (2006), "Rehabilitation of Bridges under the Umbrella of Recent Management Techniques", International conference of Bridge management systems-Monitoring, Assessment and Rehabilitation, Cairo-Egypt, March 2006.
10. Ayman H.H. Khalil and Terry J. Wipf, (2000), "Random Truck excitation for Modal Testing of Bridges", Bridge Engineering Conference, 26-30 March, Sharm El-Sheikh, Sinai, Egypt, pp. 201-212.
11. Abdel-hady H. Hosny and El-Mostafa M. Higazy (2000), "Proposed real time Montoring system for the Suez Canal Cable Stayed Bridge", Bridge Engineering Conference, Sharm El-Sheikh, Egypt, pp 143-152.

12. Diana, (2004), Software package Release (8.0), TNO Institute, Netherlands.
13. Simo, J. C., and Rifai, M. S., (1990)," A class of mixed assumed strain methods and the method of incompatible modes," *Int. J. Num. Meth. Eng. 29*, 1595-1638.
14. Andelfinger, U., and Ramim, E., (1991), "EAS-elements for 2d, 3d, plate and shell structures and their equivalence to HR elements," *Int. J. Num. Meth. Eng. 36* , 1311-1337.
15. De Borst, R., and Nauta, P. Non-orthogonal cracks in a smeared finite element model. Engineering Computations 2 (1985), 35-46.
16. Kupfer, H. B., and Gerstle, K. H., (1973), "Behavior of concrete under biaxial stresses," J. Eng. Mech., ASCE 99, 4, 853-866.
17. AASHTO (1987), "Manual for Bridge Maintenance", Washington D C, USA
18. ECOP (2003), "Egyptian Code of practice of Loads".
19. ECOP (2007), "Egyptian Code of practice of Bridges", (under discussion and preparation).
20. B. Stensvold and O. Ronnestad, (2001), "The Norwegian Bridge Management System- named BRUTUS", fourth symposium on Strait Crossings Bergen- Norway- September.
21. ISO 2394 "General Principles on Reliability for Structures", annex E4 "Specified Reliability Levels"

PREFABRICATED BRIDGE DECK AND SUPERSTRUCTURE SYSTEMS FOR RAPID BRIDGE REPLACEMENT

Sherif Yehia, Ph.D., P.E.
Assistant Professor, Department of Civil and Construction Engineering, Western Michigan University, MI 49008-5316, e-mail: sherif.yehia@wmich.edu
Osama Abudayyeh, Ph.D., P.E.
Associate Dean for Research and Graduate Programs, Professor of Civil and Construction Engineering, Western Michigan University, Kalamazoo, MI, 49008- 5314, e-mail: osama.abudayyeh@wmich.edu
Ammar Zalt
Graduate Research Assistant, Department of Civil and Construction Engineering, Western Michigan University, MI 49008-5316, e-mail: ammar.zalt@wmich.edu
John Bayha
Graduate Research Assistant, Department of Civil and Construction Engineering, Western Michigan University, Kalamazoo, MI 49008-5316, e-mail: john.j.bayha@wmich.edu

ABSTRACT

The condition of the interstate bridge network in the United States is deteriorating as the interstate highway system approaches the end of its service life. Out of the 594,000 bridges nationwide, almost 135,000 are structurally deficient or functionally obsolete, and an additional 3,000 bridges are added to this classification each year. For this reason the demand for bridge repair and replacement is at an all time high and at the same time lengthy construction time and traffic congestion associated with bridge work have become unacceptable to the traveling public. In an effort to remedy lengthy construction of an interstate bridge, the American Association of State Highway Transportation Officials (AASHTO) has partnered with the Federal Highway Administration (FHWA) to develop a system whereby prefabricated bridge elements can be utilized in an easily implemented 'Rapid Bridge Construction' (RBC) method. This paper will highlight the currently used methods of RBC and will present case studies of several bridges that are in service.

Keywords: Rapid bridge construction, prefabricated deck system, prefabricated superstructure system, case study.

INTRODUCTION

Prefabricated bridge construction is the most recent development in prefabrication technology. It is the process through which the elements of a bridge are fabricated offsite and brought to project site in a ready-to-install state. By utilizing the recent advancements in prefabrication technology the fabrication process can be completed in days or even hours rather than in months or years. The degree to which the bridge elements are prefabricated ranges from individual elements, such as caps or deck panels, to completely prefabricated bridges [1].

Prefabricated bridges offer significant advantages such as minimizing traffic disruption, improving work zone safety, minimizing environmental impacts, improving constructability, increases in quality, and lower life-cycle costs [2]. Even with their high initial cost, which is the primary disadvantage of using prefabricated technology, the use of prefabricated bridges may be justified through their ability to minimize delay for the traveling public and the avoidance of excessive lane closures. In addition, the use of high performance materials may enhance the

bridge's durability and performance [3]. Prefabricated bridge elements and systems could be a promising alternative to cast-in-place construction. This technology has achieved a reduction in construction time and decreased the traffic impact, while enhancing the durability and performance, which result in an increase in the life-span of these bridges [4].

The emphasis of this paper has been placed on the deck and superstructure systems which are typically the major structural elements of the bridge that require the most frequent maintenance and replacement. Each prefabricated system discussed in this paper will be followed by a case study.

PREFABRICATED DECK SYSTEM

Concrete deck panels are the most suitable element for prefabrication [3]. The use of these elements eliminates the need to place and remove formwork, which can accelerate the construction phase and improve work zone safety [2]. Different deck systems have been introduced in the literature some of which are:

- Full depth deck panel
- Partial depth deck panel
- NUDECK
- Fiber reinforced polymer deck
- Exodermic full depth deck

Full Depth Deck Panel System

The prefabricated full depth deck panel system is one of the oldest prefabricated systems which have been used in bridge construction. This technology has been used since the 1960s in Japan, the United States, and Canada. It was used primarily for the replacement of deteriorated cast-in-place deck panels as well as for new bridge construction [4]. Full depth deck panels have various designs and construction components such as: transverse joints between the precast panels, connection between the deck and its supporting system, post tensioning in the longitudinal direction, haunches between the top flanges of the supporting system and the deck, and overlay or waterproofing membrane system if needed [5]. Figure 1 shows a scheme of a full depth deck panel.

Longitudinal or transverse closure joints between panels introduce the biggest challenge for using this system and achieving long term durability while minimizing the maintenance costs. The most commonly used closure joints are: post-tensioned, welded, bolted, or passively reinforced [6]. Advantages and disadvantages of full depth deck systems are summarized in Table 1.

Table 1: Advantages and Disadvantages of Full Depth Deck Panel [4, 7, and 8]

Advantages	Disadvantages
Efficient and economical means of replacing a deteriorated bridge deck and a good option for new bridge construction projects.	More expensive than similar cast-in-place concrete decks.
Significant time savings over a cast-in-place slab, through eliminating the curing period for the concrete.	The long-term performance of this system is still not clear.
Eliminates the traffic impact usually caused by extensive concrete formwork.	The seismic performance has not been deeply investigated.
This system can rest either on steel or precast pre-stressed concrete girders.	Longitudinal and transverse joints, which can create reflective cracking that can affect the performance of the system.
Stage construction can be used to replace a deteriorated cast-in-place deck.	
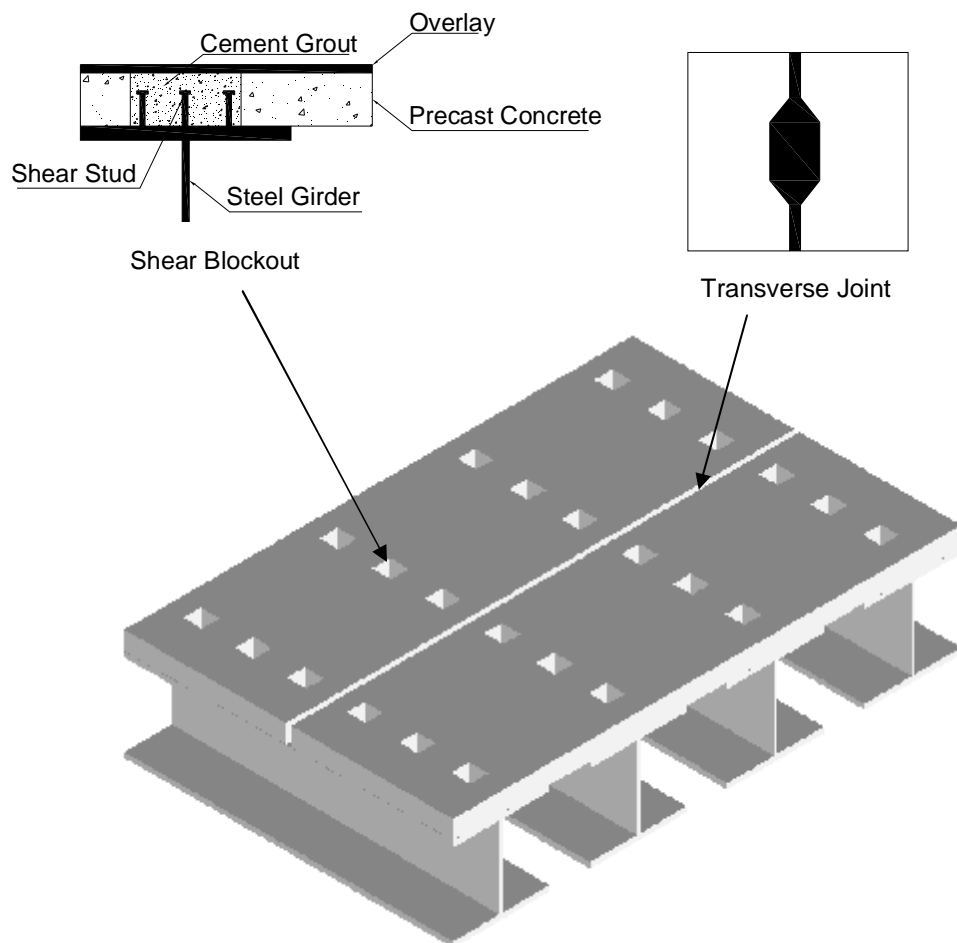
Fig. 1: Scheme of a Full Depth Deck Panel [3]

Case Study: Completed in 1993, the 214 m (700 ft) bridge carrying US 27 over Pitman Creek in southern Kentucky is a heavily traveled and congested bridge that provides a major north-south connection for the area. The deck of this bridge was heavily damaged and required immediate replacement. Using prefabricated full depth deck panels as a choice for the replacement method allowed for a modular type of construction; thereby minimizing traffic impacts, as well as providing a weight savings by reducing the dead load on the bridge's truss system. Project work was done at night, with traffic routed to one lane at 6:00 pm and opened again to two lanes at 6:00 am. Using high early strength concrete allowed the joints between the deck panels to be cured by the time the bridge was opened to traffic the next morning [9].

Partial Depth Deck Panel System

Partial or half depth deck panel systems consist of two parts: the bottom consists of a pre-stressed precast concrete panel that rests directly on the girders and serves as a leave-in-place form for the upper part which is cast-in-place concrete. The pre-stressing reinforcement in the prefabricated panel works as the bottom layer of the reinforcement, while the reinforcement in the top cast-in-place layer functions as the second layer of deck reinforcement [4]. **Figure 2** shows a scheme of the half depth deck system.

The most common problem associated with using this system is the development of cracks in the deck, either longitudinal or transverse. The characterizations of each type of crack is as follows:
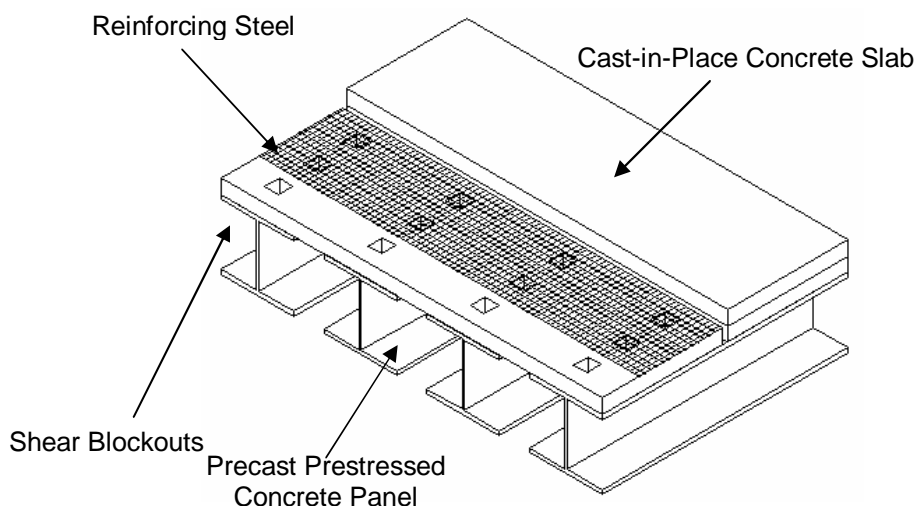
- Longitudinal cracks: this type of crack develops along the panel edges over the girders, and can be attributed to insufficient bearing under the panel for the live loads it is carrying. The effect of these cracks is a reduction in deck stiffness over the girders that may compromise the deck's load transfer mechanism [11].

- Transverse cracks: this type of crack is caused by shrinkage of the cast-in-place concrete, which is restrained from movement by the panels. Literature on this topic indicates that these cracks do not affect the structural behavior of the composite deck [11].

Half depth deck systems provide various advantages and disadvantages some of which are listed in Table 2.

Table 2: Advantages and Disadvantages of Half Depth Deck System [4, 11]

Advantages	Disadvantages
Use of the partial depth deck panel accelerates the construction and reduces the overall construction time for the project.	Requires special handling during moving and construction because the prefabricated panels are so thin.
Partial depth deck panels achieve cost savings over the other commonly used forming systems.	Longitudinal and transverse cracks in the cast-in-place portion are common.
Saves significantly of the costs incurred from site labors.	Durability problems due to the cracking of the cast-in-place portion.
Reduces the amount of concrete and reinforcement required.	The repair of this system is more difficult than traditional systems.

Case Study: Completed in 2001, the 100 m (325 ft) two span bridge over Interstate 5 (I-5) in Tacoma, Washington was replaced using precast stay-in-place deck panels. This system was used to reduce the construction time and minimize the traffic disruption. By using 9 cm (3.5 in) thick precast pre-tensioned panels, the contractor was able to limit the lane closures on the bridge for one week nighttime closures. The bridge in this project utilized a total of 766 panels [9].

Reinforcing Steel

Cast-in-Place Concrete Slab

Shear Blockouts

Precast Prestressed Concrete Panel

**Fig. 2: Scheme of a Half Depth Deck Panel [10]**

NUDECK System

The NUDECK system can be either a full or half depth deck panel. The only difference between NUDECK system and other half or full depth systems is that the NUDECK system covers the entire width of the bridge [12, 13]. The system consists of several components including open gaps over girder lines for shear studs and post tensioning, shear keys between panels, and precast concrete curbs [14]. The following steps outline the NUDECK construction procedures:

1. Determine the elevation of the supporting system and complete its installation
2. Set the precast concrete panels sequentially
3. Grout the shear keys
4. Install the post tensioning strands and perform the post tensioning operations
5. Place a flowable High Performance Concrete (HPC) grout mixture into the post tensioning channel [14]

Table 3 summarizes various advantages and disadvantages of the NUDECK system. Figure 3 shows the scheme of NUDEK system.

Table 3: Advantages and Disadvantages of NUDECK System [12, 13, and 14]

Advantages	Disadvantages
The NUDECK system has a higher construction speed because fewer pieces are required for a typical bridge.	The NUDECK system suffers from the reflective cracking over the transverse joints between the precast panels; due to a lack of continuity in the longitudinal direction.
The materials used in the production of the panel are non-proprietary and inexpensive.	
The NUDECK system has a superior structural performance under cyclic loading.	
This system has almost double the capacity of the conventional stay-in-place panel system.	Lack of long-term performance data.
Cost competitive with traditional bridge systems.	
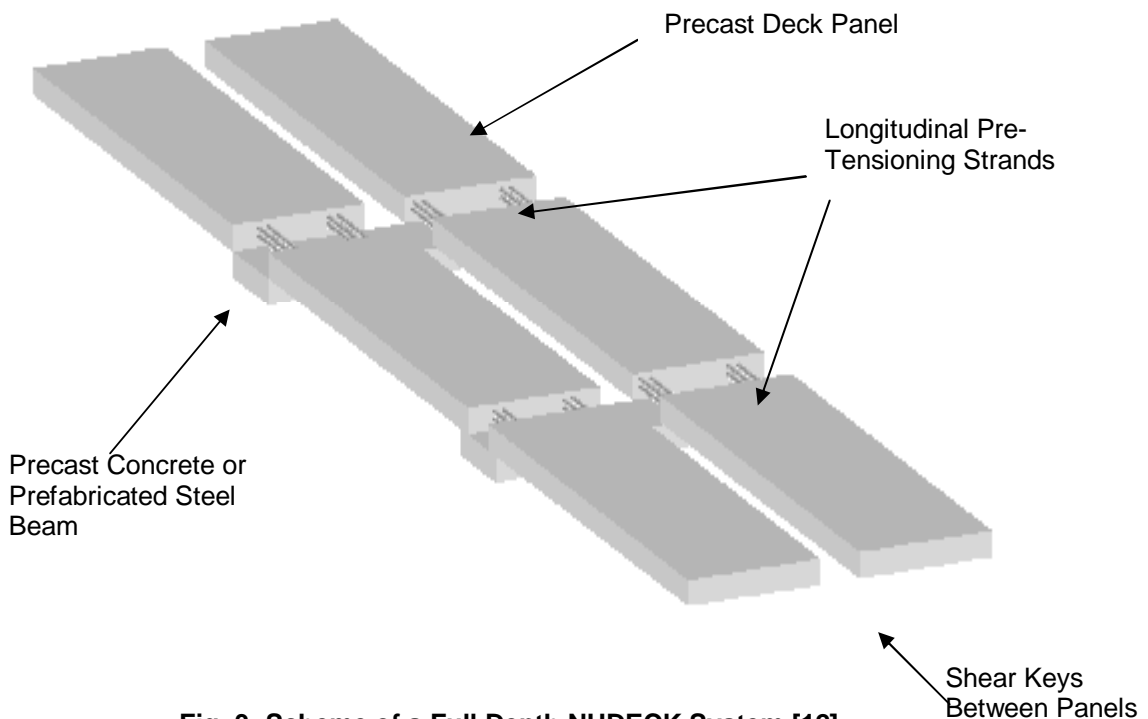
Fig. 3: Scheme of a Full Depth NUDECK System [12]

Case Study: Completed in 2004, the Skyline Bridge in Omaha, Nebraska was the first bridge constructed using the NUDECK system with self compacting concrete mix (SCC); the bridge consisted of two spans, 27 m (89 ft) and 38 m (125 ft) with a 25 degree skew. All the precast panels were shipped to the construction site and erected in place using one crane. It took about 15 minutes to position each panel at each location. The use of this system allows for a significant reduction in construction time (up to 50 percent) and it is expected to increase the service life of the bridge [14].

Fiber Reinforced Polymers Deck System

A fiber reinforcement polymer (FRP) deck system is one of the available alternatives for rapid deck replacement. It combines high strength, small dead loads, and resistance to freeze-thaw action and de-icing salts. The advantage of small dead loads is reflected in short installation times, minimum traffic delays, and an increase in the live load capacity of the bridge [15].

FRP deck systems are suitable for short span bridges up to 9 m (30 ft). However, because this system is more expensive than a more conventional concrete deck, it is valued for its light weight, rapid installation, and corrosion resistance [16]. The types of situations where the use of this system should be considered are:

1. A bridge needs to be widened without imposing large additional loads on the substructure
2. Accelerates the schedule for installing decks or superstructure components to reduce the cost of maintaining and protecting traffic, resulting in reduced congestion
3. Historic structures that must be saved due to their cultural value
4. Superstructures with spans of less than 9 m (30 ft)
5. Bridges used to carry traffic over rivers or other small bodies of water [16]

Advantages and disadvantages some FRP deck systems are summarized in Table 4.

Table 4: Advantages and Disadvantages of FRP Deck System [16]

Advantages	Disadvantages
Light weight, a FRP deck weighs just 1200 Pa (25 psf) compared to a concrete deck which weighs 5700 Pa (119 psf).	Small spans only, up to 9 m (30 ft).
Resistance to de-icing salts and other chemicals.	Thermal stresses may be as large as the stresses resulting from live loads.
Fast installation, elimination of the time consuming forming and curing processes necessary for conventional concrete deck construction.	High initial cost compared to a conventional concrete deck.
Reduces traffic delays, which leads to lower user costs.	Low modulus of elasticity leads to higher deflections.
Less expense maintenance and protection of traffic.	Limited FRP experience within the construction industry.
Long service life, useful life is estimated to be at least 75 years.	Lack of design standards and conventions for the material's characteristics.

Case Study: Completed in 2003, the Howell's Mill Bridge in West Virginia was replaced using a full depth fiber reinforcement polymer (FRP) deck system. The bridge is 75 m (245 ft) long and 10 m (32.5 ft) width and was replaced just in 3 days. The panels were attached to the girders using shear studs/grout system. The use of prefabricated FRP deck panels ensured a long service life for the bridge deck, immunity to chloride-ion induced corrosion, and increased the live-load capacity for the bridge [9].

Exodermic Full Depth Deck System

This system consists of a gird of steel girders at the bottom working with a reinforced concrete slab on the top surface as a composite section. Used in this way, the composite section will allow the reinforced concrete slab to resist the compressive forces and the steel girders to resist the tensile forces. The overall thickness of this system ranges from 15 cm (6 in) to 24 cm (9.5 in), and the total deck weight ranges form 1,870 Pa (39 psf) to 3,550 Pa (74 psf) [17]. There are two designs used for this system. The first design (or original design) has a smooth load transfer between the concrete slab and the steel girder which is achieved using shear studs. The second design (or revised design) is one in which the load transfer is achieved through embedding part of the steel girder in the concrete slab. In general the revised design is less expensive and easier to erect than the original design [17].

Exodermic deck system provides different advantages and disadvantages some of which are listed in Table 5.

Table 5: Advantages and Disadvantaged of Exodermic Deck System [17, 18]

Advantages	Disadvantages
35%-50% less weight than a traditional reinforced concrete deck.	Limited to short spans up to 5.5 m (18 ft), larger spans can be achieved by using larger main bearing bars and/or a thicker concrete slab.
Reduction in the dead load of the structure, and an increase in the live load capacity.	
The efficient use of the materials in an Exodermic deck makes the deck much lighter without sacrificing strength, stiffness, ride quality or expected life.	Although the installation is fairly simple, the construction can be hampered by a complicated and expensive fabrication process.
No special training for the construction crews is required to install this system.	
Simple installation and maintenance.	

Case Study: An exodermic deck system, specifically, the revised design was used successfully in the deck replacement of the Tappan Zee Bridge, in New York in 1998. This system was used to replace a 25.6 m (84 ft) wide deck on the east truss span that carries an area of 26,500 m^2 (285,000 ft^2). The work done during the night hours, and all seven lanes were opened to traffic by 6:00 am. The panel's depth was 19 cm (7.5 in) and the total number of panels used for the project was 1,200 exodermic panels [18].

PREFABRICATED TOTAL SUPERSTRUCTURE SYSTEM

One of the methods to minimize traffic distribution and eliminate work zone traffic congestions is to use a totally prefabricated superstructure. This allows for the prefabrication of units offsite and delivery to the construction site ready to erect in one operation. There are different types of systems that work as prefabricated total superstructure systems. Some of these systems are:

- Inverset superstructure
- Inverted "T" superstructure
- Box beam superstructure
- Segmental superstructure

Inverset Superstructure System

Inverset superstructure system consists of steel girders and a concrete slab. Shear studs are used to transfer shear forces between the slab and the steel beams of this cast-in-place system. The system utilizes a unique upside-down casting of the composite sections. Each section consists of two steel beams cast into a concrete deck of a shippable size [width of 3 m (10 ft) and length of 3.7 m (12.1 ft)] [19]. Figure 4 shows a scheme of the Inverset superstructure system.

The casting process of this system is different from other prefabricated elements and generally follows the following steps:

1. Steel beams for the composite section are placed at the designed spacing
2. The beams are placed upside-down with the shear studs facing downward
3. The concrete deck is cast in formwork supported underneath the steel beams
4. This upside-down orientation causes the steel beams to be pre-stressed by the forces from the dead weight of the assembly.
5. A deflection control device is used at mid-span during the casting process.
6. During casting the top flange of the beam is in tension and the bottom flange in compression as concrete in the forms hardens.
7. After the concrete cures and attains its design strength, the entire unit is turned right side up [18].

Advantages and disadvantages of Inverset superstructure systems are summarized in Table 6.

Table 6: Advantages and Disadvantage of Inverset Superstructure System [18, 19]

Advantages	Disadvantages
Rapid construction, construction can be completed within a few hours, even under traffic loading conditions.	The maximum weight and length of the units must be considered; as they must be fabricated, shipped, and erected in one piece.
The unit can be cast in a standard size or customized to fit any application.	
Reduced superstructure depth which allows for greater clearance underneath the superstructure.	
May be able to span up to 30.5 m (100 ft), with a maximum skew angle of about 45 degrees.	
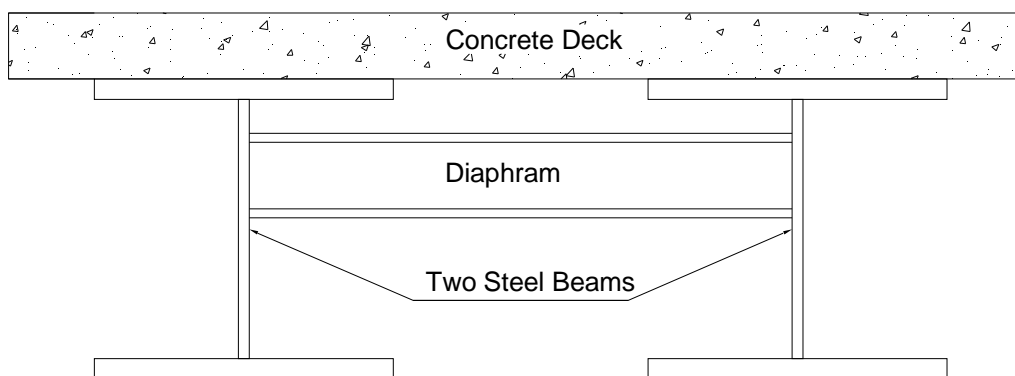
Fig. 4: Scheme of Inverset Total Superstructure System [18]

Case study: The Inverset superstructure system was used to replace part of the Tappan Zee Bridge in New York in1998. Most of the work was done during the nighttime hours between 8:00 pm and 6:00 am, without any traffic distribution. The Inverset superstructure system performed well in the Tappan Zee Bridge and the sections have shown no sign of deterioration during their years of service. Several factors have played into the success of the Tappan Zee Bridge's deck

replacement since its installation in 1998. This should be taken into consideration for any project needing deck replacement such as; careful planning, traffic control, brainstorming as a group, verifying the design and field verification [18].

Inverted "T" Superstructure System

Inverted "T" superstructure system was first used in France and is known as "The Pouter Dalle System." The system is considered effective in eliminating formwork and reducing traffic delays caused by bridge construction. This system consists of inverted "T" beam sections of specified lengths placed next to each other and then made into a composite section with cast-in-place concrete between the webs of the "T's" and over the top of the stems. The span-to-width ratio ranges from 28 to 30, and has a span range from 6 m (20 ft) to 25 m (82 ft), sometimes extending up to 32 m (105 ft) [20]. Figure 5 shows a scheme of the inverted "T" superstructure system.

Precast Inverted T

Cast-in-Place Concrete
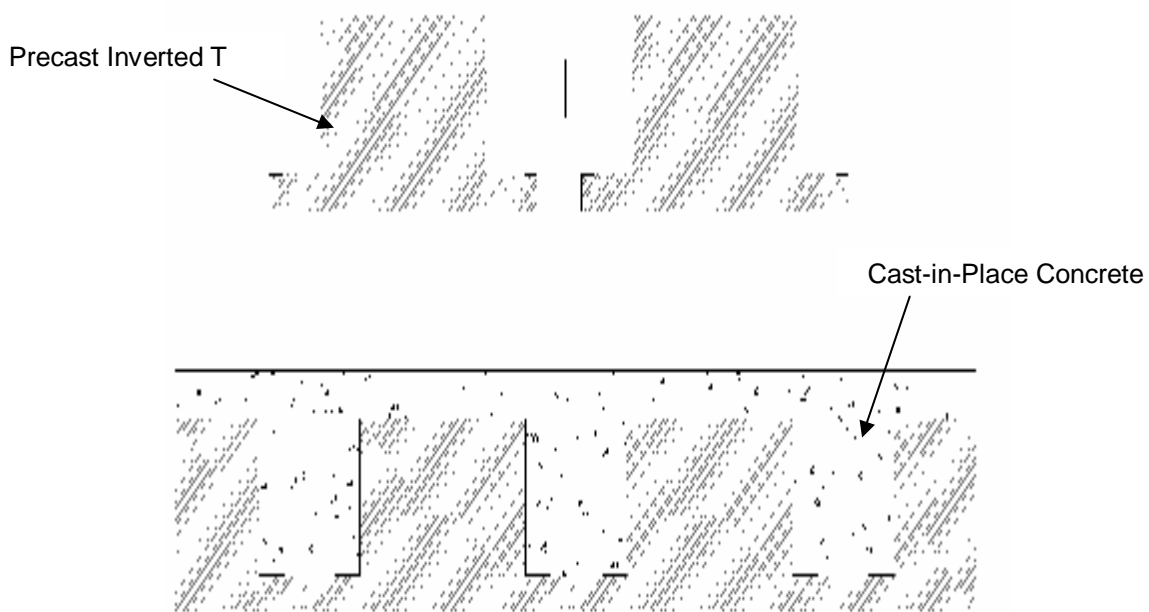
Fig. 5: Scheme of Inverted T Beam System [21]

Inverted "T" superstructure systems provide a number of advantages and disadvantages, some of which are listed in Table 7.

Table 7: Advantages and Disadvantages of Inverted T Superstructure System [20, 21]

Advantages	Disadvantages
The span is limited, but still ranges between 6-32 m (20-105 ft)	This system does not incorporate transverse post tensioning, thus longitudinal cracks may develop.
The system is simply supportive for dead loads and continuously supportive for live loads.	Cracks at longitudinal joints between panels and transverse joints at piers allow chloride intrusion causing corrosion and deterioration of the panels.
Reduced traffic delay from construction operations.	
No concrete form work is necessary.	Somewhat frequent traffic delays from construction operations.
Does not require skilled construction workers for erection.	This system is still in the developmental stage.

Case Study: Completed in 2005, the Center City Bridge, in Minnesota, had been chosen for replacement due to a deck slab that had extensive deteriorated voids. The new system consists of inverted "T" superstructure and a maximum beam length is about 8 m (27 ft). The use of this system allowed the contractor to neglect any formwork, thereby reducing the construction traffic congestion and increasing the clearance under the bridge [21].

Box Beam Superstructure System

The box beam superstructure system is considered as another effective method in eliminating formwork and reducing traffic delays caused by bridge construction. The system consists of box beams placed adjacent to each other and connected together to form a solid superstructure that is easy and quick to erect. The Michigan Department of Transportation (MDOT) considers this type of superstructure the one of choice for spans less than or equal to 30 m (100 ft). Various advantages and disadvantages of the box beam superstructure system are listed in Table 8.

Table 8: Advantages and Disadvantages of Box Girder Superstructure System [22]

Advantages	Disadvantages
Used for both short length bridges 9-18 m (30-60 ft), and medium length bridges 18-30 m (60-100 ft).	This system does not incorporate transverse post tensioning thus longitudinal cracks may develop.
Low life-cycle costs.	Cracks at longitudinal joints between panels and transverse joints at piers allow chloride intrusion causing corrosion and deterioration of the panels.
Quick and easy construction.	
Functions on a simple and reliable design.	Somewhat frequent traffic delays from construction operations.

Case Study: Completed in 2002, NASA Road 1 over Interstate 45 (I-45) Bridge in Texas was replaced using a prefabricated box beam superstructure system, which provided a structure with shallow superstructure structure depth and eliminated most of the deck formwork. All construction occurred during a very short duration; the new bridge was completed just in ten days [9].

Segmental Superstructure System

The segmental superstructure system consists of short sections that can be connected to each other to form the entire superstructure for a bridge. Segmental bridge sections are either precast or cast-in-place sections. The first precast bridge was built in France in 1962, and the first US precast segmental bridge was built in Texas in the second half of the 1900's. Segmental bridges are very economical for long spans of over 92 m (300 ft). It is the design of choice for spanning over deep valleys, wide water crossings, and a crossed highways and existing facilities without the use of costly false work [23]. The segmental superstructure system provides a number of advantages and disadvantages some of which are listed in the Table 9.

Table 9: Advantage and Disadvantages of Segmental Superstructure System [23, 24]

Advantages	Disadvantages
Long spans are possible, up to 92 m (300 ft).	Creep and shrinkage problems have been associated with this RBC system.
Good durability of the finished structure.	
Aesthetically pleasing to the eye	
Erection methods can be easily adapted for safe and rapid construction over existing roadways, rivers, and other obstructions.	
Highly skewed supports are easily accommodated by this system.	

Case Study: This is one of the methods that has been utilized to eliminate the need for a below deck support system and to increase the vertical clearance under a bridge. The use of this system increases the concrete durability and reduces the maintenance cost. New York State was the first and only state in the US to utilize this type of bridge construction. The segmental superstructure system was applied successfully on two New York bridges; Carpenter Road over the Metropolitan Transportation Authority and State Route 17M over State Route 17 in Wallkill, Orange County, both bridges were completed in 1998 [24].

CONCLUDING REMARKS

This paper presented some of the elements and systems that could be used as a prefabricated deck or superstructure system with the emphasis on reducing construction time and enhancing the durability and performance of the bridge. Use of prefabricated technology could double the service life of the bridges while minimizing the maintenance costs. The continued development and utilization of rapid construction techniques will completely revolutionize bridge construction as we know it today.

REFERENCES

1. Freeby, G., Medlock, R., Slagle, S. "Prefabricated Bridge Innovations," Texas Department of Transportation, Texas. <http://www.dot.state.tx.us/publications/bridge/prefabricated_inovations.pdf>.
2. Federal highway administration (FHWA). "Prefabricated bridge elements and systems in Japan and Europe," <http://www.fhwa.dot.gov/bridge/prefab/pbesscan.htm>. (summary report 2004)
3. National cooperative highway research program. (2003). "Prefabricated bridge elements and systems to limit traffic disruption during construction," (NCHRP Synthesis Report 324). < http://www.dot.state.tx.us/publications/bridge/prefabricated_inovations.pdf>.
4. Eberhard, M . Stanton, J. Hieber, D. Wacker, J. (2005). "State of art report on precast concrete system for rapid construction of bridges," University of Washington. (Report number WA-RD 594.1).
5. Issa, M. Yousif, A. Issa, M. (1995). "Construction Procedures for Rapid Replacement of Bridge Decks," Concrete International, 17(2), 49-52. < http://www.concreteinternational.com/pages/index.asp.>.
6. Ralls, L. Hyzak, M. Medlock, R. Wolf, L.(2004). "Prefabricated Bridges – Current U.S. Practice and Issues," Texas Department of Transportation, Texas.< http://www.anippac.org.mx/docscongreso/21.pdf>.
7. Issa, M. Khayat, S. Yousif, A. Kaspar, I. Issa, M. (1995). "Field Performance of Full Depth Precast Concrete Panels in Bridge Deck Reconstruction," PCI Journal, 40, 82-108.
8. Cumon, M. "Rapid Bridge Deck Replacement with Full Depth Precast Concrete Slabs," Transportation Research Record 1712, (paper number. 00-1220).
9. Federal Highway Administration (FHWA). "Prefabricated Bridge Elements and Systems - Superstructure: Decks," <http://www.fhwa.dot.gov/bridge/prefab/decks.htm> (March 14, 2006).
10. Wolf, L. "Texas DOT Experience with Prefabricated Bridge Construction," <http://mceer.buffalo.edu/education/webcast/Accelerated_Bridge_Construction/01Wolf.pdf>, (September 16, 2005).
11. Merrill, B. (2002). "Texas Use of Precast Concrete Stay-in-Place Forms for Bridge Decks," Texas Department of Transportation, (2002 Concrete Bridge Conference).< http://www.dot.state.tx.us/publications/bridge/precast_stay_forms.pdf>.
12. Construction Innovation Forum," NUDECK Innovation Precast Concrete Bridge Deck Panel System," 2004 NOVA Award Nomination 5, <http://www.cif.org/nom2004/nom05_04.pdf)>.

13. Badie, S. Baishya, M. Tadros, M. "NUDECK - A New Pre-Stressed Stay-in-Place Concrete Panel for Bridge Decks," <http://www.ctre.iastate.edu/pubs/crossroads/45nudeck.pdf>. (1998 Transportation Conference Proceedings).

14. Fallaha, S. Sun, S. Ladderty, M. Tadros, M." High Performance Precast Concrete NUDECK Panel System of Nebraska's Skyline Bridge," <https://www.pci.org/pdf/publications/journal/2004/September-October/JL-04-SEPTEMBER-OCTOBER-1.pdf>.

15. Keller, T. "Fiber Reinforced Polymer Bridge Decks - Status Report and Future Prospects" (Swiss Federal Institute of Technology), <http://www.cobrae.org/afbeeldingen/paperkeller.pdf>.

16. Federal Highway Administration (FHWA). "FRP Decks and Superstructure Current Practice," <http://www.fhwa.dot.gov/BRIDGE/frp/deckprac.htm>. (June 8, 2004).

17. Exodermic Bridge Deck, (D. S. BROWN COMPANY),(2003), <www.exodermic.com>.

18. California Department of Transportation. (2003). "Lessons Learned from the Tappan Zee Bridge, New York," <http://ntl.bts.gov/lib/24000/24000/24095/Tappan_Zee_Bridge_Report.pdf>.

19. Smith, J. "Turning Overnight Bridge Replacement Upside Down." <http://www.structuremag.org/archives/2004/october/D-Product%20Watch-October04-v2-CUT.pdf>. (Structure Magazine 2004).

20. Federal Highway Administration (FHWA). "Prefabricated Bridge Elements and Systems in Japan and Europe," <http://www.fhwa.dot.gov/bridge/prefab/pbesscan.htm>. (Summary Report 2004)

21. Hagen, K. Ellis, S. Fishbin, J. Molnau, K. Wolhowe, E Dorgan, D. "Development and Construction of Precast Inverted T System for Expediting a Minnesota Slab Span Bridge Project," (2005 Concrete Bridge Conference).< http://www3.dot.state.mn.us/bridge/PrecastSlabSystem/MnDOT-Inv%20T_Final.DOC.pdf>.

22. Michigan Department of Transportation (MDOT), (2005). "Box Beam Concerns Found Under the Bridge," <http://michigan.gov/documents/MDOT_RR-102_143535_7.pdf>. (Research record number: 102).

23. Federal Highway Administration (FHWA). "Segmental Concrete Bridge Design and Construction Practices". <http://www.fhwa.dot.gov/BRIDGE/segmental/task152.htm>.

24. Federal highway administration (FHWA). "The First Channels Bridge," <http://www.tfhrc.gov/pubrds/septoct98/channel.htm>. (1998· Vol. 62· No. 2).

EXPERIMENTAL STUDY OF MONO-SYMMETRIC OVER-HANGING I-BEAMS STEEL SECTIONS

Prof. Dr. Hamdy A. Mohsen
Professor of Steel Structures, Structural Engineering Department, Ain-Shams University, Cairo
Dr. Ashraf M. Fadel
Associate Professor, Structural and Steel Structures Department, Housing & Building National Research Center, Cairo
Dr. Abdel-Rahim B. Abdel-Rahim
Assistant Professor, Structural Engineering Department, Ain-Shams University, Cairo
Bassem L. Gindi
Lecturer Assistant, Structural and Steel Structures Department, Housing & Building National Research Center, Cairo

ABSTRACT

An experimental program was constructed to investigate the elastic and inelastic lateral-torsional buckling behavior of mono-symmetric over-hanging I-beam sections bent about the major axis of bending. Six full-scale over-hanging beams were tested. The ratios of the over-hanging length to the back span length were 0.5, 1.0, and 1.5. The tip of the cantilever was either laterally and torsionally restrained or laterally free. The specimens were subjected to concentrated load applied to the top flange at the tip of the cantilever. A comparison between the experimental results, the AISC Specification [1] and the BS5950 [5] was performed by using the effective buckling length coefficient *K* suggested by Nethercot [7]. The comparison shows that the results computed by the standards and specifications ranged from conservative to very conservative. In addition, using the effective buckling length coefficients to calculate the ultimate loads were not suitable for mono-symmetric over-hanging I-beam sections.

Keywords: Steel, Experimental, Mono-Symmetric Section, Over-Hanging Beam.

INTRODUCTION

The design of the mono-symmetric over-hanging I-beam did not take the same interest in any of the standards and specifications as that for the double symmetric I-beams. The effective buckling length coefficients, specified in the current standards and specifications were defined by D.A. Nethercot [7] and were proved only for the double symmetric I-section. Most of thin-walled beams had a good resistance in bending about the major axis and a low resistance in bending about the weak axis. Also, it has a low resistance in torsion. For unrestrained beams, when bend about its major axis, this exhibit instability and may suddenly go in lateral-torsional behavior. The lateral-torsional buckling was a limit state that may often control the design of steel beams.

Lateral buckling of beams can be classified into three major categories, lateral-torsional buckling, local buckling, and distortional buckling.

Lateral-torsional buckling was the simultaneous out-of-plan deflection and twisting of the beam without deformation of the cross-section.

Local buckling was generally a plate buckling in the flange and/or web of the beam without overall lateral deflection or twisting. Any significant deformations are limited to a small region along the length of the beam.

Distortional buckling was the simultaneous occurrence of lateral deflections and cross sectional distortion at buckling. Short beams with slender webs were quite susceptible to the distortion buckling mode. The buckling characteristics depend on a variety of geometric and loading parameters. The combined effect of mono-symmetric section and load position above and

below the shear center were studied, by using the finite integral method, and verified experimentally, on the elastic critical load of simply supported and cantilever beams by Anderson and Trahair [11]. Trahair [15] carried out a series of experiments to obtain the elastic buckling behavior of simply supported and continuous I-beams in order to obtain experimental confirmation of the influence of individual elastic end-restraints on the elastic buckling on symmetrical beam and of combinations of elastic end-restraints on symmetrical beam and propped cantilevers, which were prevented from twisting at the ends. Where Fukumoto, Itoh and Hahlori [18] studied experimentally the effect of the adjacent non-loaded span on the lateral buckling strength and deformation of the critical loaded span. Based on this study, the effective length concept, using the inflection points, was recommended for evaluating the ultimate strength of continuous beam. Corona and Ellison [8], [13] present the results of a combined experimental, analytical, and numerical study of plastic buckling of T-beam subjected to pure bending. The influence of initial imperfections on the response and collapse of the T-beams was studied about the major axis. The study showed that the behavior of the buckled beams was sensitive to the geometric imperfections. Kubo and Fukumoto [12] tested welded I- beam shapes with slender sections under concentrated load at the mid span of the compression flange. The interaction between the local and lateral-torsional buckling behavior was investigated in the inelastic buckling range. Kitiporcha and Trahair [16] presented a simpler, and efficient accurate form for the elastic lateral-torsional buckling of mono-symmetric I-beam and approximate formula for mono-symmetry section property (b_x).

In this study, the elastic and inelastic lateral-torsional buckling of over-hanging beams with mono-symmetric I-section subjected to concentrated load applied to the top flange at the tip of the cantilever were studied experimentally. The ultimate loads obtained experimentally were compared to those computed by AISC Specification [1] and BS5950 [5] taking into consideration the effective buckling length coefficient K suggested by Nethercot [7] to verify the validity of these coefficients.

SPECIMENS AND TESTING

Six full-scale specimens of over-hanging mono-symmetric I-beam sections were tested at the Reinforced Concrete laboratory of the Housing and Building National Research Center. The flange plates were welded to the web plate using two sided fillet weld of size 4 mm each. Stiffener plates were welded to the section plates using 4 mm size fillet welds. The ratios of the over-hanging length to the back span length, L_2/L_1, were 0.5, 1.0 and 1.5, as shown in Fig. 1.a. The nominal dimensions of the cross sections, width-to-thickness ratios of the component plates of the specimens and tip boundary conditions were listed in Table 1, and shown in Fig. 1.b.

Table 1: Average Measured Dimensions of Specimens and Tip Lateral Condition

SPECIMEN	h (mm)	t_w (mm)	b_1 (mm)	t_1 (mm)	b_2 (mm)	t_2 (mm)	L_1 (mm)	L_2 (mm)	h/t_w	$b_2/2t_2$	TIP BOUNDARY CONDITION
OH-1	200	7.4	68	8.2	101	8.4	2000	2000	27.0	6.01	* R
OH-2	200	6.0	60	8.0	100	8.0	2000	2000	33.3	6.25	***T
OH-3	200	5.0	61	8.0	101	8.0	2000	1000	40.0	6.31	*R
OH-4	202	5.5	61	8.0	101	8.0	2000	1000	36.7	6.31	**F
OH-5	200	6.0	60	8.0	101	8.0	2000	2996	33.3	6.31	*R
OH-6	201	6.0	62	8.0	101	8.0	2000	2997	33.5	6.31	**F

*R: Laterally and Torsionally Restrained,****F**: Laterally   Free,   *****T**: Top   Flange   Laterally Restrained

a: Specimen Layout

Fig. 1 Specimen Dimensions

b: Typical Cross-Section
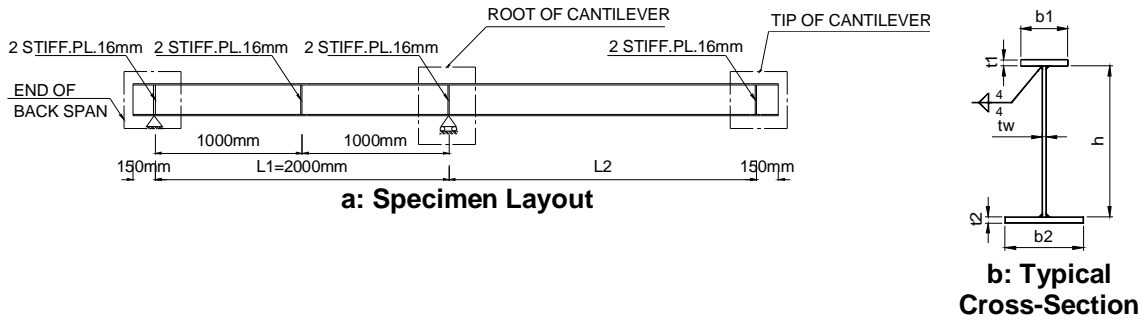
GEOMETRICAL IMPERFECTION

An initial check of all specimens was performed and showed that the flanges of the specimens bent as shown in Fig. 2.a. The warpage of the flanges, D, was listed in Table 2. These measured values were less than the permissible maximum limits given by the Egyptian Code of Practice [9], except those of the bottom flange of specimens OH-1 and OH-6. The out-of-plan deflection, $D1$, Fig. 2.b, was measured at intervals of 500 mm along the length of the specimen and was listed in Table 3. The measured values were less than the allowable limits given in the Egyptian Code of Practice [9], except those of specimens OH-1, OH-2, OH-5 and OH-6, which exceeded the code limits, as listed in Table 3. These measured values of the geometrical imperfections will be put into consideration in the finite element model.
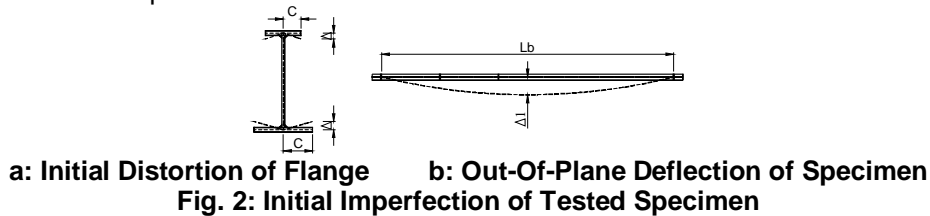

a: Initial Distortion of Flange   b: Out-Of-Plane Deflection of Specimen
Fig. 2: Initial Imperfection of Tested Specimen

Table 2: Average Measured Flange Imperfection

SPECIMEN	TOP FLANGE		BOTTOM FLANGE	
	D mm	D_{all} mm	D mm	D_{all} mm
OH-1	0.3		6.0	
OH-2	2.0		2.0	
OH-3	1.7	0.12	0.4	0.20
OH-4	6.0		0.0	
OH-5	4.0		2.0	
OH-6	4.0		7.0	
According to the E.C.P.2001 [9], the allowable imperfection $\Delta \leq C/250 \leq 6.0$ mm				

Table 3: Average Measured Out-of-Plan Straightness for the Overall Length of the Specimen

| SPECIMEN	D1 Mm	$D1_{al}$ mm
OH-1	10	4
OH-2	16	4
OH-3	2	3
OH-4	3	3
OH-5	6	6
OH-6	8	6
According to the E.C.P.2001 [9], the maximum allowable imperfection $L_b/1000$		

TENSILE COUPON TEST

To conduct proper analysis of the results, it was important to determine the mechanical properties of the steel used. The obtained mechanical properties were: the yield strength (F_y); the elastic modulus (E); and the ultimate strength (F_u). The Poisson's ratio (μ) was assumed 0.3. In total, six standard tension coupons were cut from the compression flange plates of each specimen and tested according to the ASTM A370-97a [2]. The elastic modulus was determined according to the ASTM E 111-97 Standard [3]. Two 10 mm strain gages were placed in the longitudinal direction at the mid-length of the coupon on both sides. The

interpretation of data was carried out by a combination of regression analysis and the 0.2% offset method, according to the ASTM E111-97 Standard [3], as shown in Fig. 3.b. A typical stress-strain curve of a coupon cut from the compression flange of specimen OH-1 was presented in Fig. 3.a.The mechanical properties of all coupons, as well as the average and the standard deviation, are summarized in Table 4. The tested specimens showed steel properties almost identical to the properties of steel type ASTM A607 Grade 45 [4].

Table 4: Mechanical Properties of the Tested Coupon Cut from Compression Flanges

SPECIMEN	F_y t/cm^2	F_u t/cm^2	E t/cm^2
OH-1	3.03	4.3	2199
OH-2	2.99	4.2	2042
OH-3	2.95	4.1	2095
OH-4	2.82	4.01	2021
OH-5	2.80	4.07	2106
OH-6	2.96	4.19	2041
Average	2.92	4.14	2084
Standard Deviation	0.091	0.105	65.06
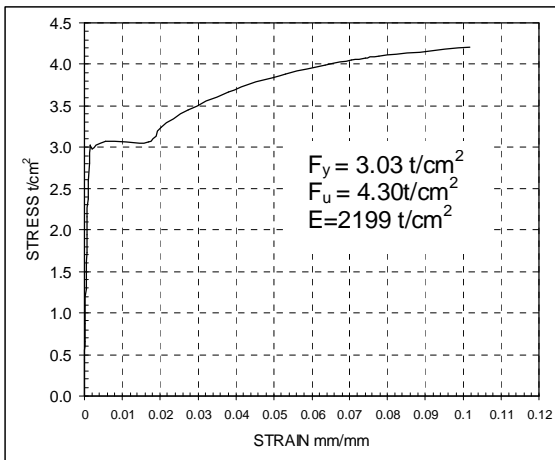
Fig. 3.a: Typical Stress-Strain Curve of a Tested Coupon Cut from the Compression Flange of Specimen OH-1
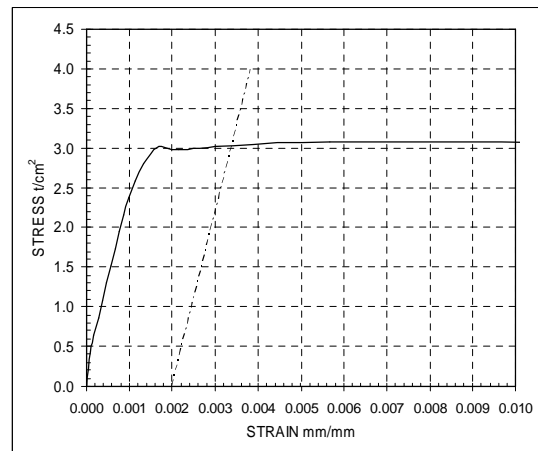
Fig. 3.b: Regression Analysis and 0.2% Offset Method of a Tested Coupon Cut from the Compression Flange of Specimen OH-1

TEST SETUP

A great effort and time had been spent in designing and constructing the test setup to study the expected deformation and behavior of the specimens. All specimens were tested using the setup shown in Fig.4. The specimens were loaded downward at the tip point of the cantilever by pushing the upper flange by a hydraulic jack. Four steel beds were used to locate the vertical and lateral supports, as shown in Fig.4

Load Equipment

A hydraulic jack of 10 ton capacity and 260 mm stroke range, was used at the loading-point. The jack was placed to react on the test frame and the load was applied to the top flange of the beam at the tip of the cantilever. The load cell was placed between the hydraulic jack and the specimen. A cylinder was welded to the top load-cell plate, as shown in Fig.4.The cylinder allowed the top plate to be in full contact with the top flange of the specimen and, in the same time, the hinge allowed the specimen to rotate at the loading point.

Lateral-Supporting Frames

Two lateral supports were placed at the mid-length of the back span and at the tip of the cantilever, for the case of the tip laterally and torsionally restrained, as shown in Fig. 5. When the tip of the cantilever was laterally unrestrained, the lateral support was placed at the mid-length of the back span. In addition, the end support and the root of the cantilever were restrained by using two angles having cross section of L60x60x6, which was welded to a plate and bolted to the structural steel bed. Acrylic sheets were placed between the column supports and the specimen to allow the specimen to displace vertically with minimum friction.

TEST PROCEDURE

Specimen Preparation

The following procedure had been followed in preparing each specimen for testing:
i)   The specimens were cleaned from rust.
ii) The dimensions of the specimens were recorded,
iii) The specimens were positioned in the test setup using an overhead crane.
iv) The specimens were attached to the vertical and lateral supports.
v) The specimens were leveled and aligned.
vi) The acrylic sheets were placed between the specimen and the lateral supporting columns.
The strain gages were mounted at the desired locations.
vii) The imperfection of the flanges and the web were determined.
viii)   All dial gages and LVDTs were positioned at the desired location by magnetic bases and metal stands, as shown in Fig. 6 and Fig. 7.
ix) All instrumentation was connected to the Data Acquisition System.

Testing the Specimen

Each test started by adjusting the loading jacks so that contact with the top flange of the specimen was achieved. The load cells at the load positions and at the ends were checked. Initial readings of all used instrumentation were then recorded. The specimens were loaded using an increment load of 100 kg to allow for the readings of the dial gages to be recorded. Visual observations were also made during the test. Loading of the specimens was terminated after the maximum load was achieved and the recorded load reduced below the maximum load achieved. Once the recorded load started to drop, it was difficult to maintain load control. This was due to the failure of the specimen.

INSTRUMENTATION

The instrumentation used in the experimental investigation were selected to measure:
i) The applied load at the tip of the cantilever and the supports;
ii) The vertical and lateral displacements of the specimens at the tip of the cantilever;
iv) The vertical and lateral deformations of the specimens at the lateral and vertical supports for each case; and
iv) The strains at the root of the cantilever of the specimens.

Load Measurements

The loads were applied through hydraulic jack, as shown in Fig.4. A pre-calibrated load cell was used to monitor and control the applied load.
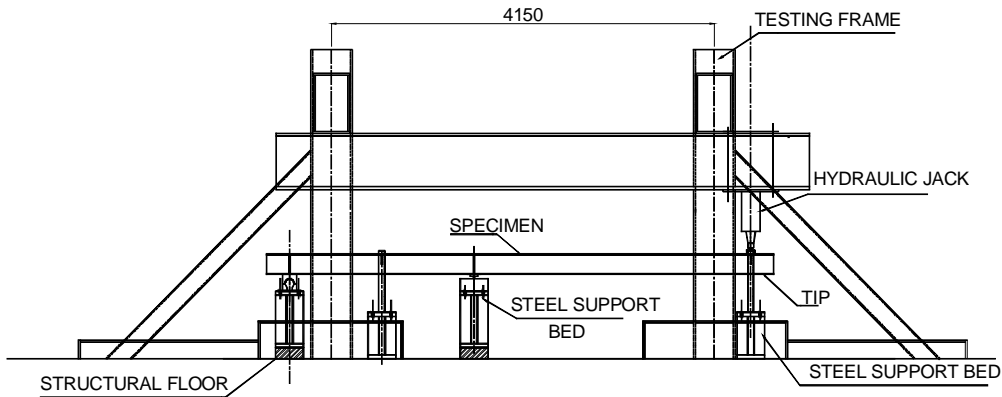
Fig. 4: Test Setup

Fig. 5: Lateral Support at Tip
Vertical and Horizontal Displacement Measurements

Linear Variable Differential Transducers LVDTs and dial gages were used to measure the vertical and lateral displacements of the specimens at various locations along their spans. Two LVDTs were placed to monitor the vertical displacement, one at the tip of the cantilever having stroke length of 160mm and the other at the mid-length of the back span with stroke length of 50mm. Two LVDTs were placed at the top and the bottom flanges to monitor the horizontal displacements. For the laterally restrained tip beams, the two LVDTs were located at the mid-length of the cantilever part. For laterally free beams, the two LVDTs were located at the tip of the cantilever, as shown in Fig. 6 and Fig. 7, respectively. The measured vertical displacements of each specimen versus the load were plotted in Fig. 8.

a: Web
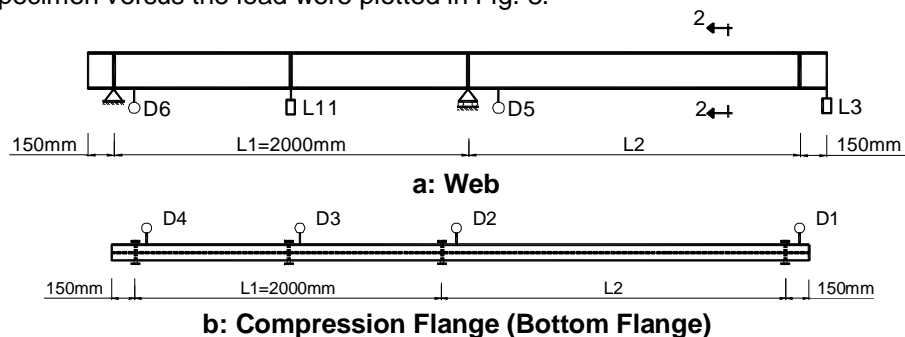
b: Compression Flange (Bottom Flange)
Fig. 6: LVDT'S and Dial Gage Distribution For laterally Restrained Beams

Four dial gages were placed to monitor the lateral movements of the lateral supports, at the tip of the cantilever, at the mid-length of the back span, at end support and at the root. In addition, two vertical dial gages were placed at the bottom flange to monitor the vertical movement under the end and the root supports.
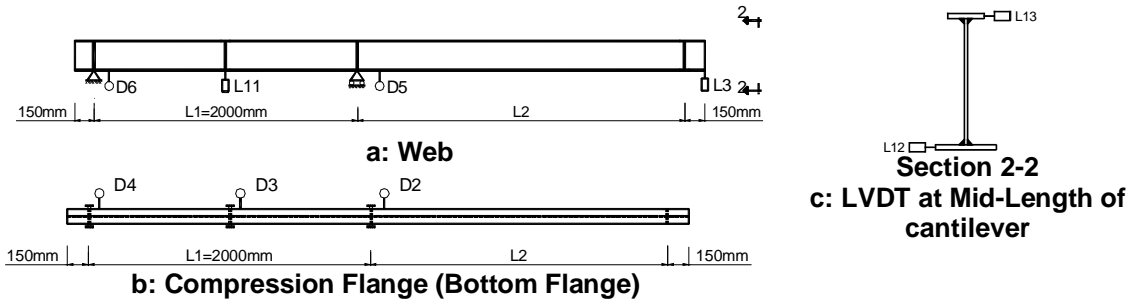

a: Web

b: Compression Flange (Bottom Flange)

Section 2-2
c: LVDT at Mid-Length of cantilever

Fig. 7: LVDT'S and Dial Gages Distribution for Tip Free
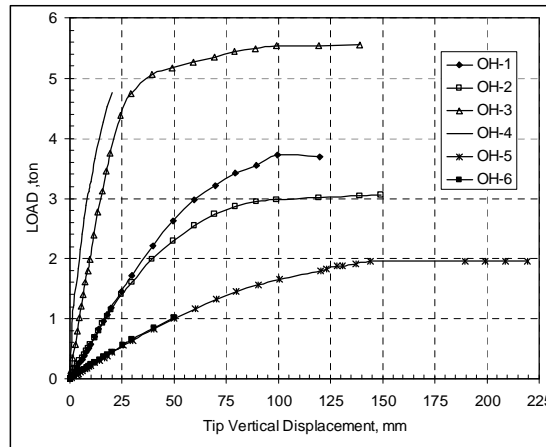

Fig. 8: Vertical Displacement Measured at the Tip of Cantilever
Strain Measurements

To measure the longitudinal strains at the root of the cantilever, seven electrical-resistance strain gages were used in each specimen. The strain gages had 10 mm gage length and 120 ohm resistance. The gages were mounted according to the specified procedures by the manufactures. The locations of the strain gages were cleaned from rust and oil before mounting the strain gages. Two strain gages were placed on the web at distance of 30 mm from the tension and compression flanges. One strain gage was placed at the mid-width of the tension flange. Another series of four strain gages were placed on both sides of the compression flange, so that each pair measures the strain at the same point of the compression flange of each specimen, the strain gage was located at 20 mm from the edge of the flange Fig. 9 shows schematically, the locations of all used strain gages. Fig. 10 through Fig. 14 show the Load-Strain relationship measured at the root of the cantilever for each specimen.
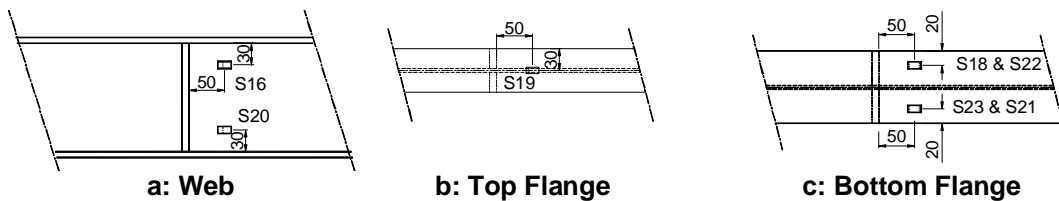

a: Web   **b: Top Flange**   **c: Bottom Flange**

Fig. 9: Strain Gage Distribution at the Root of Cantilever
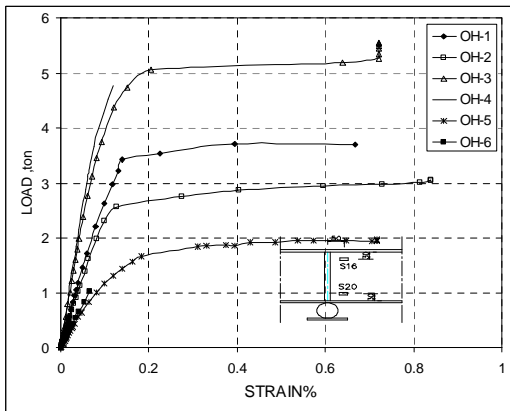
Fig. 10: The Longitudinal Strain at Web Tension Zone for S16
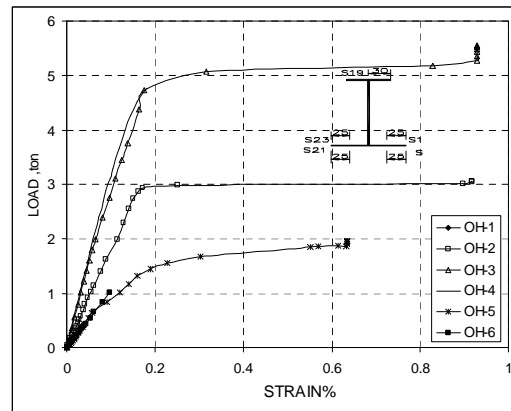
Fig. 11: The Longitudinal Strain at Tension Flange for S19
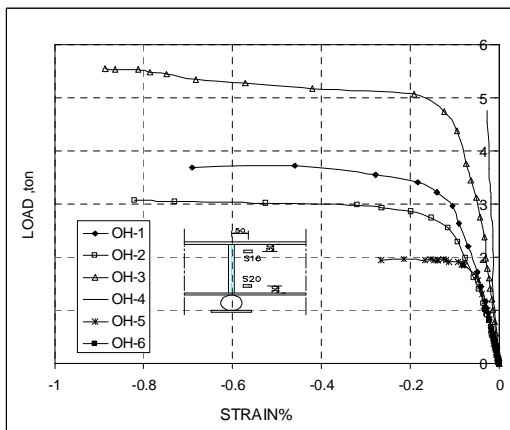
Fig. 12: The Longitudinal Strain at Web Compression Zone for S2
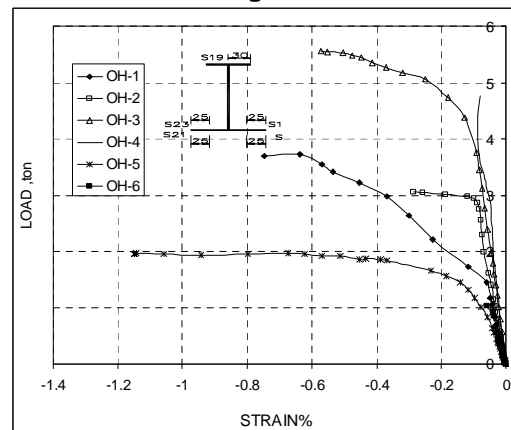
Fig. 13: the Longitudinal Strain at Compression Flange for S18 & S22
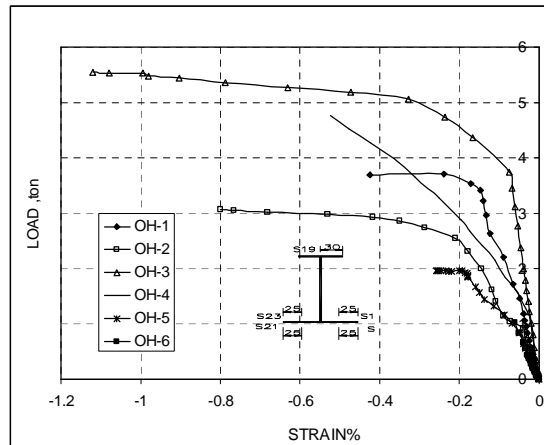
Fig. 14: The Longitudinal Strain at Compression Flange for S21 & S23

EXPERIMENTAL RESULTS

The behavior of the six tested specimens was analyzed and the experimental results were discussed as follows;

The failure mode of each specimen was shown in Fig. 15 through Fig. 20. The failure of specimens (OH-1) and (OH-2) was due to In-plane bending, as shown in Fig. 15 and Fig. 16. The ratios of the ultimate moment capacities to the plastic moments of the section (M_u/M_p) at failure were 1.12 and 1.09 for specimen OH-1 and OH-2, respectively. The failure mode of the

specimen OH-3 was due to flange local buckling. The failure occured at the root of the cantilever, as shown in Fig. 17.a and Fig. 17.b, the (M_u/M_p) ratio was 1.06. The failure mode of the specimens OH-4 and OH-6, where the tip of the cantilever was laterally free, was due to lateral torsional buckling, as shown in Fig. 18 and Fig.20. The (M_u/M_p) ratios were 0.90 and 0.54 for the studied short specimens (OH-4) and the studied long specimen (OH-6), respectively. The specimen OH-5 was laterally restrained at the tip of the cantilever. The specimen failed due to inelastic lateral buckling which occurred at the mid-length of the cantilever, as shown in Fig. 19.a and Fig. 19.b, and the (M_u/M_p) was 1.11. In practice, the rotation of plastic hinge causes the material to strain-harden and the bending moment can increase above the nominal fully plastic moment. In addition, the longitudinal stress in the web available for resisting the bending moment was reduced below the yield stress due to shear stress in the web. In tern, the plastic modulus of the section was reduced [10].

Fig. 15: Specimen OH-1 at Failure Due toIn-Plane Bending

Fig. 16: Specimen OH-2 at Failure Due to In-Plane Bending

Fig. 17: Specimen OH-3 at Failure Due to Local Buckling at Root

Fig. 18: Specimen OH-4 at Failure Due to Lateral-Torsional Buckling

Fig. 19.a: Specimen OH-5 at Failure Due to Lateral Torsional Buckling

Fig. 19.b Specimen OH-5 at Failure Due to Lateral-Torsional Buckling, Maximum Lateral Displacement at Mid-Span of Cantilever

Fig. 20.a: Specimen OH-6 at Failure Due to Lateral Torsional Buckling

Fig. 20.b Specimen OH-6 at Failure Due to Lateral Torsional Buckling

AISC SPECIFICATION, BS 5950 AND EXPERIMENTAL RESULTS COMPARISON

A comparison between the ultimate loads obtained experimentally and those computed by the AISC Specifications [1] and BS5950 [5] was performed and shown in Table 5. The considered effective buckling length coefficient K for specimens OH-1, OH-3 and OH-5 was 1.5 and 2.5 for specimens OH-2, OH-4 and OH-6, as suggested by Nethercot [7]. In this comparison, when the tip of the cantilever was laterally and torsionally restrained, the moment magnification factor C_b was assumed to be 1.67 and 1.75 as recommended in the AISC Specifications [1] and BS5950 [5], respectively. However, when the tip was laterally free, the C_b was assumed to be unity.

As shown in Table 5, the ultimate loads computed according to the AISC Specification [1] and BS5950 [5] were very conservative when compared to those obtained experimentally, especially when the cantilever length was increased. The ultimate loads computed according to the BS5950 [5] were conservative when compared to those computed according to the AISC Specification [1]. The ultimate loads computed by using the effective buckling coefficient, K=2.5, for laterally free tip, were more conservative than those computed by using the effective buckling coefficient, K=1.5, for laterally and torsionally restrained tip.

Table 5: Comparison between the Ultimate Load Obtained Experimentally, AISC Specification and BS 5950

SPECIMEN	P_u Experimental ton	P_u AISC ton	P_u BS5950 ton	P_u Experimental / P_u AISC	P_u Experimental / P_u BS5950
OH-1	3.70	3.29	2.64	1.12	1.51
OH-2	3.06	1.06	0.73	2.88	4.19
OH-3	5.55	5.44	5.44	1.02	1.02
OH-4	4.76	4.43	3.11	1.07	1.56
OH-5	1.95	1.379	0.98	1.41	1.98
OH-6	1.03	0.449	0.324	2.29	3.17

SUMMERY

An extensive experimental program was conducted to investigate the elastic and inelastic lateral torsional buckling behavior of over-hanging mono-symmetry I- beam section. Six full-scale over-hanging beams were tested. The web height-to-thickness ratio (h/t_w) was 33.33. The width-to-thickness ratio ($b_2/2t_f$) for compression flange was 6.25, which meet the compact limits for web and flanges according to AISC Specifications 2005 [1] and E.C.P 2001 [9]. The over-hanging beam was subjected to a concentrated load applied at the top flange of the tip of the cantilever. The end support and root of the cantilever are laterally and torsionally restrained at the top and bottom flanges (fork support), in addition to the mid-length of the back span to prevent lateral torsional buckling at the back span. Two cases of tip boundary conditions were studied, the first one was laterally and torsionally restrained, and the second was free. A comparison between the ultimate loads obtained experimentally and those computed by AISC Specification [1] and BS5950 [5] was performed.

CONCLUSIONS

The computed ultimate loads according to the AISC specification [1] and BS5950 [5] show that the results were ranged from conservative to very conservative, when compared to the results obtained experimentally. In addition, the effective buckling length coefficients according to the standards and specifications were not suitable for calculating the ultimate loads for the mono-symmetric over-hanging I-beam sections.

ACKNOWLEDGMENT

REFERENCES

1. American Institute of Steel Construction, (2005), "Load and Resistance Factor Design", Specifications for Structure Steel Building.
2. American Society for Testing and Materials, (1997), ASTM A 370-97a "Standard Test Methods and Definitions for Mechanical Testing of Steel Products".
3. American Society for Testing and Materials, (1997), ASTM E111-97 "Standard Test Method for Young's Modulus, Tangent Modulus, and Chord Modulus".
4. American Society for Testing and Materials, (1998), ASTM A607-98 "Standard Specification for Steel, Sheet and Strip, High-Strength, Low-Alloy, Columbium or Vanadium, or Both, Hot-Rolled and Cold-Roled".
5. BS 5950: Part1: (1990). British Standard Part1 Code of Practice for design in simple and Continuous Construction: hot rolled Section.
6. Charles G. Salmon and Johan E. Johnson (1993) "Steel Structures, Design and Behavior, Emphasizing Load and Resistance Factor Design",HaperCollins College Publishers.

7. D. A. Nethercot (1973) "The Effective Length of Cantilevers as Governed by Lateral Buckling" The Structural Engineering , Vol. 51, No. 5 May, pp.161-168.
8. Edmundo Corona, Mark S. Ellison (1997) " Plastic Buckling of T-Beam Under Pure Beding" Journal of Structural Engineering, ASCE, Vol. 123, No. 5, May, pp.2245-2262.
9. Egyptian Code of Practice for Steel Construction and Bridges (A.S.D),code No.(205),(2001).
10. John Baker and Jacques Heyman (1969), "Plastic Design of Frames- Fundamentals" CAMBERIDGE, at the Uuniversity Press.
11. John M. Anderson and Nicholas S. Trahair (1972) "Stability of Mono-symmetric Beams and Cantilevers", Journal of Structural Engineering, ASCE, Vol. 98, No.1, pp.269-286.
12. Masahiro Kubo and Yuhshi Fukumoto (1988) "Lateral-Torsional Buckling of Thin-Walled I-Beams" Journal of Structural Engineering, ASCE, Vol. 114, No.4, pp.818-825.
13. Mark S. Ellison and Edmundo Corona (1998) "Plastic Collapse Analysis of T-Beam Under Bending"Journal of Structural Engineering,ASCE,Vol.124, No.8,August,pp.818-825.
14. N.S. Trahair, (1993) "Flexural-Torsional Buckling of Structures" 1rd edition by Spon Press.
15. N.S. Trahair (1969) "Elastic Stability of Continuous Beams" Journal of Structural Division, ASCE, Vol. 95, No. ST6, June, pp.1295-1312.
16. Sritawat Kitipornchai and Nicholas S. Trahair (1980) "Buckling Properties of Mono-Symmetric I-Beams" Journal of Structural Division, ASCE, Vol.106, No.ST5 May.
17. Theodore V. Galambos (1988) "Guide to Stability Design Criteria for Metal Structures"4th Edition, John Wiley & Sons, Inc.
18. Yuhshi Fukumoto, Yoshito Itoh and Ryoji Hahlori (1982) " Lateral Buckling Tests on Welded Continuous Beam" Journal of Structural Engineering, ASCE, Vol.106, No.ST10, October.

ANALYSIS AND TREATEMENT OF DEFECTED SLABS ON GRADE EXPOSED TO MOVING VEHICLES

Ashraf M. Eid
Soil Mechanics Department, Housing and Building Research Center
Email: r5family2004@yahoo.com
Mohamed Elassaly
Civil Engineering Department, Cairo University, Fayoum Branch

ABSTRACT

The slab on grade of a "Gas Station", along the ring road, Kattamiya, Cairo, had suffered from many apparent and obvious cracks in almost all R.C. slabs designated for motor vehicle. These defects, in gas station, were noticed only three months after the station was opened for public service. The station suffered from defects in shrinkage joints, particularly in the heavy truck area. Also, there was clear separation between the curb and slabs, tilting in the perimeter walls in addition to cracks in areas around inspection chambers and relative settlement between the adjacent R.C. slab segments.

The aforementioned defects were monitored and investigated. In addition, all the available technical reports, data as well as the used stages of construction process, were investigated in order to assess the possible causes of such rapid defects. A computer analysis for models of the defected slabs using "Finite Element Method" was carried out. The models assume combined problems of the supporting soil materials underneath the R.C. slabs and the thickness and conditions of the reinforced concrete slabs to study the possible causes of the defects and assess its hazardous. Accordingly, defining methods of treatment and avoiding such problems in future could be suggested.

Description of Structure

The gas station, located in a rural area along the ring road, Kattamiya, consists of two main parts (Fig. 1):

1- First part located at the entrance of the station; this part is used for serving light-weight vehicles.

2- Second part located at the backyard of the station; this part is used for serving heavy trucks. Those trucks may weigh as much as 80 tons, as for the case of fuel tankers' trucks.

In addition, main facility structure is built at the middle of the station; this structure includes management building, supermarket, service bays, …etc. Other facility structures (car wash, ramp, …etc.) are scattered around the station. Fuel and oil tanks are placed underground.

As enriched by the technical reports and surveying maps given by the owner of the station, the natural ground level at the station location, was raised up by a sand formation having 1.5 m thickness. This backfilling process was made in order to accommodate for the required finished levels of R.C. slabs, essential for architectural and facilitation purposes of the station.

The slabs on grade were made of reinforced concrete, which were supported on a 25 cm thick layer of crushed stones serving as a base material. The R.C. slabs contained longitudinal and transversal full expansion joints spaced at 15 to 20m apart. There were also longitudinal and transversal shrinkage joints (saw cut) separating the slabs to segments ranging from 2.5 x 4.5 m to 3.0 x 5.50 m dimensions.
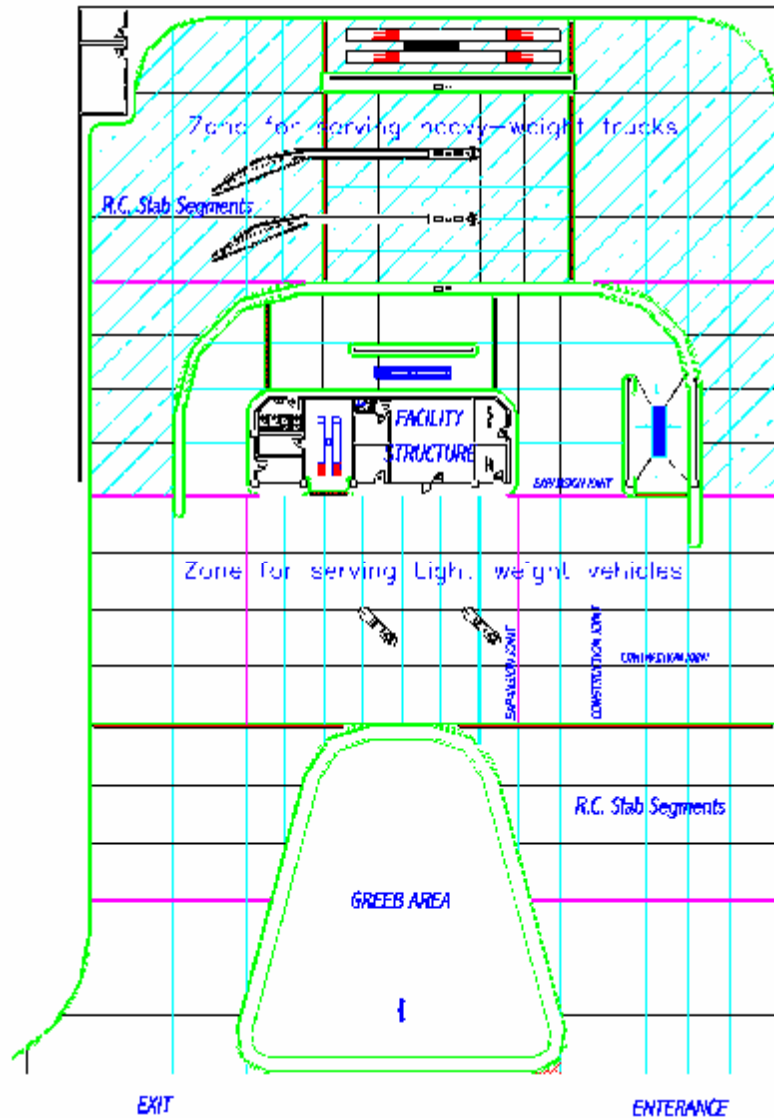
Fig 1: General Layout of Gas Station, Kattamiya, Cairo

The slabs were reinforced with upper and lower mesh of 5 ø 10/m for parts of station above fuel tanks and only one mesh of 5ø 10/m located at the top third of the cross section of the slabs for the rest of the station.

Apparent Defects

Apparent defects were observed in many parts of the station, specially in zone designated for serving heavy trucks. Figures 2 to 7 present photographs of examples of these defects. The followings represent a summary of the observed defects:

1- Obvious cracks were presented in most slabs in parts designated for motor vehicles.
The width of these cracks varied from 1 to 2 mm according to crack propagation.
Location of these cracks differed from one slab to another (Fig. 8) as follows:
a- Circular cracks around corner of R.C. slab segments (Figs. 2 and 8a).
b- Cracks parallel to the short direction and perpendicular to the traffic flow direction according to the following patterns:
i.   Cracks along one-third of some slabs (Figs.3 and 8b).
ii.   Cracks along the middle of some slabs (Figs. 4 and 8c).

iii.   Cracks along the middle as well as along one–third of the same slabs (Fig. 8d).
   2- Shrinkage joints were placed undisciplined (Fig. 2) in general, and in area of heavy truck vehicles in particular.
   3- The intersection of longitudinal and transversal shrinkage joints in many different scattered parts in the heavy truck area were crushed (Fig. 2).
   4- The filling material of the shrinkage joints was not fixed properly in different scattered parts in the heavy truck area. Also, the joints were filled with dust and deleterious matters. Parts of the filling material were cut off in different locations of the slabs (Fig. 2).
   5- Fairly high relative settlement (within 1 cm) was noticed between the nearby concrete slabs (Fig. 5), at locations of complete expansion joints between slabs. Whereas, hardly any relative settlement between nearby slabs occurred for other locations.
   6- Separation between the curbs and the floor slabs, was observed.
   7- The retaining walls around the station were tilted outwards resulting in obvious separation between them and the floor slabs as well as cracks in the end slabs (Fig. 6).
   8- Cracks spread in the R.C. slabs were noticed in areas around electrical and sanitary inspection chambers (Fig. 7).

Procedure of Investigation

Defining Possible Causes of Defects:

The possible causes of the aforementioned problems were stipulated in order to plan the procedure of investigation. The relatively recent opening of the station obstructed wide field investigation. However, the possible causes could be listed as follows:
-   The adequacy of the quality and/or the degree of compaction of base coarse/ backfill materials underneath the slabs.
- The outward tilting of the retaining walls all around the station could cause settlements in the end slabs, due to instability of the underlying soil materials even if the backfilling operation was initially satisfactory.
- The quality of concrete of the R.C. slabs as well as the constituents of the concrete mix and the thickness of these slabs in accordance with the design values.
- The used trend of construction process and agreement with the well-known engineering procedures.

Fig. 2: Circular Cracks Around the Corner of R.C. Slabs & Defects in Expansion and Shrinkage Joints.

Fig. 3: Cracks Parallel to Short Direction of R.C. Slabs and Perpendicular to Traffic Flow Direction

Fig. 4: Cracks Along the Middle of Some Slabs, Parallel to Short Direction of R.C. Slabs and Perpendicular to Traffic Flow Direction.
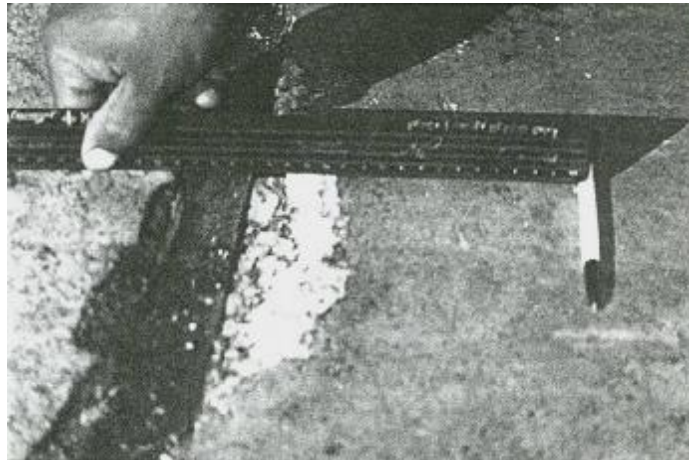
Fig. 5: Relative Settlements between Adjacent R.C. Slab Segments.

Fig. 6: Cracks in Tiles of End Walls and Separation between End Walls and Floor Tiles, due to Tilting of Retaining Wall Around the Station.

Fig. 7: Cracks Around Electrical and Sanitary Inspection Chambers.

(a)
Cracks along the corner of R.C. segment.

(b)
Cracks along one third of R.C. segment.

(c)
Cracks along the middle of R.C. segment.

(d)
Cracks along one third & middle of R.C. segment.

Fig. 8: Locations of Cracks in the R.C. Slab Segments of Gas Station

In-Situ Investigation

- Preliminarily, the executed borehole logs were studied thoroughly in order to assess the soil conditions at the project site and to recognize the possible presence of problematic soils in the region. A typical sample of the borehole logs, of the soil in the site, is presented in Fig. 9. The figure demonstrates sample of the test results being performed on the soil samples.

- The general layout of the station was plotted (Fig. 1). The cracking condition and its propagation were determined. A schematic diagram was drawn illustrating the shape of cracks (Fig. 8); the cracks were also photographed (Figs 2 to 7).

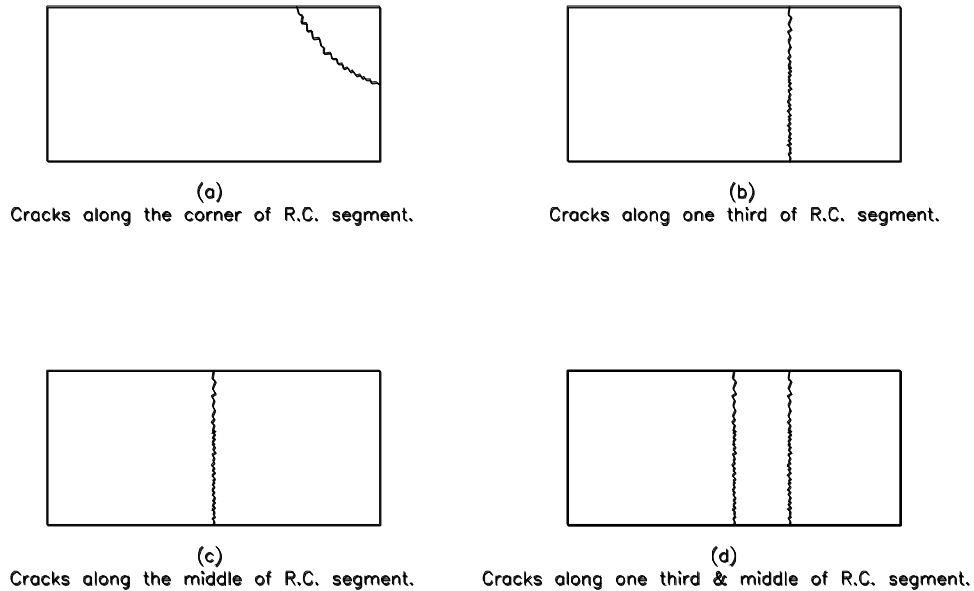- In-situ tests were conducted on the reinforced concrete slabs, where a total number of four core tests were undertaken (Figs. 10 and 11). Two core tests were performed on defected sections (cracked sections) and the other two cores were taken on sound sections in order to evaluate the variation in concrete conditions, thickness, resistance, and consequently, its cracking strength. The reinforcement mesh conditions including the used steel bar diameters as well as the concrete cover were also determined. The core tests were extended, in depth, through the base material to assess the conditions and thickness of base coarse material (Fig. 12).

- Chemical analysis on reinforced concrete samples was conducted to determine the concrete constituents (cement, coarse-grained and fine-grained materials).

- The conditions of the expansion and shrinkage joints were comprehensively studied and photographed for assessment of their roles in cracking of slabs and the possible propagation of these cracks in future.

BOREHOLE NO.(1)

Project: Gas Station   G.W.T : Not Present

Location : Ring Road   Weather: Mild

Sample depth	Sample type	S. 15	P. 15	T. 15	Legend	Layer End	SOIL DESCRIPTION	q_u Kg/cm²	W_c %	W_L %	W_P %	γ_b t/m³	Recovery %	R.Q.D
1	D.S					1.0	Light brown, graded **SAND** with some fine gravel and traces of silt.							
2	D.S		50/25				Light yellowish brown, graded **GRAVEL** with some fine gravel and traces of silt.							
3	D.S					3.0								
4	D.S		50/27				Light yellowish brown, graded **SAND** with some fine gravel and traces of silt.							
5	D.S													
6	D.S		50/30											
7	D.S						Light yellowish brown, graded **SAND** with clay pockets, partially cemented.							
8	D.S					8.0								
9	D.S						Light grey to light yellowish brown, silty **CLAY**, with traces of sand bands.							
10	D.S					10.0								
11	D.S						Light yellowish brown, **SANDSTONE**.						15	10
12	D.S		50			12							25	10
13	D.S						Light yellowish brown, graded **SAND**.							
14	D.S		50/24											
15	D.S													
							End of B.H. at 15.0 m							

Fig 9 : Typical Borehole Soil Formation at the site of the Station

Fig. 10: Samples of The Core Tests, Showing Non-Uniformity and Non-Conformity of R.C. Samples with The Required Design Dimensions.

Fig. 11: Sample of Core Test at Cracked Section (Sample # 1), Showing a Total Concrete Depth of 16 cm and RFT Mesh at Depth 10 cm from Top Surface.

Fig. 12: Core Test Extended, in Depth, Through Base Material.

Results of Field Investigation

1- According to the conducted core tests, which were extended through the base material, poorly compacted backfilling soil / base materials were found. In addition, a thin layer of weak and poorly compacted sand layer of 7–8 cm thick was found between the base layer and the reinforced concrete slabs. This sand layer was used for leveling the top surface of the base materials prior to pouring the R.C. slab.

2- The factor of safety against overturning for the retaining walls in case there is no live loads on the ground surface was 1.1; whereas, it was only 0.6 in case of imposed distributed live load of 1.0 ton/m^2. Therefore, the wall was not considered safe against soil bearing capacity and tilting. This was due to the shallowness of backfill at the back of the wall, resulting a lack in the effective passive earth pressure.

3- The results of the conducted core tests and chemical analysis (Table 1), reveal the followings:

♦   Non-conformity of the concrete sections to the required design dimensions. The required design dimension of the concrete section is 20 cm whilst some of the tested sections were only 12.50 cm, for the core test sample No. 2, above the tanks.

♦   Non-conformity of cement content of the concrete mix (270 kg/m^3, for the core test sample No. 2) to the required design value (350 kg / m^3). Consequently, the cement content is less than the design value by about 20 %, resulting in reduction in concrete strength.

♦   Non-conformity of the coarse grains proportion (975 kg/m^3) with the design value (around 1250 to 1300 kg/m^3). This proportion almost equals the detected fine-grained value (986 kg/m^3), for sample No. 1. The fine-grained value should be around 650 kg/m^3 (i.e., the ratio of the coarse grained to fine grained constituents should be around 2:1). It is worthy of note that coarse grains are responsible for maintaining the high strength of concrete.

♦   As a result of the previous defects in concrete, in addition to the anticipated inadequate workability, weak concrete strength was evident. The compressive strength of some of the samples of the concrete was only about 0.54 of its required design value (sample No. 2, Table 1).

Table 1: Summarized Results of Core Test Samples.

Sample No.	Diameter, cm	Total extracted depth, cm	Corrected strength, kg/cm^2	Cement content, kg/m^3	Coarse agregates ratio, kg/m^3	Fine agregates ratio, kg/m^3
1	7.43	16	165	N.A.	975	986
2	7.43	12.5	135	270	N/A	N/A
3	7.43	17	190	N.A.	1100	865
4	7.43	22.5	257	350	N/A	N/A

4- Depth of shrinkage joints did not exceed 1 cm, whereas the design depth should not be less than 1/6 the thickness of the concrete section, i.e., around 3 to 3.50 cm according to AASHTO specifications (1992).

5- Crushing at ends of shrinkage joints resulted in water seepage through them into the base coarse materials. This took place during the frequent floor washing operation of the station.
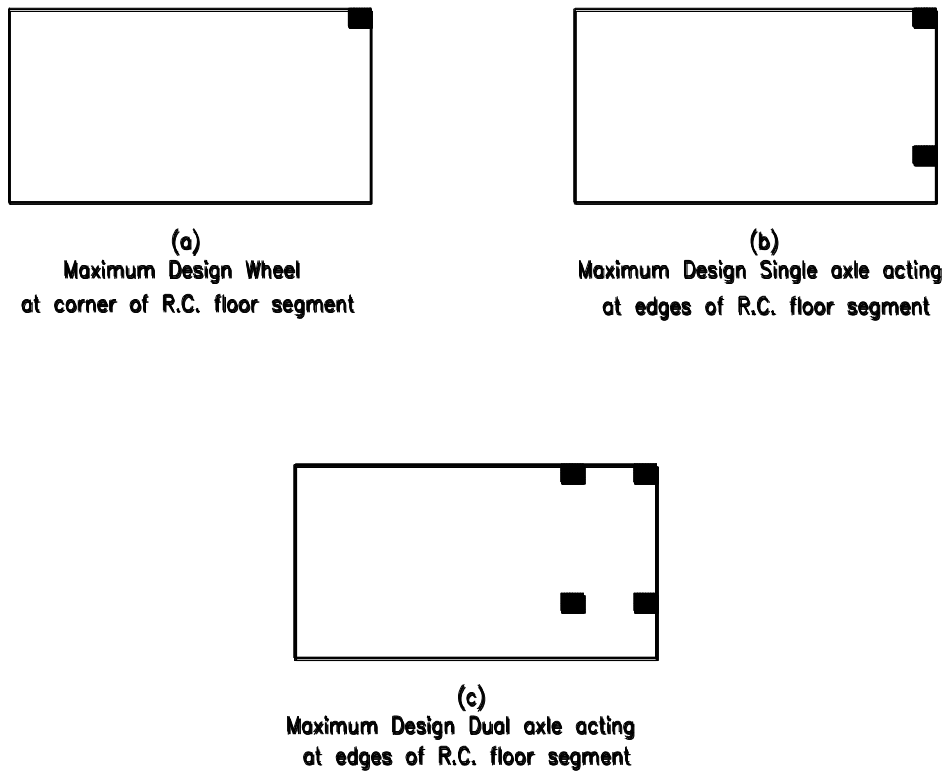
6- The depth of the filling material of the shrinkage joints did not exceed 0.50 cm (the depth of the filling material should not be less than 1.50 to 2.0 cm according to AASHTO (1992).

Computer Analysis

A detailed analysis using the computer was carried out using "Finite Element Method" in order to simulate the structural system and behaviour of the slabs on grade and to simulate the different cases of loading. Accordingly, the possible causes of cracks could be recognized and analyzed. Winkler hypothesis was utilized. It assumes that the soil media can be simulated by infinite number of elastic, non-dependent, closely spaced springs. The stiffness of the springs can be represented by the subgrade reaction modulus of the soil; this approach is called "Beam on Elastic Foundation". SAP2000 computer software was used for carrying out the engineering analysis of this problem.

The combined effects of the defected concrete and the supporting soil were involved in the computer analysis in the presumed subgrade reaction modulus. The computer analysis allowed better understanding of the possible causes of cracks with respect to the cracks shapes, propagation and directions at the different cases of loading. Knowing the critical limits of cracking would allow remedy of the soil-slab system.

Three cases of loading were investigated; each represents a specified portion of the slab being subjected to either wheel, single axle or dual axle design load (Fig. 13). For each load case, the supporting soil were simulated by three different categories of supporting media, ranging from strong and well compacted soil, to poorly compacted soil. Thus, a total number of 9 case studies, has been investigated in order to cover all possible causes of cracking. The different load cases are:

(a)
Maximum Design Wheel
at corner of R.C. floor segment

(b)
Maximum Design Single axle acting
at edges of R.C. floor segment

(c)
Maximum Design Dual axle acting
at edges of R.C. floor segment

Fig. 13: Cases of loading used in the station

1- Maximum Design Wheel load (4000 kg); the load is acting at corner of R.C. floor segment, (Fig. 13a).   Cases: Floor-1 (firm soil), Floor-2 (moderate soil) and Floor-3 (weak soil).

2- Maximum Design Single axle load (8000 kg); the load is acting at edge of R.C. floor segment, (Fig. 13b).   Cases: Floor-1A (firm soil), Floor-2A (moderate soil) and Floor-3A (weak soil).

3- Maximum Design Dual axle load (16000 kg), one of them is acting at edge of R.C. floor segment, (Fig. 13c). Cases: Floor-1B (firm soil), Floor-2B (moderate soil) and Floor-3B (weak soil).

The design load for the single axle was taken as 8000 kg, exerting maximum contact pressure = 5.60 kg/cm^2 according to Oglesby (1986). The subgrade reaction modulus was presented by three different values for each case of loading. The chosen values were as follows (Winterkorn and Fang, 1975):
1- K1 = 20 kg/cm^2/cm, which presents strong soil of crushed stones
2- K2 = 2.0 kg/cm^2/cm, which presents a moderate soil
3- K3 = 0.2 kg/cm^2/cm, which presents weak and poorly compacted soil.

Results of the Computer Analysis

i. Based on the results of the computer analysis for cases of Floor 1, Floor 2, and Floor 3, which resemble cases of one wheel load concentrated upon the corner of the reinforced concrete slab for the different assumed stiffness of the soil, it can be seen that the moments in the slab is doubled from 0.70 ton.meter/meter to 1.40 ton.meter/meter (Figs. 14a, b and c). The contour line graph shows the maximum moment (M max) for the different cases.

Considering the "Dynamic Magnification Factor", which ranges from 1.50 to 2.0 (according to the characteristics of the dynamic loads imposed by the moving trucks), the maximum moment (M max) may attain values as high as 2.10 to 2.80 ton.meter/meter.

Since the maximum moment for cracking occurrence is:

$$M \text{ cracking} = \frac{bh^2 . \sigma_r}{6}$$

Where:
b= width of section = 1.0 m
h = thickness of R.C. section = 0.20 m
σ_r= maximum tensile stress (cracking stress) = 0.6 $\sqrt{fc}$ MP$_a$ (ACI, 1995)
Thus,
σ_r=2.68 Mpa = 26 kg/cm^2
M cracking = 1.7 t.m /m

By increasing the moments beyond the M cracking, the cracks would take place diagonally at 45 degrees (circular cracks around corners), as illustrated on the net of moment contour lines.

ii. Based on the results of the computer analysis for cases of Floor 1-A, Floor 2-A, and Floor 3-A (Figs. 15a, b and c), which resemble cases of single axle load concentrated upon the edge of the reinforced concrete slab for the different assumed stiffness of the soil, it can be seen that the

(a) Case: Floor-1, M(max.)=0.7 mt/m   **(b) Case: Floor-2, M(max.)=1.1 mt/m**

(c) Case: Floor-3, M(max.)=1.4 mt/m

Fig. 14: Contour Lines for Moment M (max.), for Load Cases:

§   (a) Floor-1
    (firm soil, K1 = 20 kg/cm^2/cm),
§   (b) Floor-2
    (moderate soil, K2 = 2.0 kg/cm^2/cm), and
§   (c) Floor-3
(weak soil, K3 = 0.2 kg/cm^2/cm).

(a) Case: Floor-1A, M(max.)=0.84 mt/m

(b) Case: Floor-2A, M(max.)=1.5 mt/m

Fig. 15: Contour Lines for Moment M (max.), for Load Cases:

§   (a) Floor-1A
(firm soil, K1 = 20 kg/cm^2/cm),
§   (b) Floor-2A
(moderate soil, K2 = 2.0 kg/cm^2/cm), and
§   (c) Floor-3A
(weak soil, K3 = 0.2 kg/cm^2/cm).

(c) Case: Floor-3A, M(max.)=2.45 mt/m
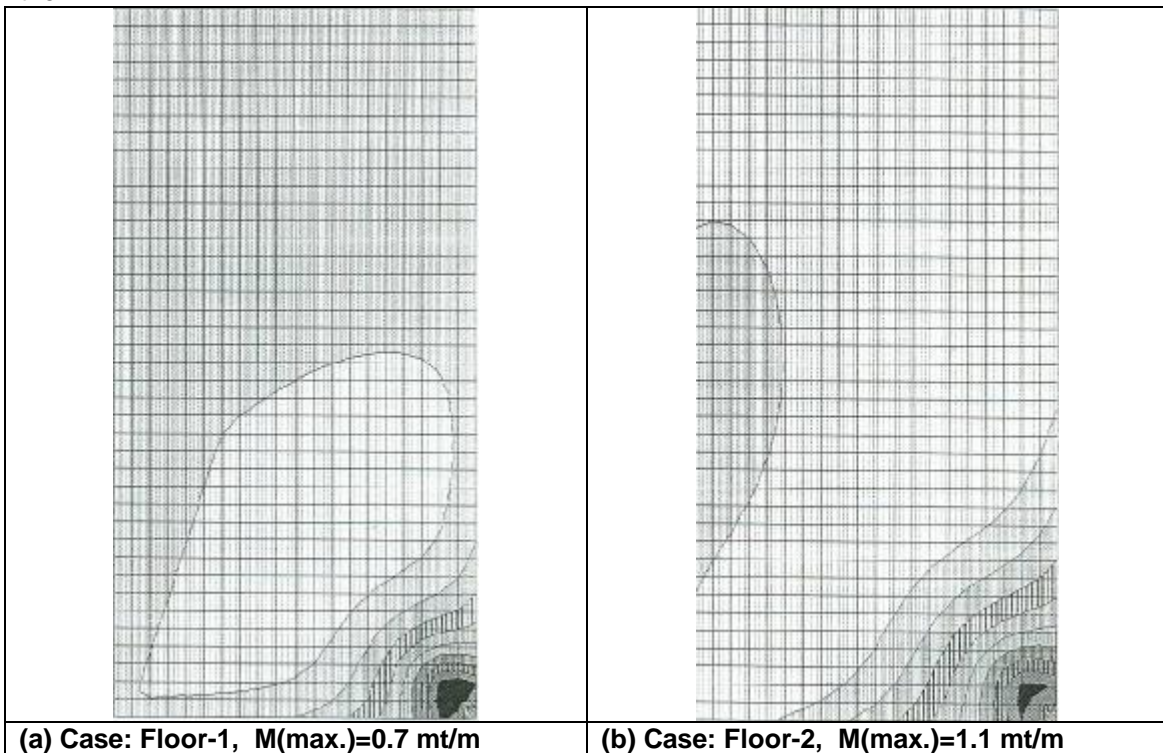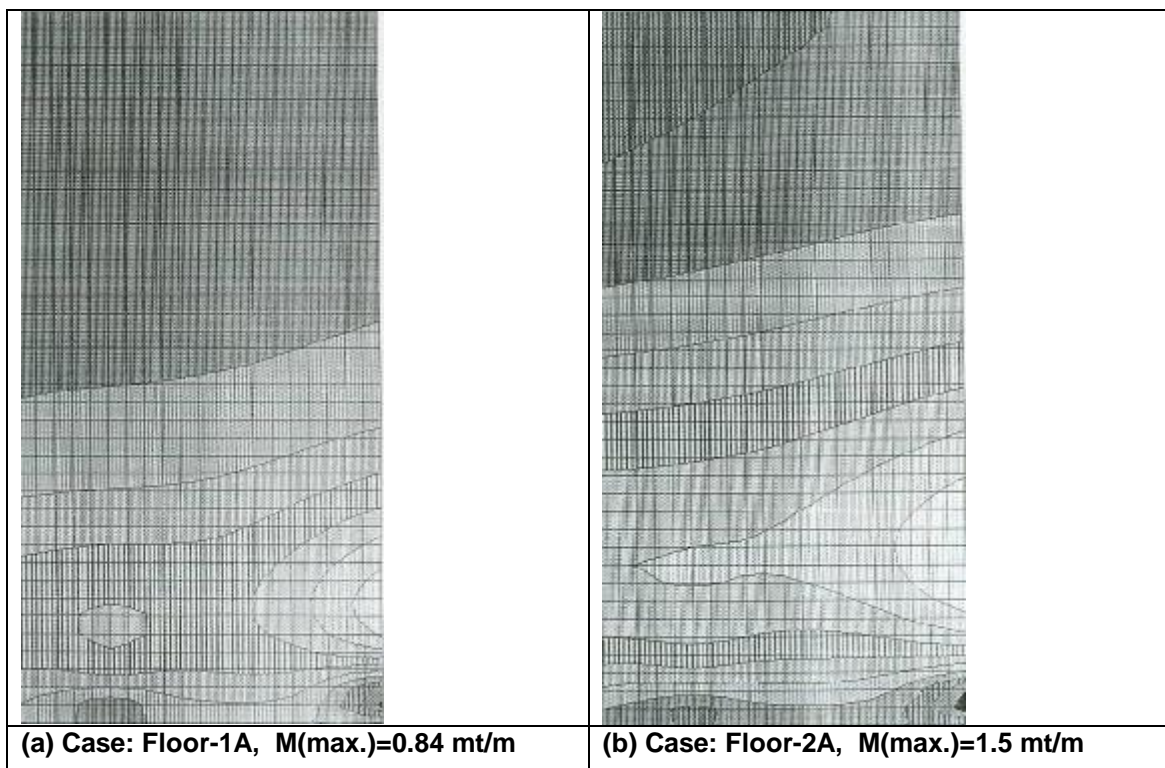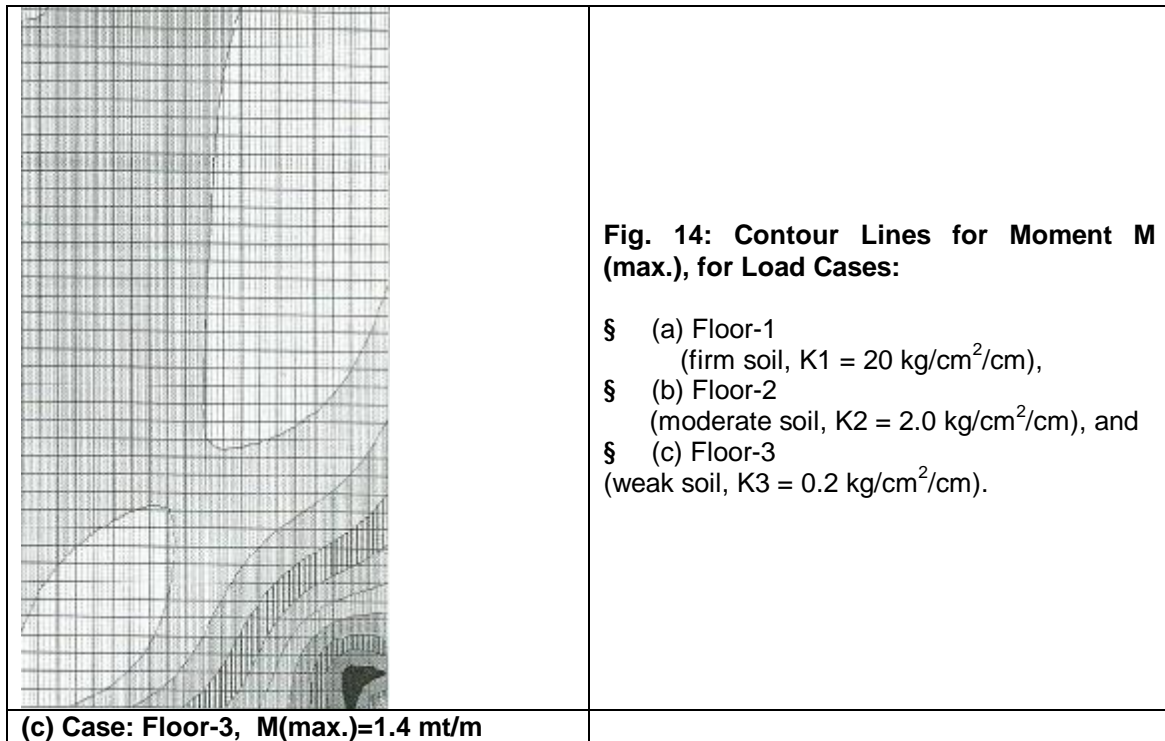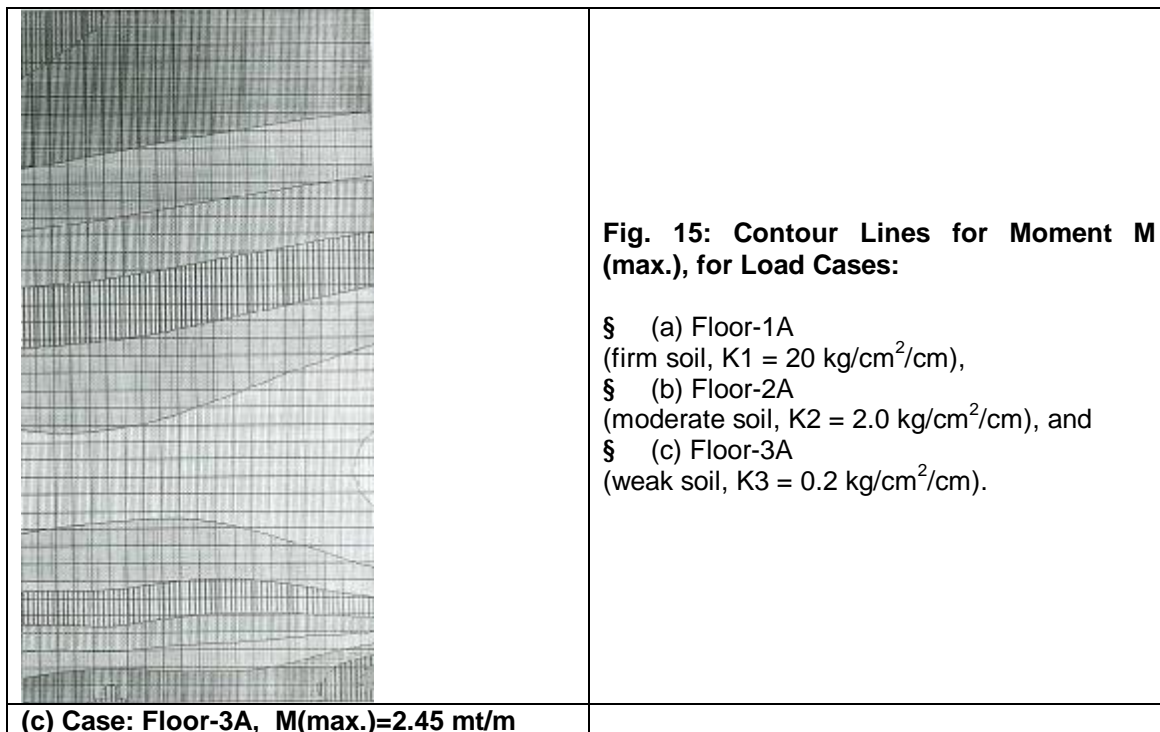
moments in the slab is almost tripled from 0.84 ton. meter/meter to 2.45 ton.meter/meter. Accordingly, the moment exceeds the cracking resistance of the slab resulting in cracks occurrence at the one-third of it, as illustrated on the net of moment contour lines of the moment for the different cases.

iii. Based on the results of the computer analysis for cases of Floor 1-B, Floor 2-B, and Floor 3-B (Figs. 16a and b), which resemble cases of dual axle loads, one of which is concentrated upon the edge of the reinforced concrete slab, it can be seen that the maximum moments in the upper fibers of the concrete section for the case of firm soil (case of Floor1-B) attains 0.88 ton.meter/meter. This value is increased to 1.68 ton.meter/meter for the case of weak soil, resulting in cracking of the concrete section perpendicular to the direction of truck flow in the one third and half of the slab when considering the "Dynamic Magnification Factor".
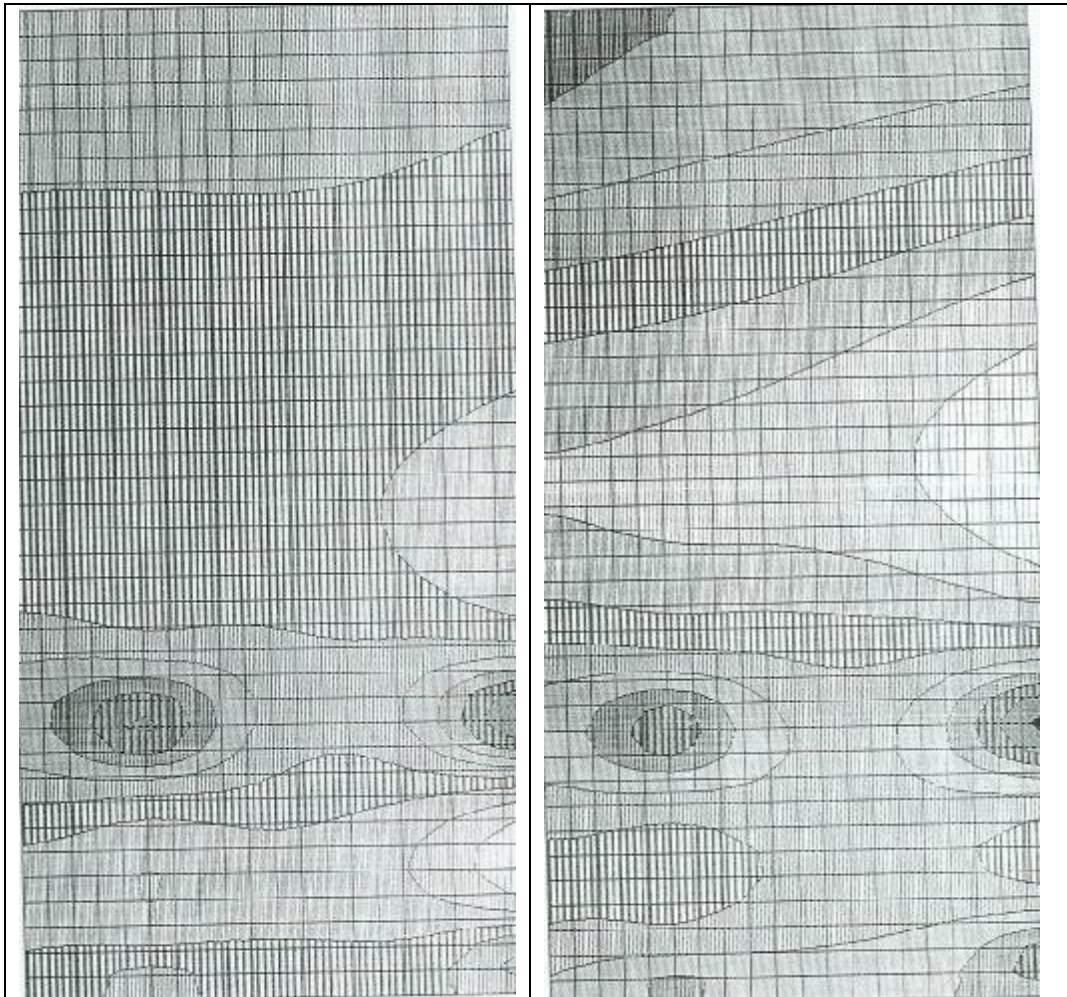
| (a) Case: Floor-1B, M(max.)=0.88 m.t./m | (b) Case: Floor-3B, M(max.)=1.68 m.t./m |

Fig. 16: Contour Lines for Moment M (max.), for Load Cases:
§   (a) Floor-1B (firm soil, K1 = 20 kg/cm^2/cm),
§   (b) Floor-3B (weak soil, K3 = 0.2 kg/cm^2/cm).

CONCLUSION

1- Considering the severe crushing of the slab' ends and cracks of slabs during their relatively short life span, it can be concluded that the cracks should not had taken place due to the plastic shrinkage of concrete or improper structural design (except for the case of retaining walls), since other parts of the concrete slabs not exposed to high loads, did not suffer of any noticeable cracks.

2- Based on the aforementioned study, the cracks should have been occurred as a direct result to the heavy loads of the trucks at specific cases of loading. The underlying soil was not adequately compacted and the concrete was weak with inadequate strength and unequal thickness. This should lead to excessive stresses and unequal settlement underneath the truck wheels at particular conditions of loading as revealed by the computer analysis.

3- The cracks around sanitary and electrical chambers, are due to the sudden change in the sub-grade reaction modulus underneath the R.C. slabs at these locations. The used construction method led to poor soil compaction at areas adjacent to these installations.

4- Cracks at locations adjacent to retaining walls were due to the tilting occurred in the walls. It took place because of the excessive stresses imposed on the soil in critical cases of loading by heavy trucks (which impose not less than 80-ton total weight) due to the shallowness of backfill at the back of the wall. I.e., the wall was not safely designed against tilting, leading to further excessive stresses on soil at the compression side of the walls' bases.

5- In the investigated locations, no relative settlement between nearby slabs occurred due to the presence of reinforcing steel mesh in the concrete section. For the case of complete expansion joints between slabs, fairly high relative settlement (within 1 cm) occurred between the nearby slabs. This confirmed the combined drawback of the defected soil and concrete conditions.

6- Because of the bad erection of shrinkage joints, the water seeped through joints to the base coarse materials, which were underlain by backfilling materials. This together with presence of high dynamic loads on the slabs, poor soil compaction and unequal slabs' thickness, resulted in compressing the soil unequally and in relative settlement between the nearby slabs. Consequently, high tensile stresses in slabs surpassing the cracking stresses in the uppermost fibers of the concrete section had occurred. These stresses caused crushing of concrete adjacent to the joints.

7- Because of the bad erection of shrinkage joints and the insufficiency of the joint's depth compared with the required design value, these joints missed their basic benefit, which is creating weak concrete plane to crack through. This resulted in the occurrence of undisciplined crack and aided in crushing the concrete beside the joints.

8- Since the filling material of the joints was not executed according to the specifications (with respect to the joints' depths and maintenance), it is therefore anticipated that secondary stresses in the slabs might have been caused at any change of temperature, particularly in the very hot summer season.

REMEDY

The treatment was undertaken through the execution of the following program:

1- The slabs that were suffering from severe cracking were demolished and re-constructed after fulfilling the specifications of compaction requirements which stipulate realizing 95% compaction according to Modified Proctor Test of the filling materials, spread in layers of 25 cm thickness using the proper machinery.

2- In the mean time, the demolished concrete slabs were re-erected following the specification requirements of concrete constituents, configuration, strength, and slab thickness.

3- The retaining walls were supported by backfilling at their backs (out side the station) up to the ground level inside the station with pre-qualified engineering materials that obey the general requirements of backfilling and compaction.

4- It is also to note that particular care should have been given to compaction at locations adjacent to the underground tanks as well as the mechanical and electrical installations. This was due to the fact that compaction at these locations was customarily of less

efficiency than compaction at the open areas, this was due to the obstructed compaction operation, entailing usage of smaller compaction equipment that couldn't fulfil the required degree of compaction.

5- According to the used construction process, the underground pipes were placed in trenches which were excavated after completion of the backfilling materials, and placing the compacted coarse materials. Expectedly, the filling operation around the pipes was inadequate due to the narrow trenches. Therefore, the thickness of backfilling materials below the pipes should be increased in order to avoid differential settlements between the locations of the pipe trenches and the dominant concrete slabs.

6- Since cracks took place around the corners of sanitary and electrical installations, such as underground chambers, tanks and manholes, these installations should have not been constructed along the path of the moving vehicles as much as possible. This is recommended in order to avoid the detrimental effects of placing one or more wheels upon the sanitary tank (or any other installation) while other wheels are resting on the concrete slabs, resulting in differential settlements and separation between the two structures.

7- In case that the sanitary and electrical works had to be placed obligatory along the path of the moving vehicles, a construction joint should be erected between them and the concrete slabs. Another precautionary measure is to increase the thickness of the filling coarse materials at the junction between them. A slope of 1:7 is suggested.

8- All expansion and shrinkage joints, as well as the filling material were re-erected following the specifications in terms of depth, fixation of filling material and rules of proper engineering construction.

9- The thin sandy layer of about 7- 8 cm, used to level the surface of the layer of base material before pouring the R.C. slabs, is considered a possible cause of inadequacy of compaction underneath the slabs due to its thin thickness and the inequality of the this thickness from one location to another. Avoiding the use of such layer and replacing it with concrete is suggested. Many stations were constructed after the completion of remedy of this station in different locations of Egypt. With fulfillment of the suggested sequences and obeying the specifications in terms of soil backfilling, concrete design and construction, no complaints were any longer raised.

REFERENCES

1. American Association of State Highway and Transportation Officials, 1992, "Standard Specification for Highway Materials", AASHTO, Washington, D.C.
2. American Concrete Institute, 1995, "Building code Requirements for Reinforced Concrete", ACI, Detroit, USA
3. Oglesby K. H., 1986, Highway Engineering, John Wiley & Sons, New York.
4. SAP2000, 1997, Basic Analysis Reference Manual - NonLinear Vevsion 6.11, Computers and Structure Inc., Berkeley, California, USA.
5. Winterkorn, H. F. and H. Fang, 1975, Foundation Engineering Handbook, Van Nostrand Reinhold Company Inc.

ANALYSIS OF PRESTRESSED ANCHORD TIE-BACK DIAPHRAGM WALL OF El-SEBAK TOWER IN MISR El-GUEDIDA CITY

Kamal Mohamed Hafez Ismail
Assistant Professor, Aswan Faculty of Engineering., South Valley Univ., Cairo, Egypt
Email: kmhi123@yahoo.com

ABSTRACT

El-Sebak tower in Misr El-Guedida is a building consisting of two garage basements, ground shopping floor, first trading floor, second offices floor, nine residential typical floors and two villas floors with sixteen floors. This tower was constructed between other nearby buildings, one of them is twenty floors constructed on pile foundation, and others are eleven floors. The most critical one chosen in this study is a five storey residential building with shallow foundation at a distance 6 meters apart from El-Sebak tower, which has 9.5 meters deep excavation.
The study is directed towards the analysis of the concrete diaphragm wall and its effect on the five story near-by building at different stages of construction.
The numerical analysis is performed using a plane strain finite element analysis assuming Mohr Coulomb elasto-plastic failure model for soil behavior. The diaphragm wall in-situ measured lateral top displacements are compared with those predicted from the program and it is found that the predicted values are reasonable to a great extent.

Keywords: Diaphragm Wall, Prestressing, Anchored tie-back, Mohr-Coulomb

INTRODUCTION

Most of the new buildings in the congested conditions of the city centers are equipped with basements used for underground parking or for placement of building service technology, bank vaults, etc.
Center areas of Misr El-Guedida are revitalizing nowadays. Erection of administrative and commercial buildings are in demand. Thus, construction work is concentrated in density built-up areas. Existing gaps in blocks of houses are filled; sometimes-existing property must be demolished prior to a new building erection.
All the standard technologies such as diaphragm walls, pile walls, micro pile walls, jet grouting, soldier pile walls and others, combined with anchors or tiebacks, struts or bracing by basement ceiling slabs are used today.
Diaphragm walls are designed of cast in place RC, usually 450 to 800 mm in thickness. Its advantage is that it seems to be an ideal structure-especially when designed as a permanent wall of an underground car park, also it has a relative enough rigidity to constrain displacements, and while its disadvantage is that, it is of relatively high price. Grabs mounted on mobile crane for excavation of diaphragm wall trenches are used
Anchorage by tiebacks – prestressed strands and rods are usually used. There have been few objections from the owners of the neighboring properties against installations below their buildings thus far and with some exceptions; the matter represents no obstacle for the issue of building permits.
Deep excavations can cause large settlement and lateral displacements of the ground around the excavation. Surrounding buildings can be damaged if the settlements are not controlled through the side support system by increasing the stiffness of the in-situ wall, by placing and preloading the braces as early as possible, or by extending the wall down to an underlying stiff layer. The lateral displacements of the side support system are often used to evaluate the

performance of braced excavation [1].

Prestressing ground anchorage proceed first by drilling the hole, placing the tendon, fixing the anchorages to the soil by bonding using a grout of mortar. The next phase involves tensioning or stressing the ground anchorage. This is the most important operation, which can be in turn broken down

Braced excavations commonly are visualized as a step-wise process of excavations and support. Following each increment of excavation, inward deflections of the walls occur, causing movements of soil adjoining the excavation that are transmitted to the ground surface as settlements and horizontal offsets [2]. With regard to stability, apparent earth pressure envelopes are recommended for a variety of soil types [3,4]. On the other hand, the patterns of settlement associated with braced excavations are summarized only in very general terms [5].

Alternatively, limit equilibrium may be used for the design of anchored walls in stratified soil and where relatively non-uniform surcharges are present. In this approach, the anchor loads are assessed, as the loads required achieving a target factor of safety for the retained soil. Another design methodology for tieback walls is the Beam-Column approach [6, 7]. This approach, however, has not been successful in predicting displacement profiles as it ignores the soil mass movement.

The finite element method (FEM) is considered a more sophisticated analysis that can be used to provide more reliable assessments of the behavior of anchored walls [8].

An extensive database for wall and ground movements due to deep excavations are presented in different soil types [9]. An evaluation of the current design methods and their implications on the wall performance.

In principle, deflections of the retaining structures and anchor forces developments are monitored, the adjacent buildings are equipped with measure points to check vertical and horizontal displacements and the widening of existing or newly arisen cracks is measured [10].

Common techniques for instrumentation and monitoring are used – inclinometers, pressure cells, precise leveling on affected constructions often with motion-controlled optical digital levels or total stations, hydrostatic leveling inside buildings, accelerometers. etc. [11].

PROBLEM DESCRIPTION

A plane strain finite element numerical analysis program is used to solve the problem of construction of reinforced concrete diaphragm wall 0.47 m thickness consisting of separate adjacent panels of width 2.3 m each, constructed by boring and then reinforced concrete is cast in place.

The wall starts from ground surface (29 m vertical coordinate) and extends to a depth 11.5 m (17.5 m vertical coordinate) from ground surface, the toe is at a depth 2.0 m below the final 9.5 m excavation depth of El-Sebak tower.

The construction site is surrounded by several old buildings, the nearest and the most critical one is a five story residential building 6.0 m apart from the diaphragm wall and its foundation level is at a depth 2.5 m from the ground surface. The building flat slab floor thickness is 0.16 m and its width is 14.0 m (starting edge horizontal coordinate is 23 m and its ending edge horizontal coordinate is 37 m, which is the nearer to the excavation side), figure 1.

Phase 1, includes construction of the five storey near-by building and construction of the continuous adjacent panels of the diaphragm walls (0.47m thick, 2.3 m width and 11.5 m depth).

Phase 2, includes excavation in front of the diaphragm wall to a depth 4.0 m.

Phase 3, includes installing the wall anchorage at a depth 3.5 m from ground surface and prestressing it by a tensile force 580 kN per diaphragm wall panel (2.30 m width).

Phase 4, includes continuing the excavation in front of the diaphragm wall up to the raft foundation level of El-Sebak tower which is 9.5 m below the ground surface.

Phase 5, includes connecting the diaphragm wall laterally by the raft foundation of El-Sebak tower. Phase 6, includes connecting the diaphragm wall by El-Sebak basement floor at a level 4.5 m depth from the ground surface and releasing the prestressing force of the anchorage of the wall.

The soil properties and stratification are got from 13 mechanical borings constructed in the site; the ground water table is not encountered at end of borings (15m).

The soil properties are as shown in table 1.

Table 1: Properties of Soil as Analyzed from 13 Constructed Borehole

Layer	Depth	E (kN/m^2)	c (kN/m^2)	f	y	Condition
Upper Sand	From 0 to 3.5 m	15000	0	34	3	Drained
Lower Sand	From 3.5 m to 6.0 m	30000	0	38	4.0	Drained
Silty Clay	From 6.0 m to 9.5 m	11500	12	15	1	Drained
Lower Sand	From 9.5 m and extended	30000	0	38	4.0	Drained

A plane strain analysis is assumed, where the soil is idealized as elasto-plastic material according to Mohr-Coulomb failure criteria. The diaphragm wall anchor extends to about 12.5 m behind the wall under the near-by building with an angle 16^0 with the horizontal. The grouting (only for the last 4.0 m of the anchor bar) material and anchor bar are idealized as elastic materials. The anchor and grouting material stiffness are chosen to be 2000 kN/m.

The residential near-by building under study consists of five storeys, the total width of building is 14.0 m consisting of two external bays 4.5 m width and an interior bay 5.0 m. The first floor level is 0.5 m higher than the ground level. The floor slab is a flat slab with average thickness 0.16 m, the total average floor load is chosen 10 kN/m^2. The building external footings are strip footings of width 1.20 m while the internal footings are of width 2.4 m, this gives an average contact stress equals to 112.5 kN/m^2, fig.1.

The problem boundary condition is hinged horizontally at the left and right vertical boundaries and totally fixed at the lower bottom horizontal boundary.
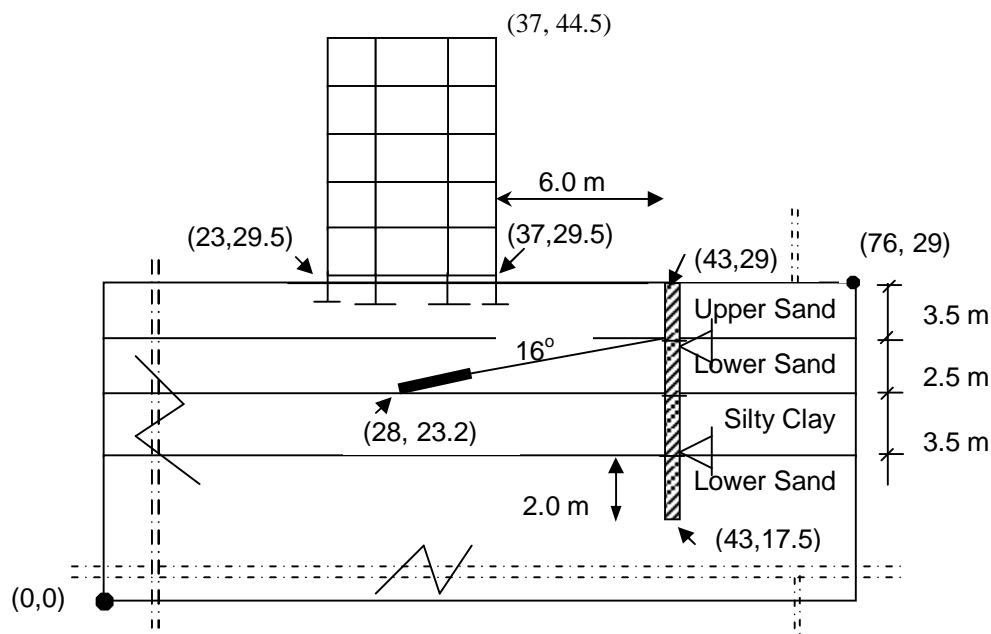

Fig. 1: Systematic Diagram Showing a Sketch of The Problem

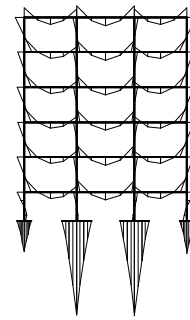## CONSTRUCTION PROCEDURE

Phase 1, Stresses and Displacements of The Near-by Five Story Building

Figures 2 and 3 show near-by building deformed mesh and structural members bending moment distribution. The calculated maximum exterior and interior footings settlements are 0.038 m and 0.0475 m respectively, while maximum interior footing bending moment is 150 kNm/m.
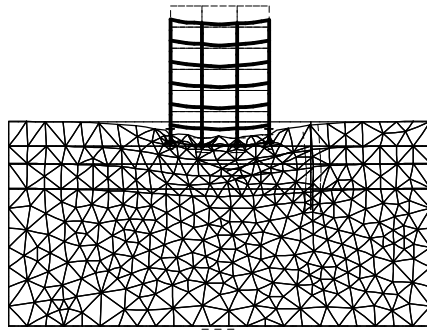
Fig. 2: Deformed Soil Mesh, phase 1   **Fig. 3: Building Bending Distribution**

Phase 2, Excavating 3.5 m Depth in Front of El-Sebak Tower Diaphragm Wall

Figure 4 shows diaphragm wall displacement due to soil excavation 3.5 m in front of the wall. The top wall horizontal displacement is 0.009 m, while the vertical component is 0.006 m upwards due to soil heave resulting from soil excavation and skin friction with the diaphragm wall.
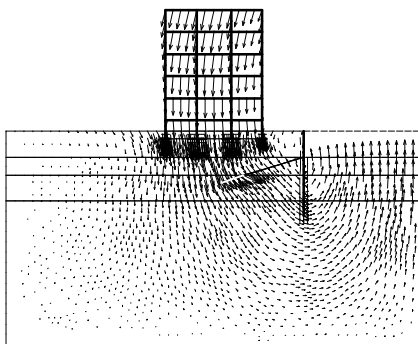
Fig. 4-a: Soil Total Displacements, phase 2   Fig. 4-b: Diaphragm Wall Displacement, phase 2

Phase 3, Prestressing the Wall Anchor by a Tensile Force 580 kN/2.3 m

Figures 5 and 6 show the near-by building tilting and its first floor resultant displacement (the initial settlement of the building in not considered here in these displacements) due to prestressing of the diaphragm anchor by 580 kN. It is found that the building first floor far edge (from excavation) displacement is 2.9 mm horizontally and 5.1 mm vertically downward, while the near floor (to excavation) edge displacement is 2.9 mm horizontally and 6.2 mm vertically upward which leads to slight tilting to the building floor as shown in figure.
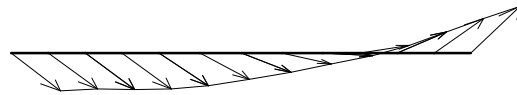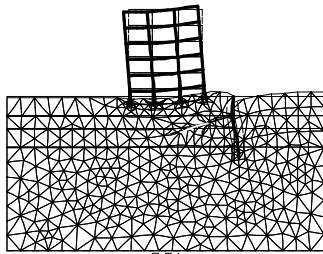
Fig. 5: Building Deformation, phase3   Fig. 6: Building First Floor Displacement, phase3

Phase 4, Completing Excavation to Foundation Level of El-Sebak Tower at 9.5 m Depth from Ground Surface

Figures 7 and 8 show the near-by building deformation and its first floor displacement wall (the initial settlement of the building in not considered here in these displacements) due to continuous excavation in front of diaphragm wall to the required foundation depth 9.5 m, it is found that the first floor far edge (from excavation) displacement is 18 mm horizontally and 12.5 mm vertically downward, while the first floor near edge displacement is 18 mm horizontally and 2.4 mm vertically upward leading to slight tilting of the building floor as shown in figure.
Phase 5, which is the construction of raft foundation of El-Sebak Tower at final excavation depth 9.5 m, is nearly having the same output as phase 4, as no additional load is applied in this phase.
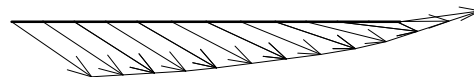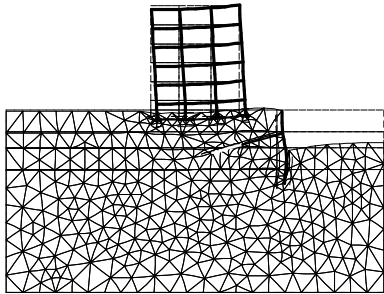
Fig. 7: Building Deformation, phase4   Fig. 8: Building First Floor Displacement, phase4

Figure 9, shows bending moment distribution of flat slab of the first floor. The bending moment at columns and intermediate spans are –23.8, 10, -20, 13, -16.3, 11, -24.5 kNm/m from left (far edge of building) to right (near building edge to excavation) respectively.
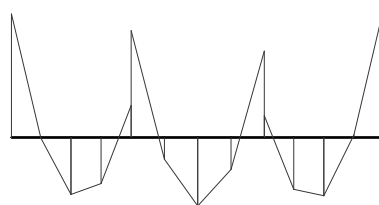
**Fig. 9: Bending Moment of Flat Slab of the First Floor
of near-by Building, phase 4**

Phase 6, Connecting El-Sebak Tower Basement Slab to The Diaphragm Wall at 4.5 m Depth And Release of Anchor Prestressing Force.

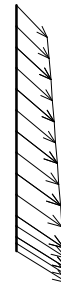Figure 10 and 11 show near-by building deformation and its nearest column (to diaphragm wall) displacements due to phase 6. If neglecting vertical settlement due to the building loads and only consider the deformation due to phase 6, It is found that the top horizontal displacement of the column is 7.6 mm and the vertical displacement downward is 7.8 mm, while the bottom of the column horizontal and vertical displacements are 12.8 mm and 7.8 mm respectively.
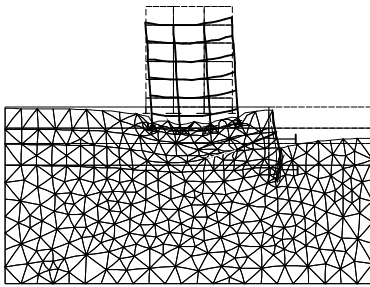
Fig. 10: Deformed Mesh, phase 6   Fig. 11 Nearest Column Displacement, phase 6

Diaphragm Wall Displacement and Bending Moment at Different Phases

Figures 12 and 13 show the horizontal diaphragm wall displacement and bending moment distribution respectively along vertical diaphragm wall height at different phases of construction. The prestressing force is 580 kN/2.3 m. The figures start by phase 2 , as the wall is not yet constructed in phase 1.
In figure 12, in phase 3 an opposite passive displacement due to prestressing force. The maximum horizontal displacement in phase 6 varies from 0.015 m at top of the wall to a maximum value 0.032 m near the toe of the wall and that's along its total height (9.5 m excavation depth).
Figure 13 shows that the extreme intensities of bending of the diaphragm wall are 380 kNm/m (behind the wall) and - 320 kNm/m (in front of the wall) from phase 3 and phase 4 respectively.
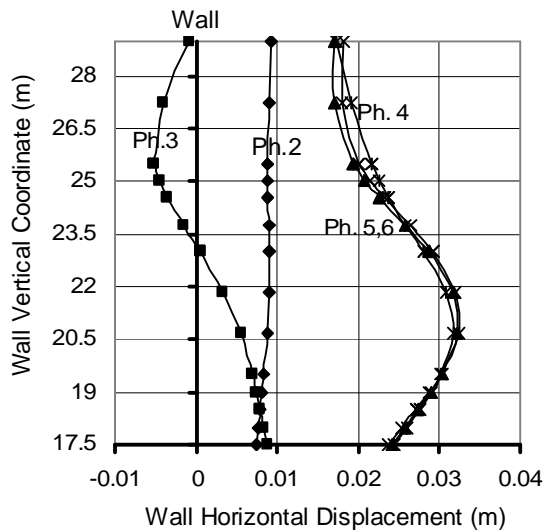
Fig. 12: Diaphragm Wall Horizontal Displacement Distribution at Different Phases (Ph.) of Construction
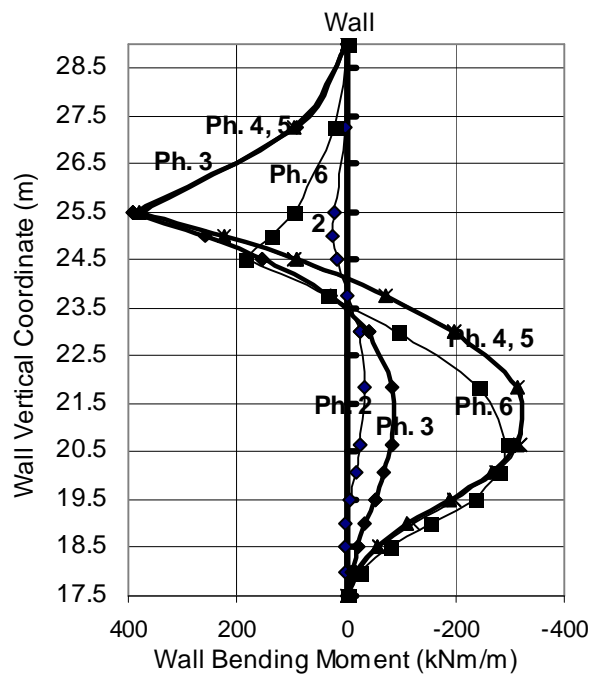
**Fig. 13: Diaphragm Wall Bending Moment Distribution
at Different Phases (Ph.) of Construction**

The Total Vertical Displacement of The First Floor of Near-by Building

Figure 14 shows near-by building first floor total vertical displacement at different phases starting from phase 1 and ending with phase 6.

In phase 3 the anchored prestressing force is 580 kN / 2.30 m panel width and all this force is transmitted to the grouting material present under the inner near-by building footing.

The tensile force cause movement to the grouting material which creates passive pressure to the soil around and in front of it and active pressure to the soil behind it, this in turn causes a field of soil movements and that is the reason for the greater final settlement of the far edge and interior columns (their footings lie in the generated active soil zone, while the near-by edge column and the interior one behind it, their footings lie in the generated passive zone).

The previous figure 6 shows the near-by building vertical displacement only due to anchorage prestressing of phase3.

Figure 4, shows that phase 4 represents the critical phase for building tilting where the total (considering building initial settlement) floor near edge undergoes total (due to building settlement and due to anchored prestressing) downward displacement equals to 3.6 cm, while the far floor edge undergoes total downward displacement equals to 5.2 cm, which means a differential settlement about 1.6 cm along the total near-by building floor width 14.0 m and this small differential settlement can be considered acceptable and can not causes any noticeable cracks.

So the tilting of the near-by building is affected by the value of the anchorage prestressing force, by the position of the grouting material and whether it is near or far to one of its building footings and by the final excavation depth in front of the wall which increases the initial anchorage force.
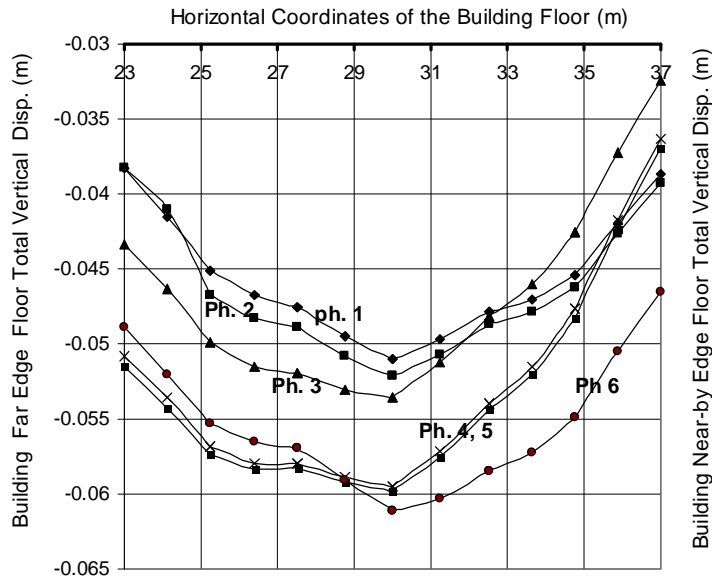
**Fig. 14: Building First Floor Total Vertical Displacement During
Different Phases of Diaphragm Wall Construction**

Effect Of Changing Anchor Prestressing Force On Diaphragm Wall

Figure 15 and 16 show the study of the effect of changing the initial anchor prestressing force (T in kN per 2.30 m diaphragm wall panel width) on both the diaphragm wall horizontal displacement and bending moment at phase 6.

It is noticed that increasing anchor prestressing force from 230 kN/2.3 m to 710 kN/2.3 m results in reducing top wall displacement from 0.032 to 0.012 m and increasing the positive wall bending moment from 85 to 245 kNm/m, while the negative moment (towards front of the diaphragm wall) is not highly affected as shown in figure.
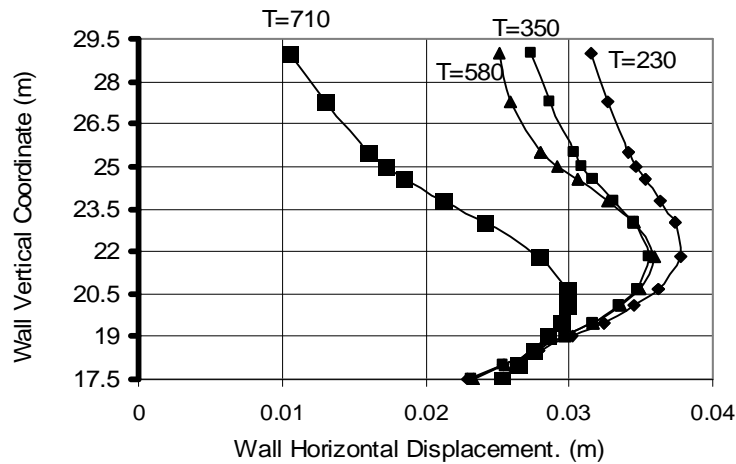
**Fig. 15: The effect of Prestressing Force (T in KN) on Diaphragm
Wall Horizontal Displacement, phase 6**
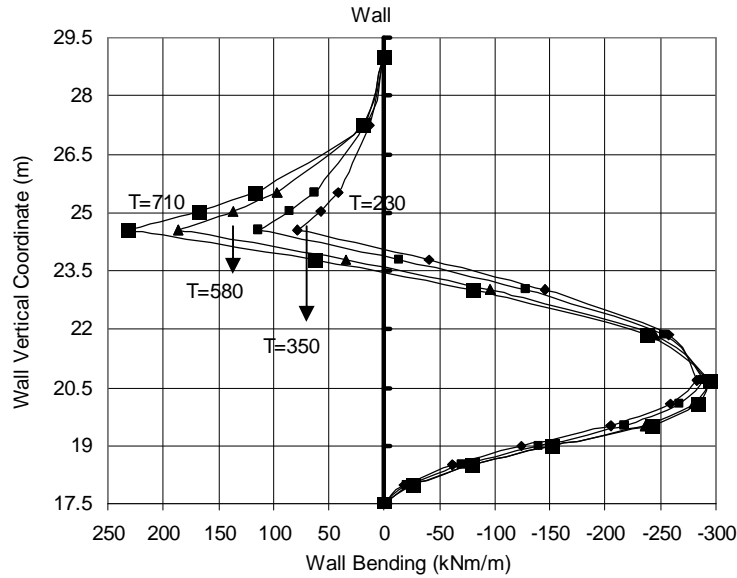
**Fig. 16: Effect of Anchor Prestressing Force (T in KN) on the
Diaphragm Wall Bending Moment, phase 6**

Figure 17 shows the effect of the initial anchor prestressing force on the vertical displacement of first floor of near-by building, (note that this displacement is due to the anchor prestressing tensile force only and not added to it the initial building settlement due to its own weight**).**
For a prestressing force 710 kN/2.3 m, the near floor edge displacement shows heave 0.0078 m while the far edge from excavation shows settle –0.0058 m (along total floor width 14.0 m.
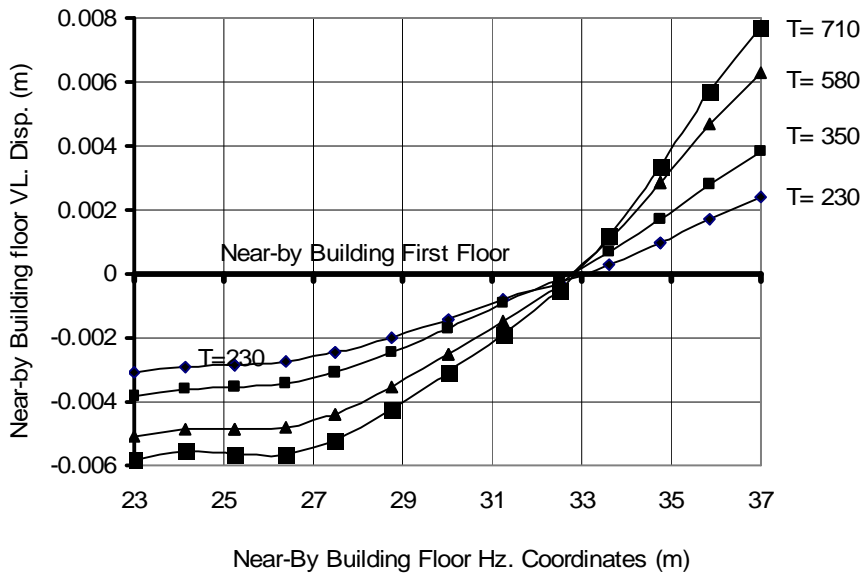
**Fig. 17: Effect of Changing Anchor Prestressing Force (T in kN) on the Vertical
Displacement of the Near-by Building First Floor, phase 3**

Effect of Changing Diaphragm Wall Thickness On Its Displacement And Bending Moment

Figure 18 shows the effect of changing diaphragm wall thickness on its horizontal displacement

for two chosen wall thickness 0.47 and 0.25 m under the same prestressing force 580 kN/2.3 m. It is noticed that increasing wall rigidity decreases significantly the maximum top displacement than that in case of 0.25 m thickness , also it causes the displacement of the wall to be more regular.

Figure 19 shows the bending moment variation due to two wall thickness 0.47 and 0.25 m. Increasing wall thickness increases the wall bending, It is noticed that the extreme negative and positive bending values are -314 and 382 kNm/m for 0.47 m wall thickness and –144 and 290 kNm/m for the 0.25 m wall thickness.
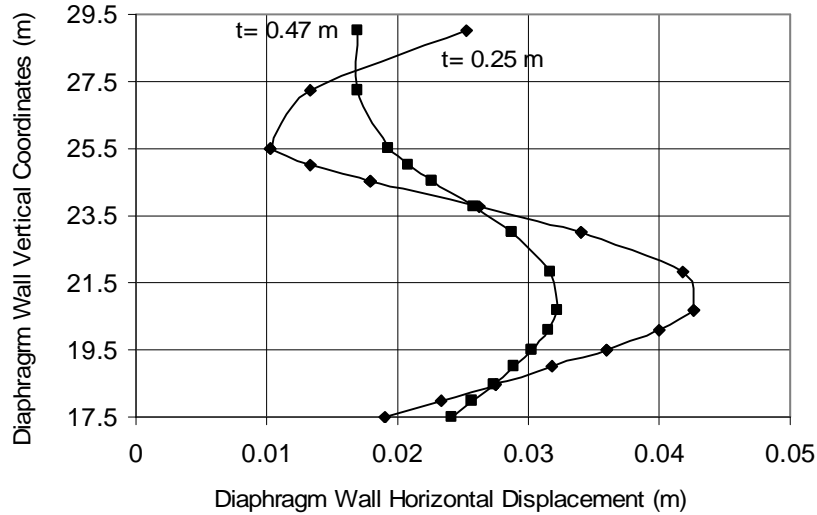
Fig. 18: Effect of Changing Diaphragm Wall Thickness (t) on Horizontal Displacement, phase 4
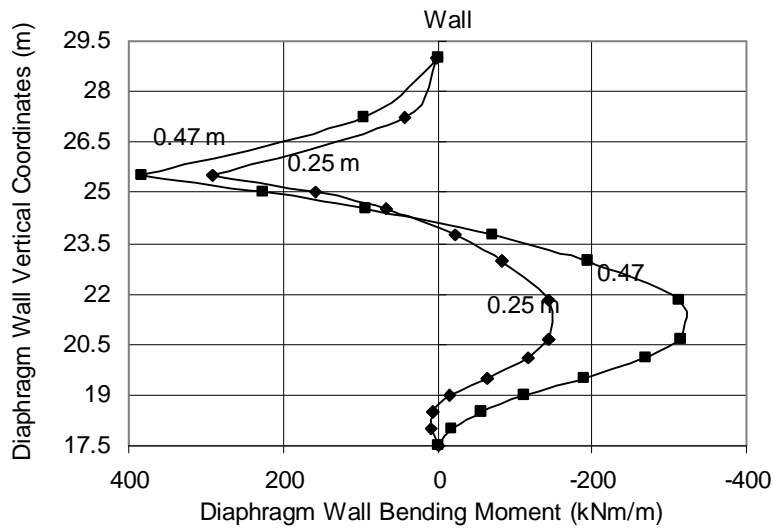
Fig. 19: Effect of Changing Diaphragm Wall Thickness on Horizontal Displacement, phase 4

Checking Program Predicted Wall Displacement Results with The Corresponding Field Measured Values

Figure 20 shows diaphragm wall top point horizontal component displacement as measured in situ at different construction phases compared with corresponding predicted values from the program outputs for 9.5 m deep excavation. It is noticed that the field measured displacement

values are relatively less and that may return to several factors, mainly assumed soil properties may not match very well with real values, also the program idealize the problem as plain strain problem for the near-bye building, while it may be more preferable to idealize it as three dimensional problem, but reasonable values are predicted from the plain strain analysis.
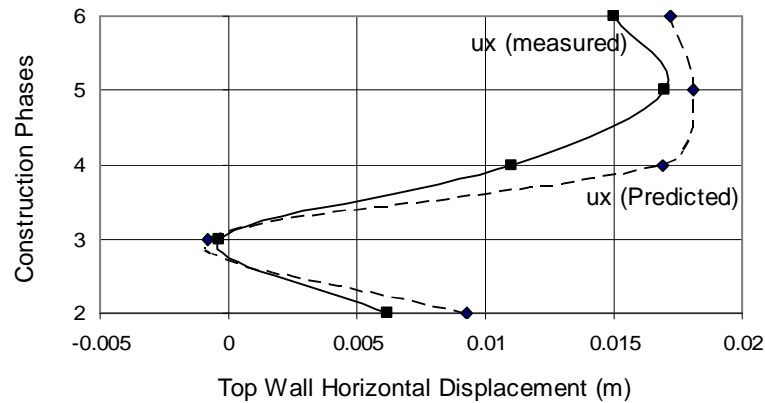
**Fig. 20: Comparison of Field and Program Predicted Displacements
for Top of the Diaphragm Wall**

CONCLUSION

(a) The calculated slight displacements which affect the building due to the near-by deep excavation ensure that the prestressed diaphragm wall can be considered as one of the effective solutions for supporting horizontal the active lateral earth pressure safely.

(b) The initial anchor prestressing force and the diaphragm wall thickness, both affects much the wall displacement and its resulted bending moments and also the affects the vertical displacements occurring to the near-by building.

(c) The diaphragm wall displacements which are predicted using the finite element plane strain analysis and Mohr Column failure model for soil can be considered satisfactory for solving such problems.

REFERENCES

1. Wong, K.S. and Brooms, B.B. (1988), "Lateral Wall Deflections of Braced Excavations in Clay", Journal of Geotechnical Engineering Division, ASCE, Vol. 115, No. GT6.
2. O'Rourke, T.D. (1981), "Ground Movements Caused by Braced Excavations", Journal of Geotechnical Engineering Division, ASCE, Vol. 107, No. GT9.
3. Terzaghi, K. and Peck, R.B. (1967), "Soil Mechanics in Engineering Practice", John Wiley and Sons, New York.

4. Henkel, D. J. (1971), "The calculation of earth pressures in open cuts in soft clays". The Arup Journal, 6 (4), pp. 14-15.
5. Peck, R.B. (1969), "Deep Excavations and Tunneling in Soft Ground", State-of-the-Art Report, 7th International Conference on Soil Mechanics and Foundation Engineering, Mexico.
6. Kim, N. K. and Briaud, J. I. (1984), "A beam column method for tieback walls", Report to Schnabel Foundation and the Federal Highway Administration, Department of Civil
7. Matlock, H., Bogard, D., and Lam, I. (1981), BMCOL 76: "A computer program foot the analysis of beam-column under static axial and lateral loading". Program Developed at the University of Texas at Austin and Documented at Ertec Inc., Long Beach, CA, USA. Engineering, Texas A & M University, College Station, TX. USA.

8. Clough, G. W. (1984), "User's Manual for Program Soil Struct", Department of Civil Engineering, Virgiria Polytechnic and State University, Blacksburg, VA, USA.
9. Long, M. (2001), "Database for wall and ground movements due to deep excavations", Journal of Geotechnical and Geoenviromental Engineering, ASCE, 127 (3), pp. 203-224.
10. Nosek, P. (1988), "Deep Foundation Pits in Czech cities", sheeting design practice and experiences, Proc. International Conference on Soil-Structure Interaction in Urban Civil Engineering, Darmstadt, Vol. 1
11. Masopust, J., Stanek, K., Nosek, P. (2003), "Foundation Pits in The City centers in The Czech", Republic XIIIth European Conference SMGE, Prague.

AN OVERVIEW OF CHALLENGES AND SOLUTIONS TOWARD IMPROVED, LOW COST BUILDING SYSTEMS IN THE US

Fernando P. Ruiz
*Owner of Brighton Homes and Builder of PATH Concept Home in Lincoln (see footnote),
Nebraska, USA, Tel (402)434-2456, E-mail: fpages@brightonconstruction.biz*
James D. Goedert, Ph.D., P.E.
*Director Construction Engineering and Management, University of Nebraska, USA, 68182,
Tel (402)554-3281, E-mail: jgoedert@mail.unomaha.edu*

ABSTRACT

The United States faces a housing affordability crises, especially among minority and disadvantaged populations in both rural and inner city, urban locations. The solutions to this challenge have come mainly through government subvention programs. However, dwindling Federal and State monetary resources cannot meet the needs of a burgeoning population requiring safe, energy-efficient, affordable housing. The United States department of Housing and Urban Development (HUD) recognized the need to address these issues from a broad, market-driven approach that relies on improved construction methods and materials, rather than simply underwriting inefficient and technologically outdated building practices. The Partnership for Advancing Technology in Housing (PATH) "is dedicated to accelerating the development and use of technologies that radically improve the quality, durability, energy efficiency, environmental performance, and affordability of America's housing." HUD's Office of Policy Development and Research manages and coordinates PATH activities. This government program in partnership with private industry is currently building a Concept House in Omaha, Nebraska, modeling the most advanced technological building methods currently in practice in the United States for residential construction. This house integrates compatible advanced building systems as an educational tool for both the housing industry and consumers of US housing. This paper will present a survey of affordable housing technologies and concepts.

Keywords: Residential, Affordable, Insulated Concrete Forms, Durable, Panelized.

INTRODUCTION

This paper describes some features of a Concept House that are relevant to the international audience because they highlight construction concepts as well as specific building techniques. The United States (U.S.) Department of Housing and Urban Development's (HUD) Partnership for Advancing Technology in Housing (PATH) in partnership with private industry is building the first concept house that integrates advanced building systems.

The U.S. Department of Housing and Urban Development's (HUD) mission is to increase homeownership, support community development and increase access to affordable housing. The Policy Development and Research (PD&R) Division of HUD is responsible for conducting research on important housing issues. Within PD&R is the PATH. PATH is "dedicated to accelerating the development and use of technologies that radically improve the quality, durability, energy efficiency, environmental performance, and affordability of America's housing" [1]. PATH has authored a library of research papers that have helped architectural engineers and manufacturers to develop more effective construction methods and materials. Examples

include studies and testing on cross-linked polyethylene (PEX) piping that lead to its broad acceptance throughout the United States at a time when copper prices made traditional water piping prohibitive. Other examples include research in concrete and wood framing techniques that provide cost savings and reduce the consumption of raw materials.

Residential construction in the United States operates, largely, within small, local code jurisdictions and without formal training. The lack of uniformity in construction regulations and a predominantly uneducated workforce makes it difficult to introduce new building technologies. The bureaucracies of municipal building departments tend to resist new construction methods. The artisan approach to training construction workers results in a labor pool that has memorized choreography of work habits. Little is learned regarding the engineering behind construction methods. Resistance to innovation is endemic to the construction industry in the Untied States.

The goal of the PATH Advisory Group is to designing and building one Concept House each year that would illustrate the best practices in residential construction and introduce a few emerging technologies. This is intended to speed the adaptation of new construction methods and to generate consumer interest in the advancing technology of homebuilding. This paper describes a few of the salient features in PATH's first Concept House. The home includes a number of innovative features that provide quality and affordability through improvements in production methods. The house is currently under construction in Omaha, Nebraska. This paper will first review the systems approach to design, then describe some energy efficiency features, and then discuss the panelized construction systems, insulated concrete foundation, and efficient mechanical systems.

SYSTEMS APPROACH

Technologies that are relatively new to the United States were introduced in the Concept House such as grey water recycling and movable interior partition walls. However, the most significant innovation came through a "systems" approach to design. This means every element in the house, from the foundation through the roof was engineered to work in coordination. The objectives of every element in the system were energy efficiency, durability, flexibility and speed of construction.

Energy efficiency came with the best weatherproof barriers available, a mechanically engineered grey water reclamation system, a water-saving tank-less water heater, expanding foam insulation derived from soybeans, and an engineered heating and air-conditioning system.

Durability was the focus of the exterior. It includes a 150-year standing seam steel roof. It also includes a panelized, insulated concrete form (ICF) used for the basement that installed in one day. A new attic wrap system assures ventilation for the sheathing and a weather-tight envelope over the attic.

Flexibility means a house that adapts to changing lifestyles. One example is movable partition walls. Wireless switches allow a homeowner the flexibility to reconfigure the floor plan to adapt to a range of lifestyles and family configurations.

Factory built components were assembled on the construction site increasing the speed of construction. The most dramatic improvements in construction time came with the panelized insulated concrete form (ICF) basement. These were manufactured in Minneapolis, Minnesota and trucked to the construction site in Nebraska. Within seven hours of the truck's arrival, workmen had finished assembling and pouring concrete into the insulated forms. Panelized floor, wall, and roof wood framing permitted similar improvements in the construction productivity of all structural components. Even millwork for windows and doors were fabricated in a factory setting and simply installed in place. With precise panelized framing and a systems approach to efficiency and durability, the home was quickly dry and under cover.

ENERGY EFFICIENCY

The double-hung windows were installed perfectly into the rough framing openings, providing further evidence of the precisely constructed shell. These Energy Star windows are efficient and durable to keep the harsh Nebraska weather out, thanks to a low U factor (0.35) and a low-emissivity film with UV protection to reduce heat gain and fading.

The weather barrier system features an innovative weather resistant barrier. It has specially designed vertical grooves to channel water to the outside while still allowing moisture vapor to pass through. The weather resistant system for the roof and attic includes a "cool" metal roof. It gives long-term durability and maximum energy performance through its pre-painted solar reflective color that reduces heat and its special zinc/tin alloy that provides enhanced corrosion resistance (see Figure 1).

Fig. 1: Energy Efficient Exterior

The attic wrap is a breathable membrane installed just under the top chord of the trusses. It helps to create an airtight seal. Its metalized surface reflects heat while allowing moisture vapor to escape. This reduces air leakage and energy loss through roof while allowing the attic to dry out.
Insulated vinyl siding was installed over the framing and weather resistant barriers, creating an energy efficient shell. Styrofoam backing provides an R-3 insulative value and increases the stiffness and rigidity of the siding. The thermal siding with the drain wrap keeps water out and allows any moisture to easily drain from the assembly. The wood trim was pre-painted and ready to install upon arrival allowing the trim to be installed along with the siding. This feature reduced installation time and rental fees associated with lift equipment as shown in Figure 2.

Fig. 2: Vinyl Siding

PANELIZED CONSTRUCTION SYSTEMS

Panelized construction systems in the United States refers to building components manufactured off site, generally in a factory, and then transported to the point of construction in flat panels ready for assembly. The Concept House used several factory built components, most notably insulated concrete forms (ICF) built in approximately 3.66 meters (12-feet) by approximately 2.44 meters (8 feet) rectangles; factory framed floors brought to the jobsite in approximately 2.44 meters (8 feet) by approximately 7.32 meter (24 feet) sections; walls in 2.44 meters (8 feet) by 3.05 meters (10-feet) sections, and truss roof framing. The benefits of panelized construction include reliable working conditions in areas of inclement weather, speed of construction and assembly, reliability based on computer driven tools and factory tolerances, and worker safety in erecting fully-built panels rather than building block-by-block in more precarious jobsite conditions.

Insulated Concrete Foundations

ICFs are appealing for the increased productivity and high insulation values. The proprietary product design and expensive distribution system coupled with high labor costs have diminished the benefits of a these super-insulated concrete walls in affordable housing. Gajda and VanGeem [4] found that homes built with ICFs had total energy reductions between 8% and 19% below traditional wood framed construction. In addition, the cost savings from reduced system capacity ranged from 16% to 30% below houses meeting the International Energy Conservation Code. Proponents argue that the benefits of additional structural insulation are often paid back in lower operating costs. Others indicate that reduced operating costs can be achieved through other less costly methods.

ICFs come in three varieties including a flat wall core system illustrated in Figure 3. Other systems include the waffle grid and the screen grid [5]. Nevertheless, when used in a panelized system, the lower onsite labor costs and speed of assembly promise to provide a bright future for ICFs. In regions of the world where facilities exist for designing and building polystyrene blocks and labor is less expensive, ICFs represent a viable alternative to concrete block.
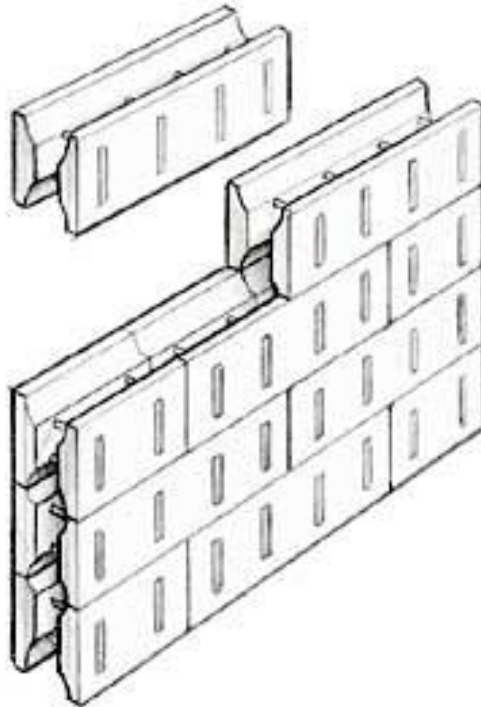
Fig. 3: Insulated Concrete Form

On the concept house, instead of stacking standard sized blocks, the manufacturer designed full height wall panels to within half-an-inch of the specified height. They were trucked to the construction site along with an expert installer. After training a local crew who were inexperienced with the product, the manufacturer delivered the basement walls for a 2,000 square-foot house at 8:00 in the morning. The walls were unloaded and erected by noon, with concrete placement beginning in the early afternoon as shown in Figure 4.

Fig. 4: Concrete Placement in Insulated Concrete Forms.

The windows were cut into place with no need to strip forms, apply waterproofing, or insulate the basement. The whole process was done in a day. The standard block or aluminum formed basement would have taken approximately two weeks to complete in two separate phases.

Factory Framing

Wood framing is of lesser relevance to projects outside North America. However, the Concept House was greatly advanced through the use of component floors and walls. Like the ICF forms, these components are built in a factory using proprietary engineering software and a computer automated factory equipment. The equipment cuts and marks all framing members. Assembly occurs on steel tables with large banks of nail guns. The panels are lifted onto trucks in reverse order of jobsite assembly, delivered to the construction, and then assembled by semi-skilled labor. Of greatest interest to the international construction community might be the component floor systems, since many countries use wood in the construction of floors and roof structure as shown in Figure 5.

Fig. 5: Component Floor System.

Ruiz [8] indicates that panelized systems result in substantial labor savings. The first floor panel required 21.36 man-hours of shop time and 6.25 man-hour of field time. Conventional framing would take approximately 31 man-hours of field time. The second floor panels required 29.64 man-hours of shop time and 7.5 man-hours of field time. Convention framing of the second floor would take approximately 41 man-hours. This is a productivity increase of approximately nine percent.

MECHANICAL SYSTEMS

The key to balancing durability with energy efficiency in the Concept House's mechanical system was to system engineer the whole rather than separate elements. Durability was provided using low-cost means while achieving longer lifespan in mechanical systems. Cross-linked polyethylene (PEX) has been used in Europe for more than 30 year and more than 10 years in North America. PEX is superior to polybutylene piping systems [3] and does not break in freezing temperatures or corrode with mineral elements [2]. Energy efficiency was accomplished with tightly sealed duct delivery system for heating and air conditioning that would not waste fuel consumption due to in-line losses and pour, unbalanced distribution of conditioned air.

A tankless water heating system produces hot water on-demand. This device won't waste energy keeping water hot when there is no demand. Even the venting of the system is advanced, relying on special 1-way air valves called Air Admittance Vents (AAVs) to let air into

the drain system when needed. These units perform the same function as a traditional vent stack but eliminate the piping requirements and most of the roof penetrations.

Engineered Plumbing

The Concept Home has a state-of-the-art integrated system, featuring an efficient design, water-conserving components, and innovative technologies that show the future in water management.
The Concept House floor plans show a centralized mechanical core with bathrooms and laundry room adjacent to this core. This innovative design strategy reduces the necessity to run pipes, wires and ducts throughout the home. Material requirements are reduced, along with the number of joints and time required for installation. In the United States, residential plumbing, heating and electrical systems are generally designed on site relying on individual tradesmen to simply figure out what and how to install based on experience. The PATH Concept House employed professional engineers to analyze and design the systems for maximum efficiency.

The PEX tubing was literally pulled from the basement to the upstairs fixtures, saving on installation time. The "home run" lines have no joints and ensure that hot water arrives quickly upon demand. Many of the lines take advantage of 3/8" tubing (instead of ½"). This further reduces line loss while waiting for hot water. The system displayed in Figure 6 allows the builder and homeowner to control each water line independently, meaning that maintenance and remodeling can take place without shutting off water for the entire home. Installation and updates to the plumbing are further simplified by quick-connect fittings that quick snap connection between the PEX and each fixture. These innovative components speed installation and make later disconnects easy.

Fig. 6: PEX Plumbing Manifold

Grey Water System

Grey water systems in the UK usually refers to water recycling from "any water source except those with fecal matter present but is mainly restricted to baths, showers and hand basins" [6]. Following filtration and sterilization, the recycled "grey water" is used for clothes washing, irrigation, and supply water to toilets. The system uses no chemicals to clean the water making it an environmentally benign product. These small scale treatment plants represent a growing trend in water conservation. This particular system represents the first grey water recycling system installed in a major metropolitan area in the United States. Many government agencies are not yet familiar with these systems and substantial hurdles exist for installation.

Issues regarding recycled water are extremely complex when considering large-scale urban environments where the opportunities abound. However, these small scale recycling technologies so real potential and have become commercially available. Jeffrey, et.al. [7] indicates that "a simple reuse system which takes water from the bath and shower to be used for toilet flushing, average water savings of about 20%." This saving is significant when multiplied by the large number of households in a given municipality.

CONCLUSION

The HUD PATH program is attempting to educate home builders across the United States through the concept home. Innovative technologies are developed and then incorporated into the home. This is followed by a series of promotions including a website with links describing those new technologies. The first concept home built in Omaha, Nebraska incorporates a number of innovative systems. Most of these systems are proven technologies that have not gained wide acceptance. Some systems may be cost prohibitive in a competitive market. Others may have higher initial cost with lower overall life cycle cost. Technologies such as the ICFs are gaining market share. The concept house used the ICF only for the basement. Some builders are using the ICF for the entire structure including affordable home builders. PEX water distribution systems make good economic sense and are allowed by the International building code. This alternative to copper piping is economical in terms of both materials and installation. It is not yet widely accepted in the United States due in large part to the lack of information but probably more from resistance to change. This resistance to change is endemic in the United States construction industry. The construction industry has no single leader that creates or establishes a competency with economic advantage for other to follow. Rather it is a fragmented industry with a number of competitors with little will to affect change. It is efforts like the HUD PATH program working with industry on the concept home that will create the change agent necessary to influence the industry as a whole.

ACKNOWLEDGEMENT

REFERENCES

1. "About PATH", http://www.pathnet.org/sp.asp?id=15221 (2007), accessed April 20, 2007
2. "Crosslinked Polyethylene (PEX) Tubing", (1998), Plastic Pipe Institute, TN-17.
3. "Differences Between PEX and PB Piping Systems for Potable Water Applications", (2004), Plastic Pipe Institute, TN-31.
4. Gajda, J., & VanGeem, M. (2000), "Energy Use in Residential Housing: A Comparison of Insulated Concrete Form and Wood Frame Walls", Portland Cement Association, Research and Development Serial No. 2415.
5. "ICFs in Residential Construction", http://www.forms.org, (2007) accessed April 22, 2007.
6. Jefferson, B., Laine, A.L., Judd, S.J., & Stephenson, T. (2000) "Membrane bioreactors and their role in wastewater reuse", Water Science and Technology, Vol. 41, No. 1, pp. 197-204.
7. Jeffrey, P., Seaton, R.A.F., Parsons, S.A., Judd, S.J., Stephenson, T., Fewkes, A., Butler, D., & Dixon, A. (2000), "An interdisciplinary approach to the assessment of water recycling technology options", International Journal of Water, Vol. 1, No. 1, pp. 102-117.
8. Ruiz, F.P., (2005), "Better Framing with Factory-built Walls", Fine Homebuilding, February/March, pp. 68-71.

EFFECT OF BACTERIAL ADDITIVES ON THE PERFORMANCE OF SEPTIC TANKS FOR WASTEWATER TREATMENT IN THE UPPER EGYPT RURAL AREA

A.H. Mostafa
Housing and Building National Research Center, Water Pollution Control Dept.,Cairo,Egypt.
M. H. Mostafa
Housing and Building National Research Center, Water Pollution Control Dept.,Cairo,Egypt.
H. T. El-Zanfaly
Housing and Building National Research Center, Water Pollution Control Dept.,Cairo,Egypt.
I. Fahim
Sanitary Waste Company, Cairo, Egypt.

ABSTRACT

The experimental work was executed on 6 septic tanks represent two modified types located in villages of the Upper Egypt. Three of them receiving waste with medium organic load, while the others receiving waste with high organic load. Mixture of five selected, adapted, enzyme active producer, bacillus bacterial species has been used as additive to the septic tanks under investigation in order to test its ability to improve the effluent quality as well as increase the efficiency.

Regarding the septic tanks receiving the medium load, a slight improvement in the effluent wastewater quality was achieved few days after the addition of the bacteria. At the 6th day, the effluent showed gradual increase in the percentages of removal in the examined parameters reaching the maximum values at day 30 and showed ranges for removal percentage (%) reaching: 91.3-94.4, 93-95.8, 90-91.7, 75-87, and 99.95 – 99.99 for COD, BOD_5, TSS, oil & grease and total coliforms, respectively. After 36 days a gradual decrease in percentages of removal was observed, showing higher values than that achieved in the absence of bacterial additives. At the end of the experimental period (60 days) the effluent of the septic tanks that supported with cultured bacteria had the following characteristics: COD; 77.2-104.8 mg O_2/ l , BOD_5; 44.1-58.7mg O_2 /l; TSS; 52.9-70.6 mg/l, Oil & Grease; 4.1-15 mg /l and total coliform 10^4-10^6 MPN/ 100ml. It is important to mention that at the same time, septic tanks without bacterial additives were able to show removal percentages (%) ranged as: 79.3-88.5 , 80 - 85.5, 75.1 - 83, 28 - 41.7 , and 98.5 - 99.85 for COD, BOD_5, TSS, oil & grease and total coliforms, respectively.

Regarding the other three septic tanks that receiving influent with high load of pollutants, again the actual improvement in the effluent quality appeared at the 6th day with maximum removal after 36 days, and may extend to 42 days, after addition of bacteria. During this period, the removal percentages for COD, BOD_5, TSS, oil & grease and total coliform were ranged as 93.8-97.2, 94.5-97.0, 94.0-97.9; 64.0-93.8; 99.81-99.99, respectively. Septic tanks without bacterial additives showed percentages of removal efficiency ranged as 64.7 – 87.2, 73.4 – 89.6, 56.7 – 86.9, 34.6 – 45, and 92.8 – 99.28 for COD, BOD_5, TSS, oil & grease and total coliforms, respectively.

Although, the removal efficiency of septic tanks with bacterial additives was higher in case of those receiving the high load of pollutants than those receiving medium load, the pollutants residual in the final effluent (after 60 days) of the first case are higher.

Key Words: Wastewater Treatment , Septic Tanks , Bacterial Additives

INTRODUCTION

Septic tanks/soil absorption systems are an option to consider wherever a centralized treatment system is not available. It has been the most popular on-site method (U.S. EPA, 1980) [17]. The septic tank is an underground, watertight vessel installed to receive wastewater from the home. It is designed to allow the solids to settle out and separate from the liquid, to allow for limited digestion of organic matter, and to store the solids while the clarified liquid is passed on for further biological, physical and chemical reactions through the subsurface wastewater infiltrations system (SWIS). Collected solids undergo some decay by anaerobic digestion in the tank bottom and depending on the activity of natural microorganisms that exist in the waste with minimal human intervention. Scum and grease float to the surface and the baffles keep it out of the soil absorption system. If an excessive amount of sludge is allowed to collect in the bottom of the septic tank, wastewater will not spend a sufficient time in the tank before flowing into the soil. Depending on the retention time of liquids in the septic tank, further biological treatment is expected from the natural microorganism existed.

Clarified septic tank effluent exits the septic tank and enters the soil absorption system where a biological biomat forms, contributing to even distribution of the waste into the soil (Hoover et al., 1996) [7]. The character of wastewater flowing into the soil absorption area is a critical variable for proper functioning of septic system. Soil absorption systems work most effectively when the influent does not contain significant levels of settleable solids, greases and fats. To avoid infiltration soil clogging by grease and scum, outlet baffles are suggested. Also, the use of two-compartment tanks recommended over single- compartment design. Absorption beds and trenches are the most common design options for soil absorption systems (U.S. EPA, 1980) [17].Since digestion of wastes in septic tanks is performed biologically, it is a temperature dependent process and colder temperature as well as the addition of toxic substances (as detergents, bleaching agents, acids, solvents, etc.) which may hinder the effective biological breakdown of wastes in septic tanks (Montgomery, 1990 and Seifer, 1999) [10,13] and cause septic tank upset. In addition, other cases such as when someone in the home is on chemotherapy for an extended period of time and the unused septic tanks for long period or the high loads of the hard biodegradable materials, may destroy or stress the biological activity in the septic tank. Under all these conditions, it is possible to suggest the addition of biological additives in the form of enzymes or microorganisms to help speed the re-establishment of biological activities.

 Failure of systems to adequately treat wastewater may be related to inadequate site, inappropriate installation, or neglectful operation. Hydraulic overloading has been identified as a major cause of system failure (Jarrett et al., 1985) [8].

Septic systems can act as sources of nitrogen, phosphorus, organic matter, and microbial pathogens, which can have potentially serious environmental and health impacts. Since septic wastewater contains various nitrogen compounds (Brown, 1998) [3], installation of septic systems in areas that are densely developed can, in combination with other factors, result in the introduction of nitrogen contaminants into groundwater. Groundwater impacts can occur even when soil conditions are favorable because the unsaturated aerobic treatment zone located beneath the drain-field promotes conversion of wastewater-borne nitrogen to nitrates. If nitrate contamination of groundwater is a concern in the rejoin, control methods or denitrifying technologies may be required for safe operation of a septic system (U.S. EPA, 1999) [18].

Conventional septic systems are designed to operate indefinitely if properly maintained. However, because most household systems are not well maintained, the functioning life of septic systems is typically 20 years or less (U.S. EPA, 1999) [18].

MATERIALS AND METHODS
A. SEPTIC TANKS:

Septic tanks were modified by some organizations as on-site, simple and low cost wastewater treatment system in a group of villages in the Delta and Upper Egypt.
The modified septic tank, as shown in Fig.1, consists of the same components of the traditional one and represented by:
a- Entrance chamber   b-Sedimentation chamber
c- Distribution chamber   d-Outlet chamber

There was anaerobic filter contained two layers of gravel .The bottom layer contained gravel (40 – 60 mm in size) of two third of the depth. The top layer contained gravel (20 – 40 mm in size) of one third of the depth. According to the design criteria for the modified septic tank, the retention time for the wastewater is ranged as 1-3 days according to the tank type.

The experimental work was executed on two types of modified septic tanks. The 1st type which represented the medium organic load served (10 persons) with a sedimentation chamber capacity of 2.4 m^3 and dimensions (L= 2m, W = 1 m, and D = 1.2 m). This type achieved sedimentation retention time = 3 days .There was only one filter chamber with dimensions = (L2 = 1 m, W=1 m ,d=1 m). The 2nd type which represented the high organic load served (200 persons) with a sedimentation chamber capacity of 35.5 m^3 and dimensions (L=13 m, W = 1.7 m, and D = 1.6 m). This type achieved sedimentation retention time = 2.2 days .There was two filter chambers with dimensions of each chamber = (L2 = 1.5 m, W=1.7 m ,d=1.2 m).The bacterial additives were added in one package to the wastewater inside the distribution chamber of the two types of the septic tanks as a ratio of the quantity of the wastewater found in the sedimentation chamber .The results of the effluent were monitored and compared with results without bacterial additives until reaching the same results. At that time the bacterial additives must be added again.
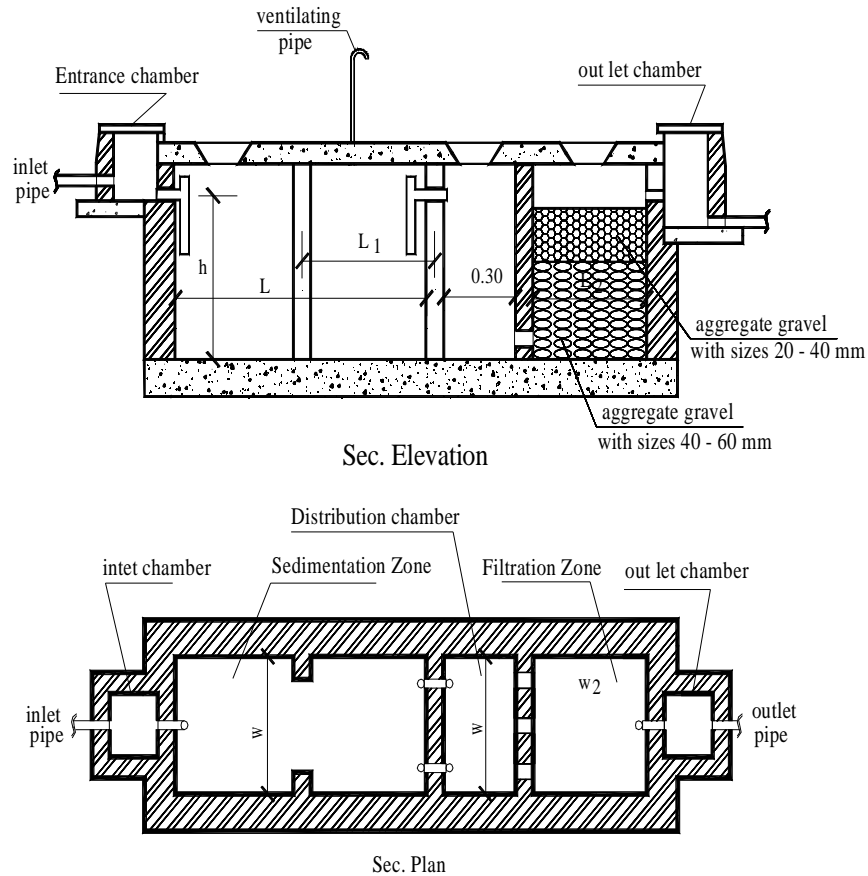
Fig. 1: Typical Modified Septic Tank

B) BACTERIAL CULTURES

From sewage samples collected from septic tanks, 800 bacterial isolates were isolated, purified by streaking on tryptic soy agar medium and microscopically examined to ensure its purity. All the isolates were assayed for their enzymatic activity using different substrates and focusing on:

protease, amylase, lipase, esterase, cellulase, xylanase and urease production. Two hundred and forty isolates were selected according to their high enzyme production activity and only 158 of them that were able to show stability in activity through twenty times of sub-culturing. Another adaptation program was carried out on these 158 isolates through testing their ability to produce the mentioned enzymes at different temperature and pH values. Only 78 isolates that was able to show the ability to produce enzymes at wide ranges of temperature (10-55°C)and pH values (4-10). Stability of the characters was tested by sequential culturing program using media containing sewage and finally only 23 isolates that could pass the screening tests. The API identification system was followed and showed that the last 23 isolates could be grouped as belong to 5 bacillus species.

One strain of each species was selected, cultured on tryptic soy agar slants and kept in the refrigerator as stock culture to be used in the present study.

Two days before the experiment, the five strains were inoculated in nutrient broth and incubated at 37°C for 24 hr. Each cultured strain was centrifuged at 4500 rpm for 10 min and the sediment from every 1 liter culture was collected separately in sterile bottle and kept in the refrigerator. The sediments were transported to the site of the experiment in icebox. Every septic tanks gravel filters were seeded with the culture sediments (the sediment resulted from 1 liter culture/m^{3} of the tank capacity).

C) SAMPLING

The effluent from the septic tank under study before and after inoculation with the mixture bacterial was collected in sterile glass bottles and transported in icebox to the laboratory for bacteriological and chemical examinations. The parameters were determined according to the Standard Methods for the Examination of Water and Wastewater (APHA, 1998) [1] and included: total coliforms MPN/100 ml, biochemical oxygen demand (BOD$_5$), chemical oxygen demand (COD), total suspended solids (TSS) and oil & grease.

RESULTS AND DISCUSSION

1- The application of bacteria for sewage treatment in septic tanks should ensure that it was conducted close to the recommendations prescribed by U.S. Environmental Protection Agency (U.S.EPA) [17,18,19] for minimizing the environmental and/or users risk.

2- U.S.EPA standards ensure that the number of micro-organisms emitted from the site where microorganisms are used is minimized. It does not specify specific limits for the emitted microorganisms. EPA specified that the introduced genetic material, in case of genetic engineered strains, must be limited in size to reduce the risk of introduction uncharacterized genetic material. In the present study, the used strains were selected from the natural habitat which have high rate of enzymatic activity as well as it can grew at wide range of pH and temperature and not genetically engineered strains.

3- Although direct monitoring data are unavailable, worst case do not suggest high levels of the public exposure resulting from the application of these bacteria in well designed and maintained septic tanks. However, human exposure via dermal and ingestion routes as well as release to the environment may occur if the effluent from the treated septic tanks is discharged on an open area or directly on surface water.

4- In the present study, the used strains were isolated from sewage and commonly exist in soil and ubiquitous nature. They are un- pathogenic nor toxigenic (Banerjee et al. 1988, and Edberg,1992) [2,6].

5- When B. licheniformis enter the human digestive system it is not able to colonize to any large degree. However, if challenged by large numbers of this microorganism, it may cause limited gastroentertities for only the compromised individuals (Edberg, 1992) [6]. Outside the gastrointestinal tract, it would likely be a temporary inhabitant of skin (Claus and Berkeley, 1986) [4]. It is widely known as a contaminant of food, but not thought to be causal agent for food poisoning (Norris et al., 1981) [11]. There was no mention of any plant pathogenic activity in Bergey's Manual of systemic Bacteriology (Claus and Berkeley, 1986) [4].

6- The base considered in strains selection was to cover the various conditions at which the degradation of pollutants may occur (aerobically or anaerobically, and wide ranges of pH

and temperature). The selected species of bacteria through their enzymatic activity can breakdown the different pollutants that usually occur in sewage such as carbohy- drates, proteins, cellulose, urea, oil and grease (Table 1).

7- Three septic tanks located in villages namely Gragoos; Quina Governorate, El-Mahameid; Aswan Governorate, and Bany sanad; Asuot Governorate were selected on the base that they receive wastewater influent with medium load of organics (COD 560 – 640 mg O_2/ 1 and BOD_5 350 – 400 mg O_2 /1). A slight improvement in wastewater quality was achieved

Table 1 : Characteristics of the Selected Strains Used as Septic Tank Additives

Character	Bacillus amylo-liquefaciens	Bacills licheniformis	Bacillus subtilis	Bacillus megaterium	Bacillus pumilus
Growth	Facultative	Facultative	Aerobic	Aerobic	Aerobic
pH range	6-10	5-10	4-10	5-10	6-10
Temperature	10-50	10-55	10-50	4-45	10-50
Production of: Protease (break down of proteins)	++	++	++++	+++	+++
Amylase (break down of carbohydrates)	++	++	++++	+	+
Lipase (break down of grease)	++	++	++++	+++	+++
Esterase (break down of fats)	++	++	++++	+++	+++
Cellulase (break down of cellulose)	++	+	++++	+++	++++
Xylanase (break down of plant materials)	++	+	++++	+++	++++
Urease (break down of urea)	+++	++	++	++++	++

+ Moderate   ++ = Good   +++ = Very Good   ++++ = Excellent.

during the first few days after the addition the mixed culture of bacteria to the gravel filter. From the 6th day, the gradual increase in the percentages of removal in the examined parameters was observed reaching the maximum values at day 36 for the effluents of the three septic tanks. The maxi-mum percentage of removal achieved was ranged as 91.3-94.4 for COD, 93-95.8 for BOD5, 90-91.7 for TSS, 75-87 for oil & grease, and 99.95 – 99.99 for total coliform.

After 42 days a gradual decrease in percentages of removal for all determined parameters was observed, but still higher than the values achieved in the absence of bacterial additives.

At the end of the experimental period (60 days) the effluent of the septic tanks had the following character:

COD; 77.2-104.8 mg O_2 / l , BOD5; 44.1-58.7mg O_2 /l; TSS; 52.9-70.6 mg/l, Oil & Grease; 4.1-15 mg /l and total coliform 10^4-10^6 MPN/100 ml (Tables and Figures. 2 ,3, 4).

8- It is important to mention that septic tanks without bacterial additives showed removal percentages ranged as 79.3-88.5 for COD, 80 - 85.5 for BOD5, 75.1 - 83 for TSS, oil & Grease 28 - 41.7 for oil & grease, and 98.5 - 99.85 for total coliform (Tables and Figs 2,3,4).

9- Other three septic tanks were selected in three villages, namely Enibis; Souhag governorate, Bani Sanad; Asuot governorate, and El-Mahameid; Aswan governorate to represent tanks receiving influent with high load of pollutants (COD; 1072 – 2180 mg O_2 /l and BOD5; 714-1200 mg O_2 /l, TSS 205 - 1144 mg/l, oil & grease 40-104 mg/l al total coliform 10^8-10^9 MPN/ 100

ml.Again the actual improvement in the effluent quality appeared at the 6th day after bacterial addition to the tanks. Microorganisms used for wastewater treatment are likely to be exposed to a wide variety of environmental stresses. Stress factors can range from high concentration of contaminants, detergents or solvents, through extremes in pH, oxygen tension, ionic strength, and nutrient concentrations (Morita, 1988). Microorganisms must adapt to these conditions to be able to degrade the pollutants. In some cases genetic engineering may be helpful in augmenting resistance to such stress, thereby facilitating good performance of degradative organism under adverse conditions (Clark, G.H.1999) [5].

Table 2: Changes in Parameters Rested after the Addition of Bacterial Additives to Septic Tank at El Mahamid Village, Aswan Governorate

parameters	Time in days after bacterial addition											
	0	3	6	12	18	24	30	36	42	48	54	60
COD inf.	560	565	568	578	585	605	615	620	635	640	650	655
COD eff.	116	113	98.3	87.9	76.6	70.2	60.9	54	62.2	71	91	104.8
% Removal	79.3	80.3	82.7	84.8	86.9	88.4	90.1	91.3	90.2	88.9	86.0	84.1
BOD inf.	400	405	418	428	435	450	470	465	440	435	430	425
BOD eff.	80	67.1	72.3	64.2	54.4	45.5	37.1	32.6	35.6	41.8	51.2	58.7
% Removal	80	81.2	82.7	85	87.5	89.9	92.1	93.0	91.9	90.4	88.1	86.2
Tss inf.	654	348	355	350	365	375	388	393	375	370	365	360
Tss eff.	88	85.6	78.8	65	58.4	50.3	42.3	39.3	41.3	44.8	49.6	52.9
%Removal	75	75.4	77.8	81.4	84	86.6	89.1	90.0	89.0	87.9	84.4	85.3
Oil & grease inf.	64	63	65	70	71	73	75	70	78	65	63	60
Oil & grease eff.	46	42.8	35.7	30.8	22.7	15.3	11.3	9.1	10.9	12.4	12.2	15
%Removal	28	32	45	56	68	79	85	87	84	81	79	75

Table 3: Changes in Parameters Rested after the Addition of Bacterial Additives to Septic Tank at Benisand Village, Asuit Governorate

parameters	Time in days after bacterial addition											
	0	3	6	12	18	24	30	36	42	48	54	60
COD inf.	600	610	625	635	660	690	700	710	735	715	710	720
COD eff.	87	86	81.3	73	64	56.6	50.4	47.6	52.2	60.8	65.3	79.2
% Removal	85.5	85.9	87	88.5	90.3	91.8	92.8	93.3	92.9	91.5	90.8	89.0
BOD inf.	350	353	358	360	365	368	375	388	390	385	383	380
BOD eff.	59.7	54	49.4	42.8	36.9	29.1	24	22	27.3	33.5	38.3	44.1
% Removal	84.1	84.7	86.2	88.1	89.9	92.1	93.6	94.3	93.0	91.3	90.0	88.4
Tss inf.	434	440	450	455	459	465	473	470	465	475	480	478
Tss eff.	73.8	73	69.3	63.7	56.9	50.7	44	39	41.1	47.5	52.3	66
%Removal	83	83.4	84.6	86.0	87.6	89.1	90.7	91.7	91.1	90.0	89.1	86.2
Oil & grease inf.	12.0	12.5	12.8	12.5	13.0	13.2	13.8	14.0	12.9	13	12.8	12.5
Oil & grease eff	8	8.1	7.54	6.34	5.5	4.5	3.6	3.5	3.47	3.73	3.84	4.1
%Removal	33.3	35.0	41.1	49.3	57.6	66.0	74.2	75.0	73.1	71.3	70.0	67.6

Table 4: Changes in Parameters Rested after the Addition of Bacterial Additives to Septic Tank at Garagoos village, Quina Governorate

parameters	Time in days after bacteria addition											
	0	3	6	12	18	24	30	36	42	48	54	60
COD inf.	640	635	655	670	678	690	710	715	720	705	712	720
COD eff.	96	90.8	81.9	72.4	62.4	53	46.2	40	49	55.7	69.8	85.4
% Removal	85	85.7	87.5	89.2	90.8	92.3	93.5	94.4	93.2	92.1	90.2	88
BOD inf.	400	408	418	435	450	468	477	489	494	490	480	492
BOD eff.	58	57.5	53.5	47.9	41.9	35.1	27.2	20.5	24.7	32.8	41.8	54
% Removal	85.5	85.9	87.2	89	90.7	92.5	94.3	95.8	95.0	93.3	91.3	91.3
Tss inf.	380	388	395	398	415	420	428	435	430	428	420	415
Tss eff.	69.2	68.7	64.8	59.7	56.9	51.7	46.6	42.6	48.2	52.6	59.2	70.6
%Removal	81.8	82.3	83.6	85	86.3	87.7	89.1	90.2	88.8	87.7	85.9	93
Oil & grease inf.	12	11.8	12.5	12.8	13.3	13.7	13.9	14.2	14	12.9	13.2	13.0
Oil & grease eff.	7	6.7	6.5	5.8	5.2	4.5	3.6	2.94	3.3	3.4	4	4.3
%Removal	41.7	43.2	48	54.5	60.9	67.5	74.3	79.3	76.5	73.8	69.8	67.1
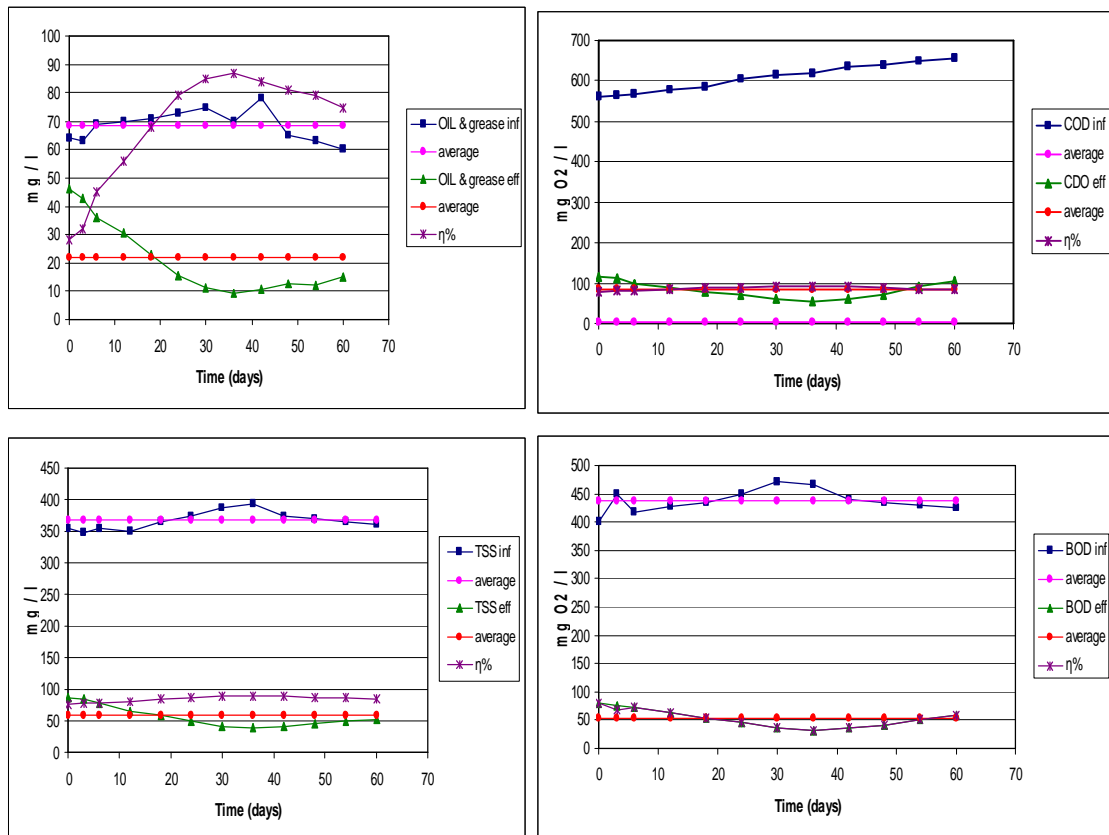
Fig. 2 : Changes in Parameters Rested after the Addition of Bacterial Additives to Septic Tank at El Mahamid Village, Aswan Governorate.
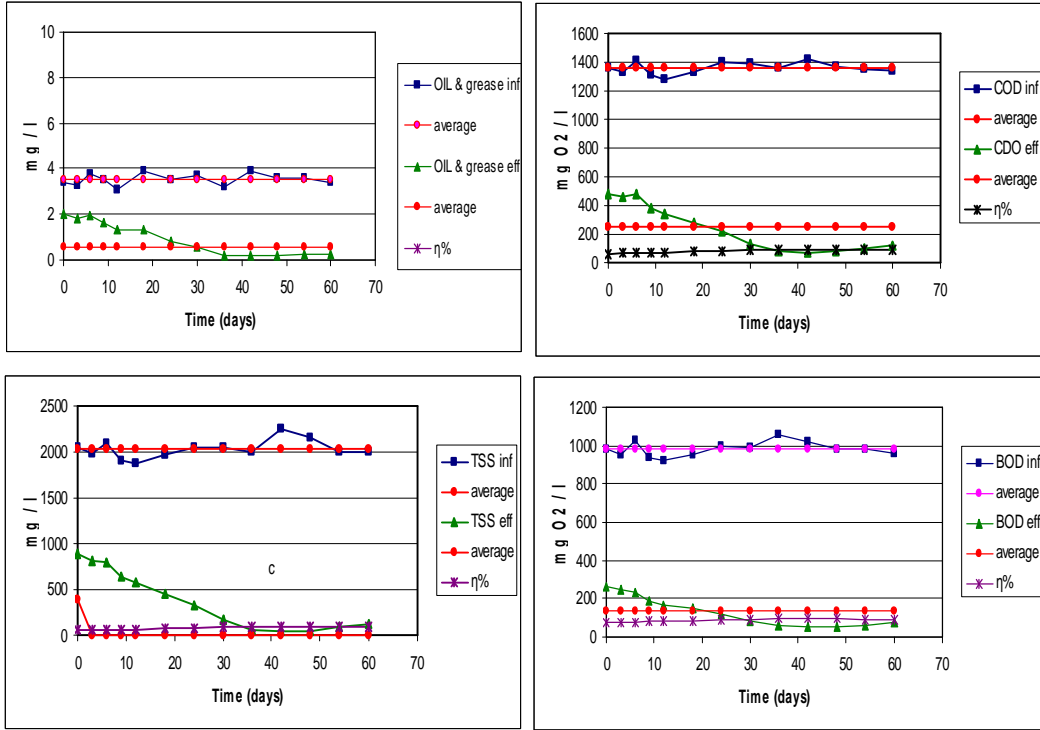
Fig. 3 : Changes in Parameters Rested after the Addition of Bacterial Additives to Septic Tank at Benisand Village, Asuit Governorate
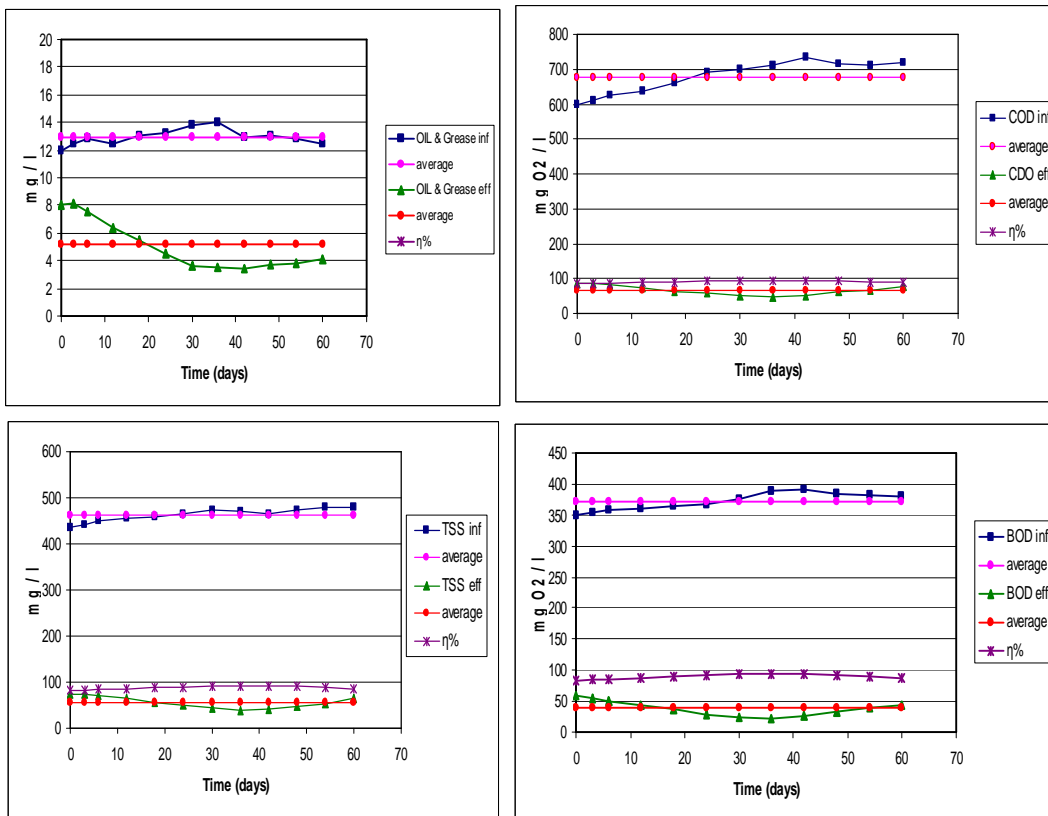

Fig. 4 : Changes in Parameters Rested after the Addition of Bacterial Additives to Septic Tank at Garagoos Village, Quina Governorate

10- In the present study, the maximum removal efficiency appeared after 42 days and may extend to 48 days. During this period, the removal percentages for COD, BOD5, TSS, oil & grease and total coliform were ranged as 93.8-97.2, 94.5-97.0, 94.0-97.9; 64.0-93.8; 99.81-99.99, respectively (Tables and Figures. 5,6,7).

Septic tanks without bacterial additives showed removal efficiency (as %) ranged as 64.7 – 87.2 , 73.4 – 89.6, 56.7 – 86.9, 34.6 – 45, and 92.8 – 99.28 for COD, BOD5, TSS, oil & grease and total coliform, respectively.

Table 5 : Changes in Parameters Rested after the Addition of Bacterial Additives to Septic Tank at El Mahamid Village, Aswan Governorate.

parameters	Time in days after bacteria addition											
	0	3	6	12	18	24	30	36	42	48	54	60
COD inf.	2180	2210	2230	2260	2290	2280	2310	2340	2380	2350	2280	2220
COD eff.	280	2785	245.5	214.7	176.3	139.1	101.6	74.9	66.6	82.3	114	162.1
% removal	87.2	87.4	89.0	90.5	92.3	93.9	95.6	96.8	97.2	96.5	95.0	92.7
BOD inf.	1200	1190	1230	1250	1280	1290	1295	1310	1330	1360	1290	1300
BOD eff.	125	120.2	114.4	100	88.3	72.2	58.3	45.9	39.9	55.8	77.4	102.7
% removal	89.6	89.9	90.7	92.0	93.1	94.4	95.5	96.5	97.0	95.9	94.0	92.1
Tss inf.	1144	1160	1180	1210	1225	1250	1270	1290	1310	1325	1320	1310
Tss eff.	150	148.5	139.2	127	111.5	98.8	81.3	67.1	61.6	79.5	100.3	115.3
%removal	86.9	87.2	88.2	89.5	90.9	92.1	93.6	94.8	95.3	94.0	92.4	91.2
Oil & grease inf.	104	106	109	112	115	120	123	108	118	120	117	115
Oil & grease eff.	68	67.8	65.7	61.9	58.4	55	48.8	37.4	40.5	43.2	44.7	46
%removal	34.6	36	39.7	44.7	49.2	54.2	60.3	65.4	65.7	64	61.8	60

Table 6 : Changes in Parameters Rested after the Addition of Bacterial   Additives to Septic Tank at Anebas Village Sohag Governorate.

parameters	Time in days after bacteria addition											
	0	3	6	12	18	24	30	36	42	48	54	60
COD inf.	1072	1082	1120	1070	1090	1115	1135	1100	1150	1125	1110	1100
COD eff.	234	233.7	224	181.9	157	127.1	96.5	62.7	51.8	58.5	81	99
% removal	78.2	78.4	80	83	85.6	88.6	91.5	94.3	95.5	94.8	92.7	91.0
BOD inf.	714	720	730	755	770	790	805	820	810	825	800	790
BOD eff.	142.1	140.4	126.3	111.7	93.2	75.8	55.5	36.1	34	41.3	52.8	53.7
%Removal	80.1	80.5	82.7	85.2	87.9	90.4	93.1	95.6	95.8	95.0	93.4	92.2
Tss inf.	852	850	870	887	900	920	938	960	985	970	930	900
Tss eff.	160	158.1	147.9	131.3	112.5	93.8	72.2	56.6	50.2	58.2	67	82.8
%Removal	81.2	81.4	83	85.2	87.5	89.8	92.3	94.1	94.9	94.0	92.8	90.8
Oil & grease inf.	40	40.1	40.3	40.8	41.0	41.7	42.3	43	72.7	42	41.8	41.0
Oil & grease eff.	22	21.5	20.2	17.95	15.79	13.43	11	8.6	8.33	8.44	9.4	10.25
%Removal	45	46.5	50	56	61.5	67.8	74	80	80.5	79.9	77.5	75

Table 7 : Changes in Parameters Rested after the Addition of Bacterial Additives to Septic Tank at Benisand Village, Asuit Governorate

parameters	Time in days after bacteria addition											
	0	3	6	12	18	24	30	36	42	48	54	60
COD inf.	1360	1330	1410	1280	1330	1400	1390	1360	1425	1370	1350	1340
COD eff.	480	463	481	339	279.3	217	132	84	74	82.2	95.85	124.6
% Removal	64.7	65.2	68	73.5	79	84.5	90.5	93.8	94.8	94.0	92.9	90.7
BOD inf.	980	950	1030	920	950	1000	990	1055	1020	980	980	960
BOD eff.	260	247	226.6	165.6	147.3	120	84.2	58	49	49	93.7	74.9
% Removal	73.4	74	78	82	84.5	88	91.5	94.5	95.2	95	93.5	92.2
Tss inf.	2051	1980	2100	1880	1970	2050	2040	2000	2250	2150	2000	2000
Tss eff.	888	817.74	798	573.4	457	329	177.5	60	47.25	47.3	96	124
%Removal	56.7	58.7	62	69.5	76.8	84	91.3	97	97.9	97.8	95.2	93.8
Oil & grease inf.	3.4	3.3	3.8	3.1	3.9	3.5	3.7	3.2	3.9	3.6	3.6	3.4
Oil & grease eff.	2	1.8	1.92	1.3	1.29	0.84	0.56	0.2	0.22	0.22	0.27	0.28
%Removal	41.1	45.5	49.5	58.0	66.8	76.1	85.0	97.8	94.4	93.9	92.6	91.8
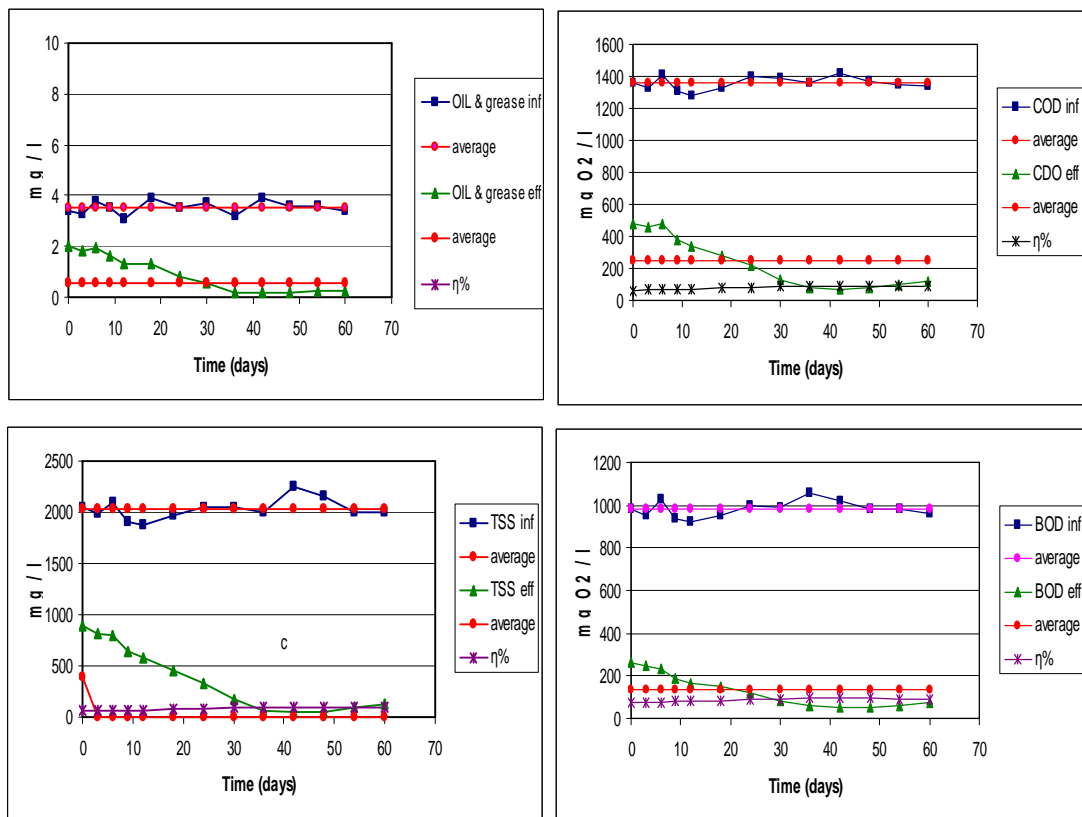
Fig. 5 : Changes in Parameters Rested after the Addition of Bacterial Additives to Septic Tank at El Mahamid Village, Aswan Governorate.
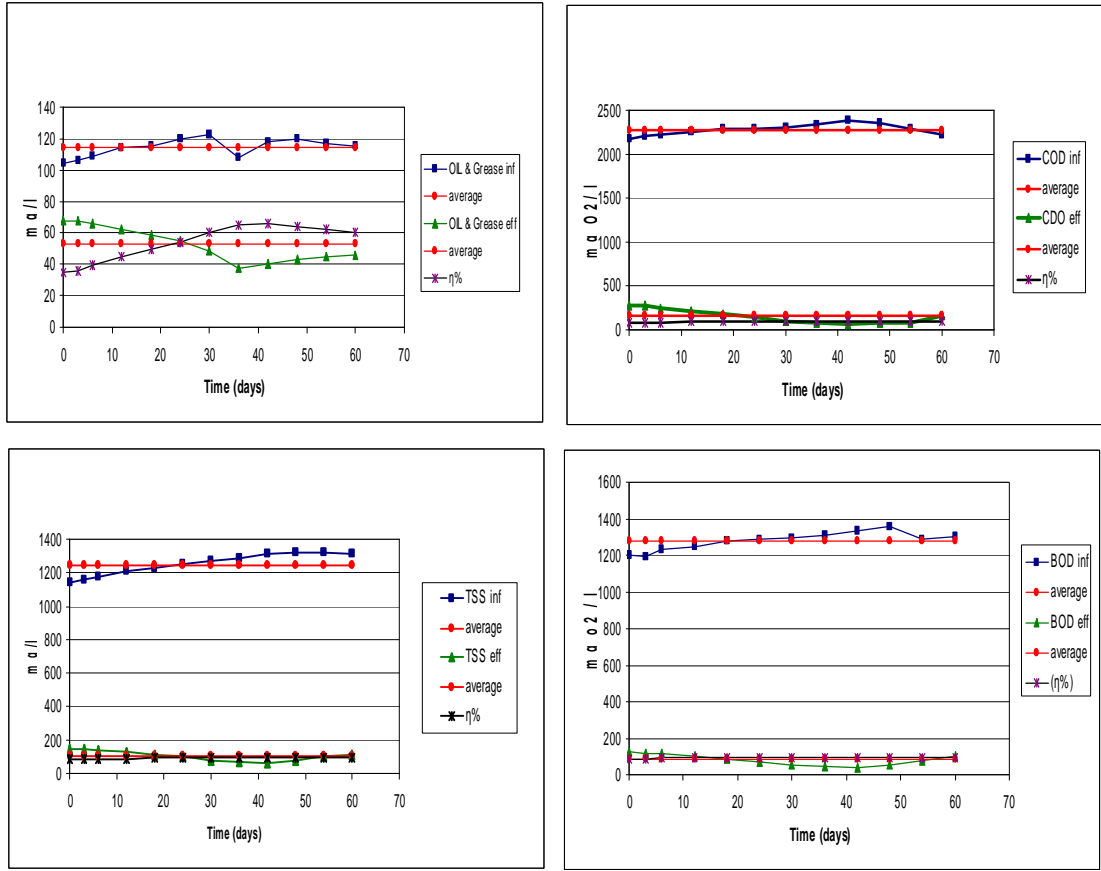
Fig. 6 : Changes in Parameters Rested after the Addition of Bacterial   Additives to Septic Tank at Anebas Village Sohag Governorate.
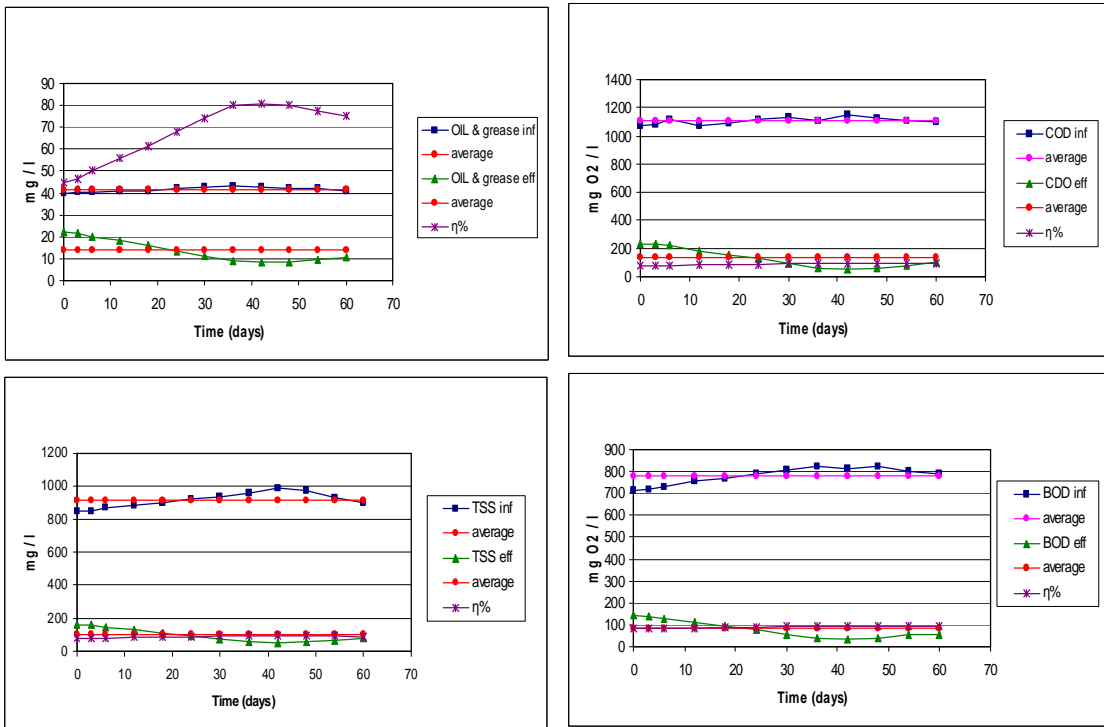

Fig. 7 : Changes in Parameters Rested after the Addition of Bacterial Additives to Septic Tank at Benisand Village, Asuit Governorate

CONCLUSIONS

1- Although, the removal efficiency of septic tanks with bacterial additives was higher in case of those receiving the high load of pollutants in the influent than in those receiving medium load, the pollutants residual in the final effluent (after 60 days) of the first case are higher (Tables and Figs 2,3,4,5,6,7).

2- The further decrease in the total colifrom density resulted after using bacterial additives may be due to the possibility of antimicrobial agent production. For example, *B. licheniformis* is capable of producing several antimicrobial agents such as licheniformin. In addition, metabolite(s) produced by *B. licheniformis* and *B. amyloliquefaciens* showed antifungal activity (Shigemistsu et al., 1983, Scharen & Bryan, 1981 and Yoshida et al., 2001) [14.12, 20].

3- From the results, it seemed that septic tanks need to re-inoculated with the selected strains after 30-45 days. Cells inoculated in the gravel filter start to reproduce firm biofilm on gravel surfaces as well as on the tank walls. The decrease in bacterial activities and pollutants removal efficiency may be due to one or more of the following reasons.a) The first is the presence of toxic materials in the wastewater which can inhibit the survival of the community. b)The second, is that such chemicals may produced and bio-chemically incompatible with the effective catabolism of the target compound and may poison the process.c) The third reason is the interactions between microorganisms such as the lytic activity of amoebicin m-4-A that produced by *B. licheniformis* against *B. megaterium* (Lebbadi et al., 1994)[9] d)The forth possibility is that biofilm formed may slough out and lost by the time with the effluent. The use of other material than gravel which have rough surface may be much more helpful.

4- Concerning the use of cultured bacteria as additives to septic tanks in order to provide the system with types of bacteria at density necessary to improve and enhance system function, there are two approaches. a)The first say that because of the presence of significant numbers and types of bacteria, enzymes, yeasts, and fungi in typical residential and commercial wastewaters, the use of septic system additives containing these or any other ingredients is not recommended (U.S. EPA, 2005) [19].b) The second approach recommended the use of bacterial additives for septic tanks under normal as well as adverse conditions. This approach based on the studies which proved that biological additives are usually won't cause problems if they won't provide help (Clark, 1999) [5].

5- The use of selected and adapted natural bacteria as additive have the same advantage as the home field ones and the competition with the native bacteria of the system won't exist. These bacteria can reduce retained organic molecules to soluble compounds and gases. This digestion can significantly further reduce sludge volume especially in warm climate of the Upper Egypt. Material degraded by bacteria does not contribute in increasing the loading of BOD5, TSS.

6- Users must aware that the application of bacterial additives is not the solution for all symptoms of septic tank failures. The cause of failure should be identified and appropriate corrective action taken to prevent recurrences.

7- Finally, at any case, bacterial additives are not an alternative to proper maintenance and do not eliminate the need for routine desludging of the septic tank.

ACKNOWLEDGMENTS

REFERENCES

1- American Public Health Association (APHA). 1989. Standard Methods for the Examination of Water and Wastewater APHA, 20th Edit., Washington, D.C.

2- Banerjee, C., Bustamante, C.I., Wharton, R., Tally, E., and Wade, J.C. 1988 *Bacillus* infections in patients with cancer. Arch. Intern. Med.. 148 : 1769-1774.

3- Brown, R.B. 1998 Soils and septic systems. Fact sheet SL-118 University of Florida Cooperative Extension Service.

4- Claus, D. and Berkeley, R.C.W. 1986. Genus *Baillus* chon 1872, pp. 1105-1139. In : P.H.A. Sneath , et al. (eds.) Bergey's Manual of systematic Bacteriology, vol. 2. Williams and Wilkins Co., Baltimore, MD.

5- Clark, G.H. 1999. The effect of bacterial additives on septic tank performance. Master's Thesis, North Carolina state University, Department of Soil Science, Raleigh, NC.

6- Edberg, S.C. 1992. USEPA human herlth assessment: *Balillus licheniformis.* Upublished U.S. Environmental Protection Agency, Washinton, D.C.

7- Hoover, M.T., Disy. T.M., Pfeiffer, M.A., Dudley, N., Mayer, R.B., and Buffington, B. 1996. North Carolina Subsurface System Operators Training School Manual. Raleigh , N.C.: Soil Science Department, College of Agriculture and Life Sciences, North Carolina State University and North Carolina Department of Environment, Heath and Natural Resources

8- Jarrett. A. R., Fritton, D.D., and Sharpe, W.E. 1985. Renovation of failing absorption fields by water conservation and resting. American Asssociation of Agricutural Engineers Paper 85-2630.

9- Lebbadi, M., Galvez, A., Valdivia, E., Martinez-Buen, M., and Maqueda, M. 1994. Biological activity of amoebicin m-4 from *B. licheniformis* M-4. Antimicrobial Agents Chemother 38, 1820 – 1823.

10- Montgomery, T. 1990 On-site wastewater treatment systems: A brief description of ecological economic and regulatory factors. The New Alchemy Institute T.echnical Bulletin No. 6.

11- Norris, J.R., Berkeley, R.C.W., Logan, N.A., and O'Donnell, A. G. 1981. The genera Bacillus and sporolactobaillus, pp. 1711-1742. In : M.P. Starr et al. (eds.), The prokaryotes: A Handbook on Habitats, Isolation and Identification of Bacteria , Vol. 2. Springer-Verlag, Berlin.

12- Scharen, A.L., and Bryan, M.D. 1981. A possible biological control agent for net blotch of barely. Phytopathol. 71 : 902-903.

13- Seifer, R. 1999. Septic system fact sheets. Alaska Cooperative Extension, University of Alaska , Fairbanks.

14- Shigemitsu, H., Hirano, K., Kohno, M., Eshizaki H., and Kunoh, H. 1983. Effect of Bacillus licheniformis on Fusarium oxysporum f. sp. Cucumerinum. Trans. Mycological Society of Japan 24: 477-486.

15- Sohnson, B.A., Anker, H, and Meleney, F.L. 1945 Bacitracin: A new antibiotic produced by a member of the *B. subtilis* group. Sci. 102 : 376 – 377.
Callow, R.K., and Hart, P.D. 1946. Antibiotic material from *Bacillus licheniformis* (weigmann, emend Gibson) active against species of mycobacteria.. Nature 15 : 334.

16- Tolman , A.L., Gerber, R.G., and Hebson, C.S. 1989.Nitrate loading methodologies for septic system performance prediction: State of an Art. In proceedings of the FOCUS Conference on Eastern Regional Groundwater Issues, pp. 167-180. Dublin, Ohio: National Water well Association.

17- U.S.EPA. 1980 Design manual for onsite wastewater treatment and disposal systems. U.S.EPA 625/1-80-012, U.S.EPA, Washington, DC.

18- U.S. EPA. 1999. Decentralized systems technology fact sheet, septic tank – soil absorption systems. United State Environmental Protection Agency, EPA 932-F-99-075, Office of Water, Washington, D.C.

19- U.S.EPA. 2005 Onsite wastewater treatment systems, special issues Fact sheet 1- septic tank additives. U.S Environmental Protection Agency, National Risk Management Research Laboratory. EPA 625/R-00/008.

20- Yoshida, S., Hiradate, S., Tsukamoto, T., Hatakeda, K., and Shirata, A. 2001. Antimicrobial activity of culture filtrate of *Bacillus amyloliquefaciens* RC-2 isolated from mulberry leaves. Phytopathology 91: 181 – 187.

EFFECT OF WINDOW TO WALL RATIO AND DIFFERENT CLIMATE CONDITIONS ON ENERGY CONSUMPTION FOR RESIDENTIAL AND COMMERCIAL BUILDINGS IN EGYPT

S. S. Shebl

Housing and Building National Research Center, P. O. Box 1770, Cairo, Egypt
e-mail: ssshebl@yahoo.com, Tel: +20127193844, Fax: +2-02-3351564

ABSTRACT

This study evaluates the effect of window to wall ratio (WWR), for all different buildings to save energy associated with the total electricity consumed. It summarizes the results of a simulation analysis to determine the effectiveness of WWR for different outdoor climate conditions in reducing electrical energy consumption for building sector in Egypt. Typical four buildings that represented both residential and commercial buildings in Egypt were tested. This study takes into consideration different runs for Alexandria, Cairo, and Aswan that represented the different climate regions in Egypt. This study is based on thermal performance analysis with respect to thermal comfort and energy conservation with the software Visual DOE-3.1. It has been proved that decreasing of WWR generally saves more energy and WWR upto about 17 % is preferred for energy efficient residential buildings in Egypt. The outdoor climate conditions in Egypt, affect strongly the rates of energy consumption for residential buildings, especially for the very hot dry regions. So, reduction of WWR as much as possible and prevention of natural ventilation during the day is generally recommended. The results for the commercial sector case indicate generally that outdoor climatic conditions slightly affect the rates of energy consumption, and a WWR up to 20 % is preferred for commercial buildings to be energy efficient.

Keywords: Energy; saving; efficient; window to wall ratio; visual DOE3.1; thermal comfort.

INTRODUCTION

The building sector in Egypt generally consumes a large percentage of the total energy, therefore, it becomes necessary to enhance the efficiency of energy utilization to increase the benefit of the energy resources and minimize requirements for energy efficient buildings. Both ASHRAE/ANSI 90.2-01 [1], and energy codes that has been developed recently [2,3,4] specify minimum requirements in order to improve the thermal performance of buildings to achieve comfort conditions. These codes has been effectively used to reduce heating and cooling loads and to moderate indoor temperature swings. Increasing energy loads may be due to improper use of building envlope fenestration, such as larger window area with aluminum frame without external shutters and also in addition, to using of glass type of high solar heat gain coefficient SHGC …etc. As a result, these buildings have higher solar heat loads and additional utilization of air conditioning to offset the resulting increase of cooling loads. An acceptable indoor environment can be achieved by natural ventilation and a good passive thermal performance. Glazing provide alternate means of regulating the amount of passive gain in buildings as size and type, thus helping to reduce energy consumption for winter heating, summer cooling, ventilation and lighting.

M. S. Imbabi and A. Musset [5] demonstrated that building energy performance simulation programs such as PSS6, Energy Plus and DOE-2.1E neglect thermal comfort. Such programs assume that HVAC system provides comfort as long as the air temperature is maintained as

specified by the program user. However, thermal comfort depends on other variables such as wind speed, mean radiant temperature, etc, that are not taken into consideration by such simulation programs. The energy performance of building can model hourly using Visual Doe3.1 building simulation program, which is a computer program, designed to explore the energy behavior of buildings.

S. S. Shebl [6] summarized the results of a simulation analysis for determining the effectiveness of envelope fenestration on energy saving for residential buildings in Egypt using of the software DOE-2.1E. It was concluded that using of sash ratio with high values, shutting ratio with low values, glass type of low solar heat gain coefficient, overhang with high projection factor and WWR up to 15% increasing the energy savings.

G. B. Hanna et. al. [7], evaluate theoretically using of the software DOE-2.IE, the effect of building envelope on the total energy consumption. The results of a simulation analysis to determine the effectiveness of envelope construction in reducing electrical energy consumption had been summarized for residential buildings in Egypt. The study takes into consideration the building envelope, orientations, window-opening size as a ratio of wall area, and the glazing type for Cairo and Alexandria. For most residential buildings in Egypt with SHGC values above 0.61, an increase of the total electrical consumption by 25% can be concluded. Roof and wall insulation provides significant energy saving, 40% and 12% respectivly.

R. M. A. Selim et. al. [8] illustrated that the use of new building technologies had a bad effect on increasing of energy consumpion. This was due to the excess use of glass and the indiscriminate transfer of western technologies without their being localized. Visual DOE3.1 program had been used for modeling the energy performance of buildings. Parametric runs were performed to examine the effects of orientation, building material, WWR and glass type. Most of the required thermal resistance of building envelope elements were tabulated and it was found, that recommended by the Egyptian Energy Efficient Code.

This study is based on thermal analysis with the software Visual DOE3.1. This program is an important tool for energy simulation aimed at achieving energy efficiency solutions. In this study, thermal performance of window to wall ratio alternatives under different climatic conditions in Egypt were evaluated in terms of energy consumption. The climatic condition for Alexanderia, Cairo and Aswan were tetsed. These represent the climates of humid, hot-dry and very hot-dry regions respectively. Two different models that represents the residential building sector and another two different models that represents the commercial building sector had been evaluated. The performance of different alternatives is discussed in comparative form with respect to the base case. Consequently, the emphasis is placed on the thermal performance of alternatives from the point of view of thermal comfort and energy consumption.

ASHRAE/ANSI 105-99 [9] provides a uniform basis for reporting energy use, and compliance of Standard 105-99 requires also, reporting of sufficient information about the building such as its use, local climate, orientation, construction and fenestration details, calculation or measurement method used, …etc. In the present work, sufficient data of tested models are presented and analyzed as shown hereinafter.

DESCRIPTION OF LOCAL CLIMATE DATA

Building performance varies strongly with the outdoor climate conditions because of the special impact of solar intensity and outdoor relative huimitiy and dry bulb temperature. Therefore, description of the local climate data is essentially important. Three different climate conditions representative to all Egypt are tested. Alexandria is situated at 31.12 ^{o}N Latitude and 29.53 ^{o}E Longitude. Cairo is situated at 30.13 ^{o}N Latitude and 31 ^{o}E Longitude. Aswan is situated at 24°N Latitude and 32.53 ^{o}E Longitude. These represent the climates of humid, hot dry and very hot dry regions respectively.

DESCRIPTION OF SAMPLE BUILDINGS

Typical four buildings located in Cairo and represented both residential and commercial buildings in Egypt were tested, Fig. (1). Ramadan and Ghazala apartments, can be considered as representative models for residential buildings while, Electricity and Omar-Effendi buildings

are for commercial buildings. Handling of sample buildings under different climates, that representing all Egypt, as mentioned before has been carried out.

DESCRIPTION OF BASE CASE FOR ALL MODELS

Ramadan Apartment

The model consists of one block with 3 facades and Azmiuth angle of 280°. It has 5 floors above ground with 4 units per floor. The floor height is 2.7 m. It is a medium apartment as a one unit in the third floor. It has a gross area that totally conditioned of 105 m^2. Base case constructions and fenestrations summary is shown in Table (1) & (2). Window to wall ratio for base case is 0.088. Summary of alternatives is shown in Table (3).

Ghazala Apartment

The model consists of one block, with Azmiuth angle of zero. It has 10 floors, with 4 units per floor and floor height of 2.7 m. The tested model is a medium apartment as one unit in eighth floor. It has a gross area that totally conditioned of 99 m^2. The WWR for the base case is 0.121. Summary of alternatives is shown in Table (3).
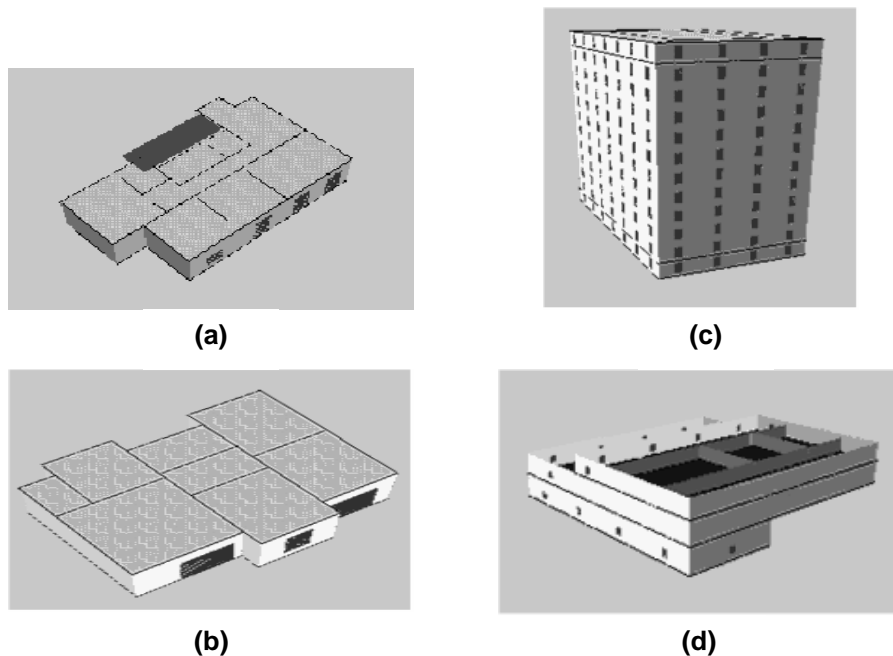
Fig. 1: Isometric View of (a) Ramadan Apartment; (b) Ghazala Apartment; (c) Electricity Building; and (d) Omar-Effendi Building

Table 1: Construction Summary for Different Tested Models

Model	Construction element	Area (m²)	U-Factor (W/m²-°C)
Ramadan apartment	Conc. 100 mm, 75 mm insul., 30% reflectivity	105	0.4
	*CMU Partition 200mm	101	3.28
	H Clay 120 mm	53	1.65
	Insul. H Clay 120 mm	72	0.66
	Insul. Floor 200mm	105	0.73

Ghazala apartment	CMU Partition 200mm	99	3.28
	H Clay 120 mm	88	1.65
	Insul. 120 mm H Clay	30	0.66
	Insul. Roof 210 mm	99	0.35
	Insul. Floor 200 mm	99	0.73
Electricity building	CMU Partition 200mm	4,258	3.28
	Brick Wall 287 mm	4,084	1.73
	Conc. Roof 175 mm	1,008	0.81
	Ground Floor 200 mm	1,008	1.4
	Internal Floor 215 mm	11,088	1.26
Omar-Effendi building	CMU grouted 128 mm	1,740	0.98
	Mtl Deck 27 mm	1,848	0.42
	Simulated Slab 1000 mm	1,848	0.14
	R-0 Mass 100 mm	2,520	1.03
	Partition 31 mm	781	2.19
	Gyps. board ceiling 16 mm	4,368	4.23

*CMU: Concrete Masonry Units

Table 2: Fenestrations Summary for Different Tested Models

Model	Fenestration element	Area (m²)	SHGC
Ramadan apartment	single clear 0.75x0.75 m	1	0.815
	Ballacon 1.2x2 m	7	0.815
	single clear 1.2x1 m	4	0.815
Ghazala apartment	6040 double bronze 1.2x2.1 m	4	0.492
	single clear 1.2x1.2 m	1	0.815
	Ballacon 2.5x2.2 m	10	0.815
	single clear 0.8x0.8 m	0	0.815
Electricity building	6040 double bronze 1.2x2.1 m	589	0.492
Omar-Effendi building	Skylight	19	0.815
	6040 double bronze 1.2x2.1 m	80	0.492

Table 3: Alternative WWR Summary for Different Tested Models

Model	Alt 1	Alt 2	Alt 3	Alt 4	Alt 5	Alt 6	Alt 7
Ramadan apartment	0.061	0.101	0.171	0.304	-	-	-
Ghazala apartment	0.05	0.091	0.139	0.185	0.21	0.298	0.318
Electricity building	0.051	0.113	0.198	0.266	0.288	-	-
Omar-Effendi building	0.116	0.158	0.231	0.27	0.314	-	-

Electricity Building

The model consists of 3 rectangular shaped blocks has dimensions of 24x42 m, with Azmiuth angle of zero. It has 10 floors in addition to ground and roof floors, with floor height of 2.7 m. The gross area of the model that totally conditioned is 12096 m^2. The WWR for the base case is 0.126. Summary of alternatives is shown in Table (3).

Omar-Effendi Building

The model consists of 3 rectangular shaped blocks has projected dimensions of 44x42 m, with Azmiuth angle of zero. It has two floors in addition to ground floor, with floor height of 3 m. The gross area of the model that totally conditioned is 4368 m^2. The WWR for the base case is 0.054. Summary of alternatives is shown in Table (3).

RESULTS AND DISCUSSION

Figure (2) shows the effect of WWR on improvement of total electricity consumption for Ramadan apartment with different climate conditions with respect to the base case. The percentage consumption improvement is calculated as [(Alternative – Base case) ×100/ Base case]. It can be seen that, decreasing of WWR generally saving more energy. The outdoor climate conditions in Egypt, affect strongly the rates of energy consumption for residential buildings, especially for the very hot-dry regions. It has very high rates of energy consumption. It reaches sometimes, to about 100 % beyond the base case. So, for thermal comfort and energy saving purposes, reducing of WWR as possible, and preventing natural ventilation during day is generally recommended for the very hot-dry regions. While, the humid regions and hot dry regions has the lower rates of energy consumptions. Increasing WWR upto 17 % showed little variation in energy consumption, while for any more increase; the curve suffers more inclination which means more energy consumption. Increasing of WWR to about 30% has a very bad effect on the total energy consumption. It consumes nearly twice the consumption rates for the base case, due to the rapid increase in internal cooling loads during summer months.
Figure (3) shows the effect of WWR on improvement of energy consumption for Ghazala apartment with different climate conditions with respect to the base case. It can be seen that, same trends as for Ramadan apartment had carried out.
The results for residential sector generally in Egypt indicate that, for humid and hot dry climate conditions, WWR up to 17 % is preferred for residential sector. While, for very hot dry climate conditions, reducing of WWR as much as possible is preferred for residential sector in Egypt.
Figures (4, 5) indicate the effect of WWR on improvement of total electricity consumption for Electricity and Omar-Effendi building, respectively, in different climate conditions with respect to the base case. A downward trend can be noticed. The results for commercial sector in Egypt indicate generally that, increasing of WWR to about 20 % has a small effect on the total energy consumption. The outdoor climate conditions in Egypt, slightly affect the rates of energy consumption for commercial buildings. For all possible climate conditions, WWR up to 20 % is preferred for commercial sector in Egypt. Generally, although the energy consumption has small values for residential buildings compared with those for commercial buildings, the effect of WWR is very sensitive for only residential buildings.
Figures (6, 7) illustrate the monthly total electricity consumption for Ramadan and Ghazala apartment with different WWR at climate condition of Alexandria, Cairo and Aswan. The results indicate that, increasing of WWR increase the total electricity consumption during summer season to values reaches to nearly twice in some months with respect to the base case. This is due to the increasing of the cooling loads during summer months. This leads to increasing of the yearly total electricity consumption. These intervals reach to about four months for Alexandria, seven months for Cairo and nine months for Aswan.
Figures (8, 9) illustrate the monthly total electricity consumption for Electricity and Omar-Effendi buildings with different WWR at climate condition of Alexandria, Cairo and Aswan. It can be seen that, there was an increase of cooling electricity consumption due to the increasing of WWR although, it represent a small ratio with respect to the total electricity consumption for commercial sector in Egypt.
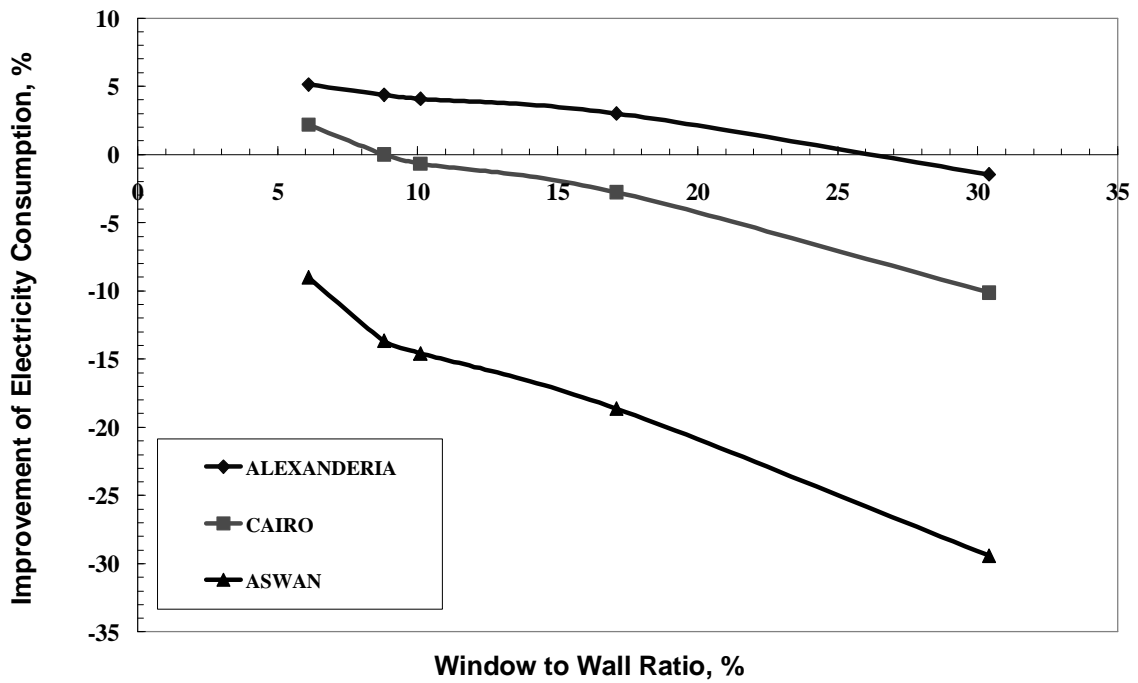
Fig. 2: Effect of Window to Wall Ratio on Improvement of total Electricity Consumption for Ramadan Apartment with Different Climatic Conditions
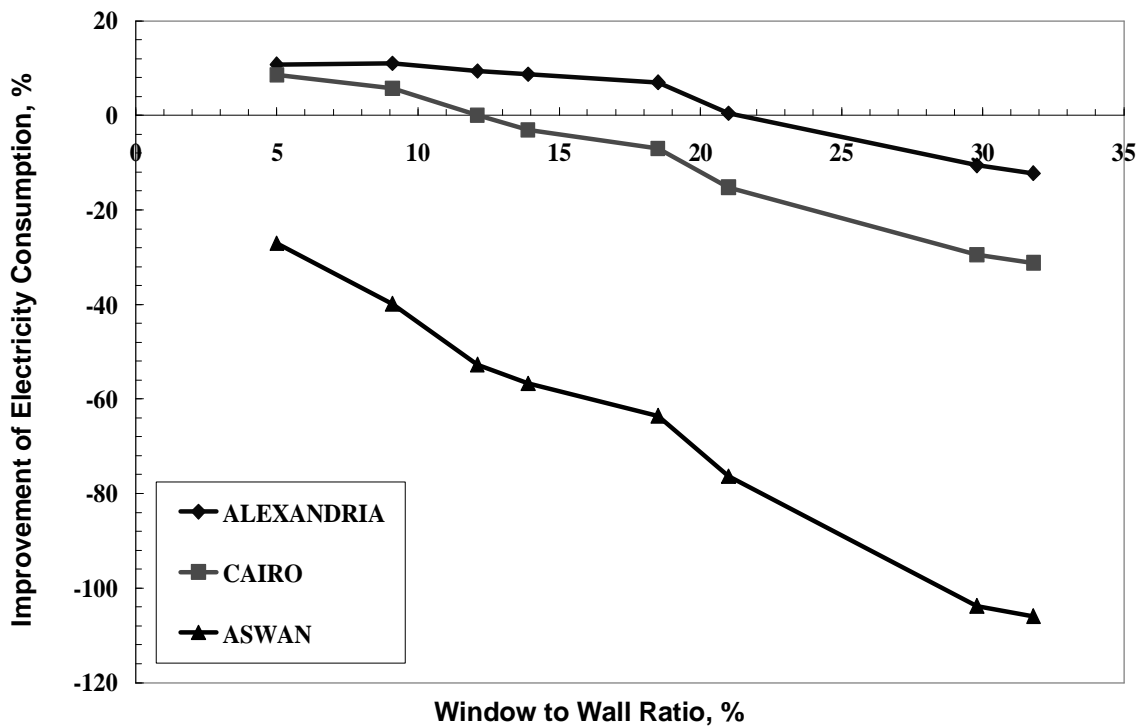

Fig. 3: Effect of Window to Wall Ratio on Improvement of Total Electricity Consumption for Ghazala Apartment with Different Climatic Conditions
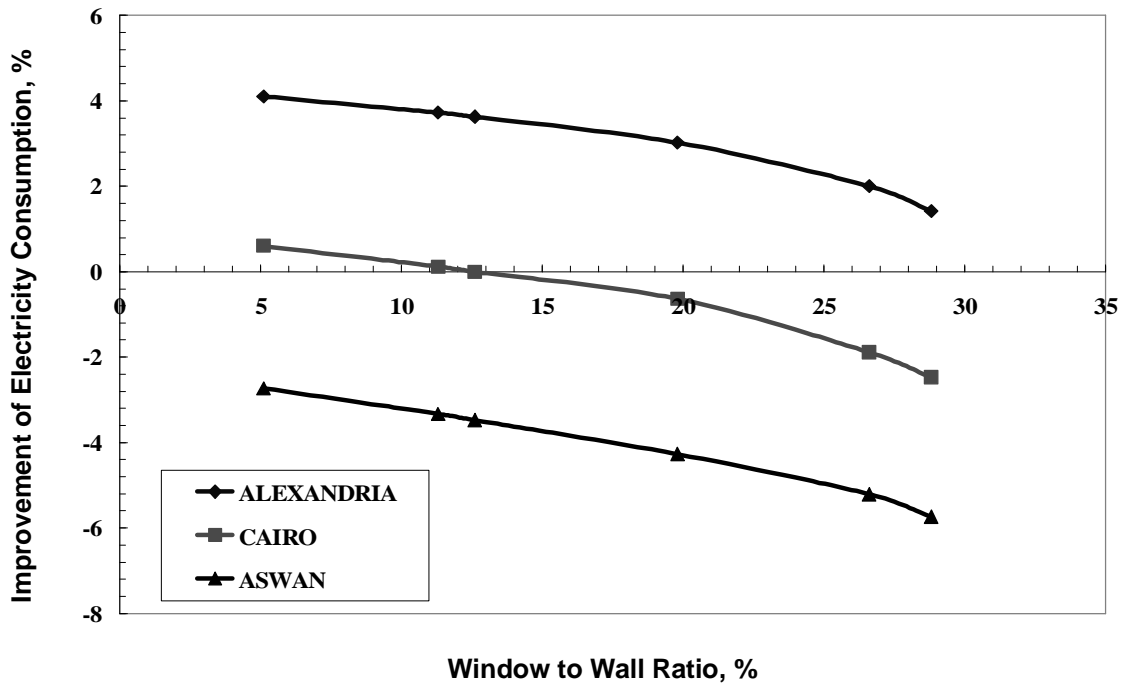
Fig. 4: Effect of Window to Wall Ratio on Improvement of Total Electricity Consumption for Electricity Building with Different Climatic Conditions
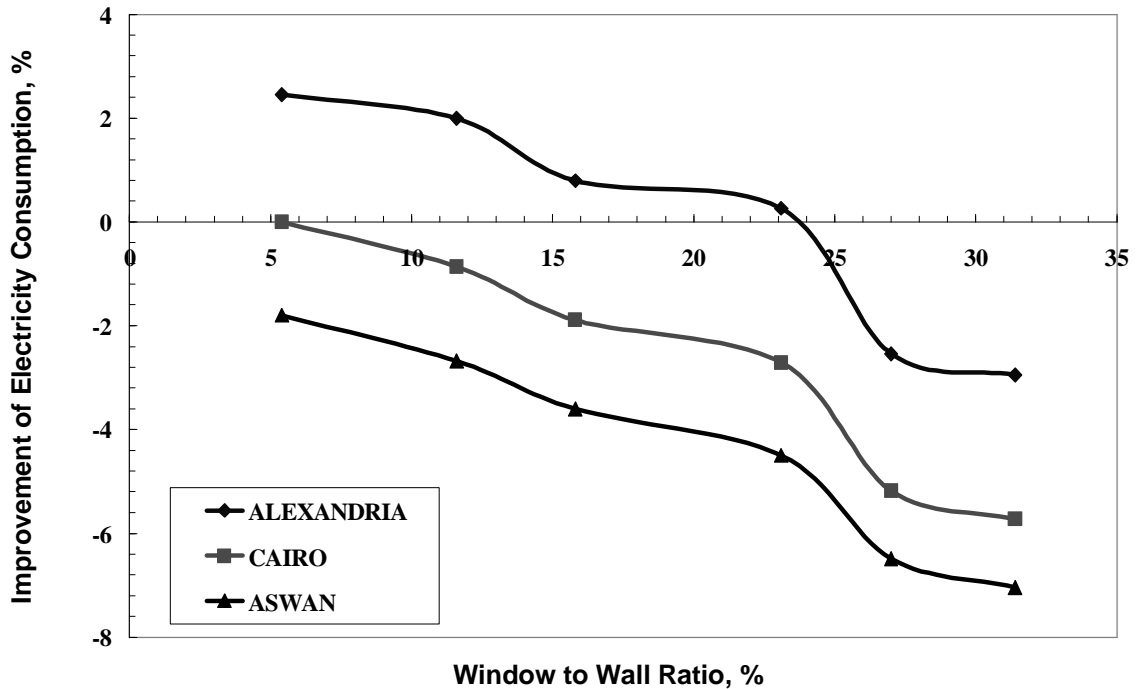

Fig. 5: Effect of Window to Wall Ratio on Improvement of Total Electricity Consumption for Omar-Effendi Building with Different Climatic Conditions
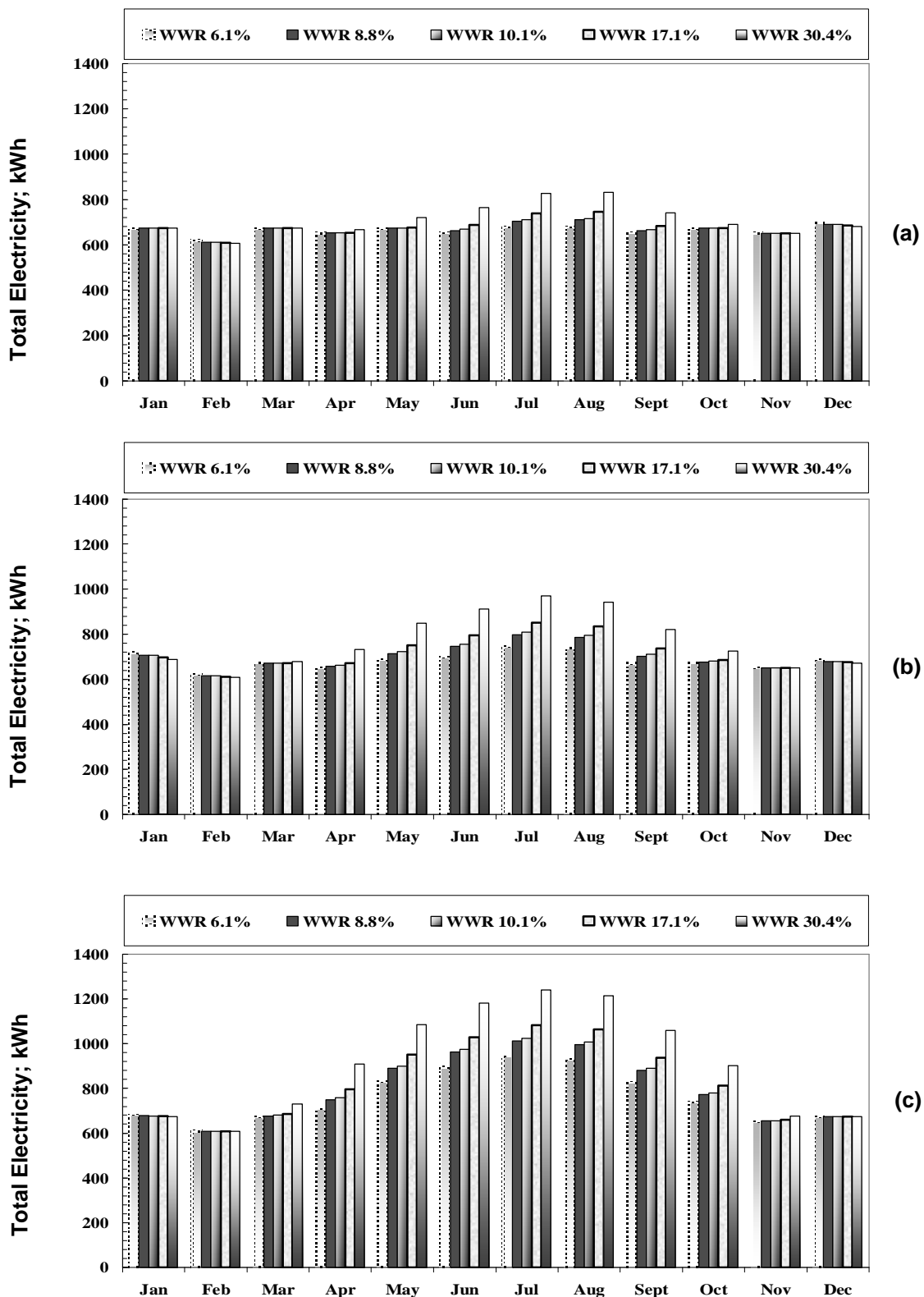
Fig. (6): Monthly Total Electricity for Ramadan Apartment with Different Window to Wall Ratios at Climatic Conditions of (a) Alexandria (b) Cairo (c) Aswan
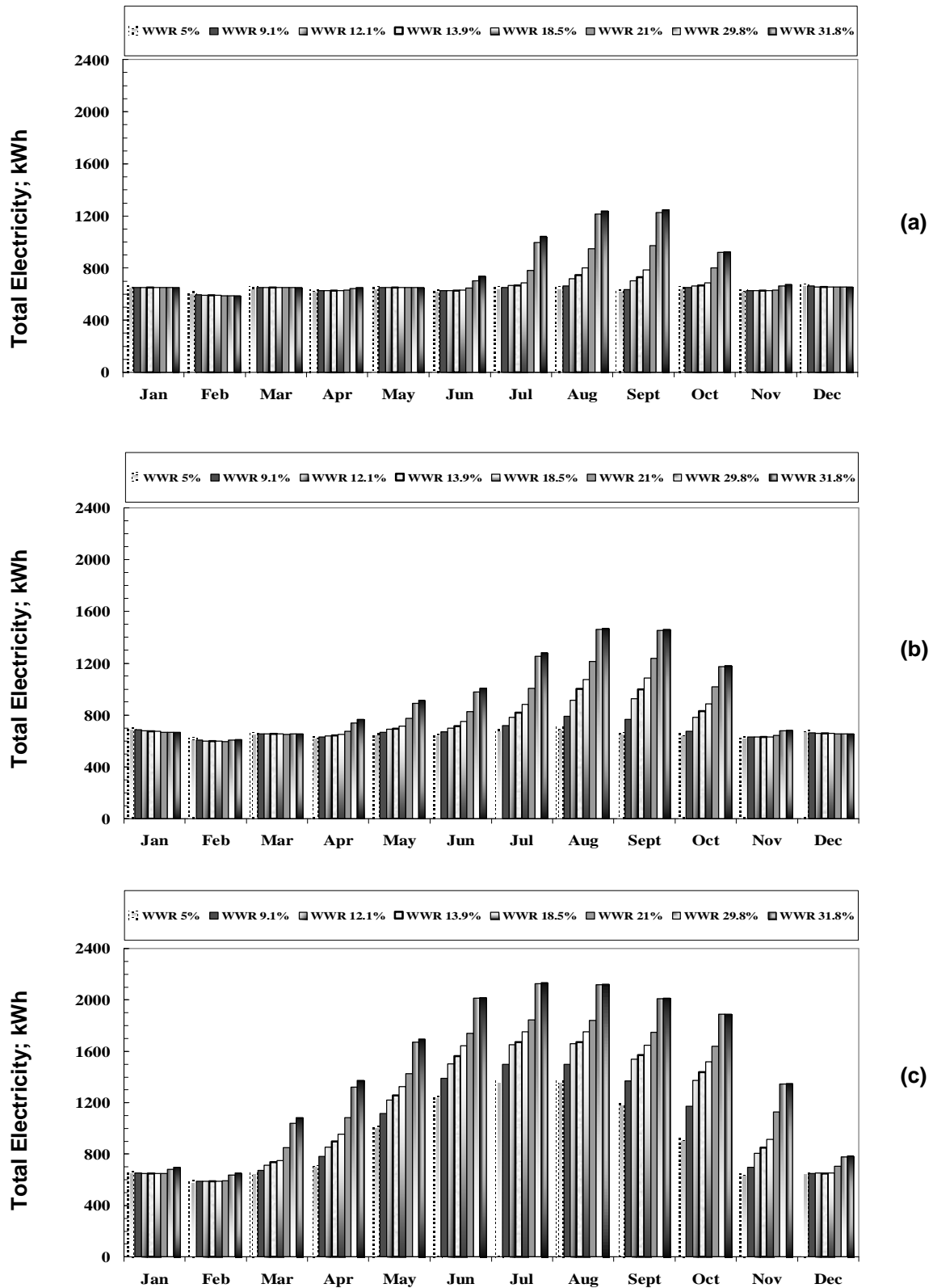
Fig. 7: Monthly Total Electricity for Ghazala Apartment with Different Window to Wall Ratios at Climatic Conditions of (a) Alexandria (b) Cairo (c) Aswan
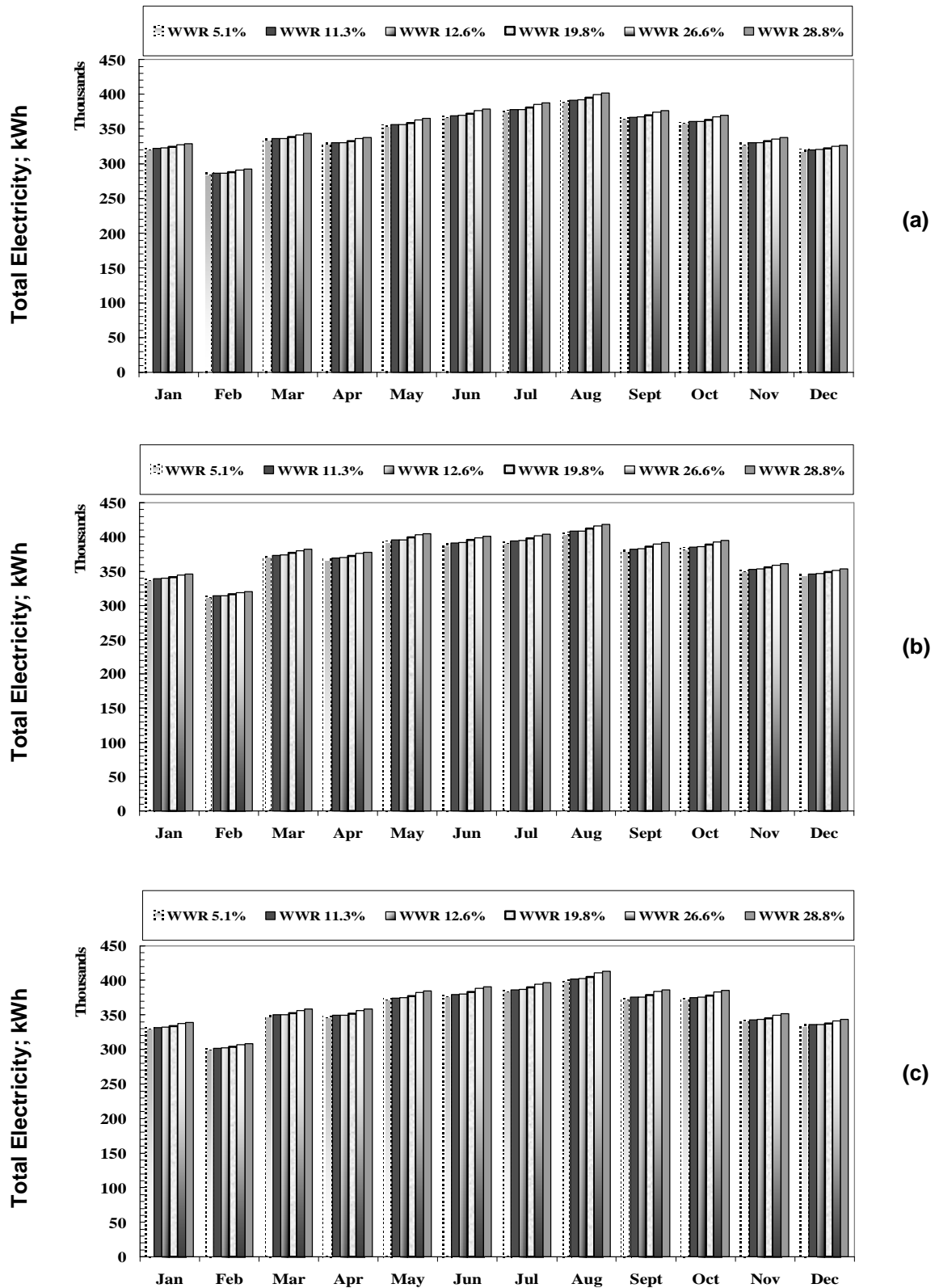
Fig. 8: Monthly Total Electricity for Electricity Building with Different Window to Wall Ratios at Climatic Conditions of (a) Alexandria (b) Cairo (c) Aswan
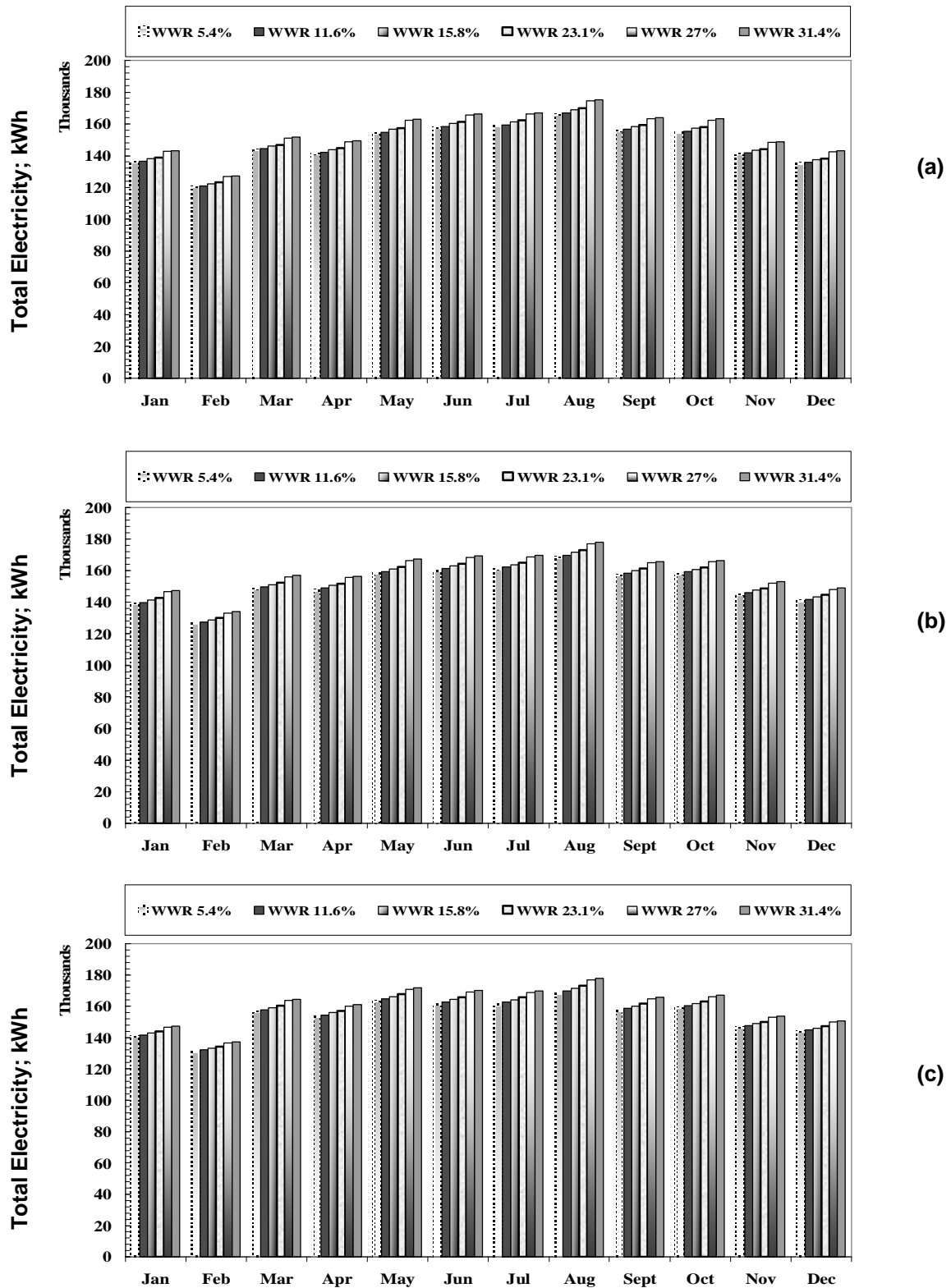
(a)

(b)

(c)

Fig. 9: Monthly Total Electricity for Omar-Effendi Building with Different Window to Wall Ratios at Climatic Conditions of (a) Alexandria (b) Cairo (c) Aswan

CONCLUSION

It has been proved that, decreasing of WWR generally saves more energy, and WWR of about 30 % has a very bad effect on the building performance due to the rapid increase of internal cooling loads during summer months. The outdoor climatic conditions in Egypt, affect strongly the rates of energy consumption for residential buildings, especially for very hot dry regions. Therefore, the reduction of WWR as much as possible for those regions and preventing natural ventilation during the day time is generally recommended. The humid regions and hot-dry regions in Egypt has the lower rates of energy consumptions. Thus, WWR up to 17 % is concluded from humid and hot dry climatic conditions, for energy efficient residential buildings in Egypt. The results for commercial sector in Egypt indicated generally that outdoor climatic conditions, slightly affect the rates of energy consumption. So, for all possible climatic conditions, WWR up to 20 % is preferred, for commercial buildings to be energy efficient. Implementing energy efficient features at design stages, leads to more economical and practical housing solutions.

REFERENCES

1. ASHRAE/ANSI Standard 90.2, (2001), "Energy Efficient Design of Low-Rise Residential Buildings", Atlanta.
2. Ministry of Housing, Housing & Building Research Center, (2003), "Energy Efficiency Residential Building Code", Egypt.
3. G. L. Robertson, (1998), "Residential Energy Code – A New Zealand proposal", pp. 926-930.
4. "Energy Efficiency Commercial Building Code of Vietnam - 1st draft", (2001).
5. M. S. Imbabi and A. Musset, (1995), "The Monymusk Hybrid Solar Heating and Project", Building and Environment, Vol. 30, No. 1, pp. 91-98.
6. S. S. Shebl, (2006), "Energy Analysis for the Effect of Envelope Fenestration for the Different Orientation", Proc. Of the 2nd Int. Conf. on Thermal Engineering Theory and Application, Al Ain, United Arab Emirates.
7. G. B. Hanna, N. M. Guirguis, H. S. Osman and M. A. Hussein, (2004), "Energy analysis for new residential buildings in Egypt", Int. Conf. Future Vision and Challenges for Urban Development, Housing & Building Research Center, Egypt.
8. R. M. Selim, M. M. Razek, A. R. Abdin and M. M. Ewaida, (2004), "Energy Performance of building envelope in Egypt", Int. Conf. Future Vision and Challenges for Urban Development, Housing & Building Research Center, Egypt.
9. ASHRAE/ANSI Standard 105, (1999), 'Standard Methods of Measuring and Expressing Building Energy Performance", Atlanta.